Discovery and Application of Neoepitopes in an Oncolytic Rhabdovirus Vaccine Approach to Treat Glioblastoma Multiforme

Zachary Keavin Jilesen

A thesis submitted in partial fulfilment of the requirements for the degree of
Master of Science in Microbiology and Immunology

Department of Biochemistry, Microbiology and Immunology
Faculty of Medicine
University of Ottawa

Supervisor
Dr. David Francis Stojdl

ABSTRACT

Glioblastoma multiforme is the most common and lethal primary brain tumour in adults. Its aggressive and invasive phenotype makes it resistant to current standards of care, with a patient median survival following treatment of only 14 months. Potent and safe therapeutics are necessary to improve patient prognosis. Globally, efforts are being made in immunotherapies to combat such deleterious tumours. Preliminary work in the Stojdl lab has developed a novel oncolytic virus platform for brain cancer therapy that is non-toxic and exhibits potent anti-tumour efficacy. This platform is based on the rhabdovirus Farmington, identified for its potent oncolytic properties and engineering malleability. Herein, we begin to show our capability to discover and vaccinate against immunogenic neoepitopes derived from a mouse cancer mutanome. Engineering Farmington virus to express neoepitopes, allows for robust tumour specific immune proliferation following a prime vaccination. Overcoming problems of targeting self-antigen and antigen loss variants, a multi-neoepitope vaccine, presented here, is one of many alternative approaches to help combat cancer resistance. Despite achieving robust anti-tumour immunity by vaccination, selectivity of the tumour microenvironment remains an enormous challenge. Cumulative efforts in immunotherapy research will help drive novel therapeutics, like Farmington, into clinic and, ultimately, improve patient's prognosis and quality of life.

ACKNOWLEDGEMENTS

To begin, I would like to thank Dr. David Stojdl for not only providing me the opportunity to pursue graduate studies within his lab but also giving the support required to successfully complete this body work. Working in the Stojdl lab has given me the opportunity to grow independently as a scientist, while allowing me to gain a unique perspective on research. The opportunity to challenge myself and explore endless hypotheses was always available during my time in his lab. Dr. Stojdl worked endlessly to provide support and keep my experiments progressing without delay. I will complete my time in his lab with a new way of thinking and a set of skills that I could not have obtained anywhere else.

Next, I would like to thank Charles for taking the time to mentor me into becoming a competent scientist. I cannot express how appreciative I am for Charles's extreme patience during my initial strides into research. Having come into the Stojdl lab with no prior laboratory experience, it was a relief to know I would start everyday beside him. I can confidently say that Charles not only provided me with everything I know about engineering rhabdoviruses today but also gave me the confidence and encouragement required to complete my M.Sc. degree. Charles's limitless support and excitement with every result, positive or negative, helped me progress through every step of my project. I cannot be thankful enough for the positive experience in science Charles provided for me.

I want to thank Dr. Stefanie Swift and Dr. Justyna Kmiecik for teaching all mouse handling techniques and protocols I know today. Their patience and availability helped me garner these techniques and begin experiments promptly. I also wanted to thank Robyn, my fellow M.Sc. candidate, for being such a good support through the entirety of my project.

I want to thank Philippe Charron for working endlessly to provide the neoepitope prediction pipeline in time for my project. Always available to help or answer questions, he has provided substantial support within the lab. I also want to thank Dr. Persano for teaching me how to produce nanoparticle vaccines and helping encapsulate peptides for the screen.

I also want to thank Animal Care and Veterinary Services who worked endlessly to ensure proper welfare was had with all of our animals. They provided the support required to always begin and finish experiments on time.

I would also like to thank my TAC members, Dr. Michele Ardolino and Dr. Rebecca Auer, for taking the time out of their busy schedules to help mentor me and review my project as it progressed. Thank you for providing the support and resources required to complete my thesis. Additionally, I would like to thank the BMI faculty for always being available to help with all of my administrative needs.

Finally, I would like to thank my friends and family for always providing support with every decision I have ever made. Making it through graduate school would have not been possible without my parents' mentorship and support. I cannot show my appreciation enough for what my parents have provided for me. Ultimately, I would like to thank my partner and best friend, Kristina, for patiently listening and providing help whenever and wherever needed.

TABLE OF CONTENTS

1 - INTRODUCTION

Textbook Treatment

The silver bullet, a treatment described by the renowned German scientist Dr. Paul Ehrlich to have curative potential and no side effects, is what scientists strive for when designing novel therapeutics for the clinic (1). With increased understanding of the heterogeneity of diseases like cancer, discovering a silver bullet that works across populations is currently arduous and typically unattainable. To achieve potent efficacy across the heterogeneity of cancer, current medicine has given up at least one of the two silver bullet characteristics, for example chemotherapies efficacy is limited due to the abundance of detrimental side effects (2). In demand for new strategies to fight cancer with less side effects and consistent results, personalized immunotherapy has emerged.

1.1 - Malignant brain tumours – A look into relevancy

Malignant brain and other central nervous system (CNS) tumours are estimated to have a incidence of 8.71/100,000 in Canada (>3000 new cases per year), based on a study spanning 2009 to 2013 (3). In an effort to more accurately depict the Canadian population effected by brain and other CNS tumours, the Canadian Brain Tumour Registry (CBTR) has been put in place and expects to publish their first report in spring 2019. Following this, the United States reported an average incidence of ~7/100,000 (>22,000 new cases per year). Both majorities falling within the 40+ age range (4).

Tumours understood to be of glial cell origin are referenced as ‘glioma’. Gliomas can be further dissected into four categories depicted by the World Health Organization (WHO) as

astrocytic tumours (astrocytoma grades I, II, III, and **IV**), oligodendrogliomas, ependymomas, and mixed gliomas (4,5). Particularly, astrocytic grade IV tumour, also known as glioblastoma multiforme (GBM), accounts for 54% of all gliomas and 16% of all primary brain tumours (4,6). Incidence rate for GBM in the United States is 3.19 per 100,000, ranging from 0.59 to 3.69 per 100,000 persons globally, affecting mostly adults, with a median age of 64 (7–9). While GBM can affect children, it is considered uncommon (4).

Male incidence of GBM is 1.6 times higher than in females and 2.0 times higher in Caucasians compared to people of African origin and lesser so in people of Asian, Hispanic and Indian origin (9). Whilst increased incidence of GBM is observed in patients with tumour syndrome: Turcot syndrome (10) and Li-Fraumeni syndrome (11), GBM otherwise occurs sporadically lacking any known genetic predisposition.

GBM is the most common and lethal primary malignancy of the central nervous system due to its resistance towards the standard of care: surgery, chemotherapy and radiotherapy. Despite such potent therapeutics, median survival time for treated GBM patients is only 14.6 months (4,12). Being extremely invasive, GBM makes curative surgical resection nearly impossible. Some evidence even points to GBM tumour microenvironments (TME) to have subpopulations of highly tumorigenic cells (e.g. glioma/GBM stem cells) supporting these recurrent GBM phenotypes (13–15). Global efforts are being made to improve the horrible prognosis of GBM.

1.1.1 – Glioblastoma multiforme: primary versus secondary

GBM can be categorized into primary (90%) and secondary (10%) malignancies. Primary GBM originates *de novo*, with no known malignant precursor. In contrast, secondary GBM develops from the aforementioned low-grade astrocytoma (grade II diffuse or grade III anaplastic

astrocytoma). In short, primary GBM genetic abnormalities include gene EGFR overexpression, PTN mutation and loss of chromosome 10. Whereas secondary GBM encompasses IDH1 mutations, TP53 mutations and chromosome 19q loss (11,16–21). Molecular understanding of the GBM mutanome can assist in prognosis and can better direct treatment. For example, IDH1 mutations found in secondary GBM predict a better prognosis and rate of survival. Occurring in only 5% of primary GBM cases, identifying IDH1 mutations can moreover be used to differentially diagnose primary from secondary GBM (22). By mid 2010, GBM, through genetic identification, had been categorized into four molecular sub-types: classical, mesenchymal, proneural and neural (18). Each with distinct molecular profiles and differing response to aggressive treatments; classical GBM responding well to aggressive chemotherapy when compared to no improvement seen when equally treating proneural GBM (11). Additionally, PD-L1 that inhibits T cell activation, is significantly higher expressed in IDH1 wildtype gliomas vs mutant gliomas, elucidating the potential for anti-PD-L1 checkpoint inhibitors in IDH1 wildtype gliomas (23). Uncovering the genetic and molecular profiles of individual GBMs can distinguish subtypes and elucidate options for personalized therapy.

1.1.2 - Neural stem cells and the origin of glioma

The most common and invasive glioma, GBM, has had median survival remain unimprovement for over a decade. An argument can be made that clinical advancement has been put on hold for ignorance of cellular glioma orgin. Being an astrocytoma, GBM, retains some morphologic characteristics of mature astrocytes but the appearance of neoplasm is not a predictor of cellular function. Gliomas of comparable histological structure have been shown to exhibit vastly different behaviours, supporting the need for an in-depth molecular understanding

of each tumour. Furthermore, gliomas can contain non-neoplastic astrocytes and endothelial cells within their stroma to create a germinal niche, which is an unfavourable stage in tumour progression. Recreated via coexistence of neoplastic and non-neoplastic cells of the CNS, this niche becomes highly evocative between the adult neural stem cells and accompanying cells, further supporting a potential shift toward incomplete differentiation of progenitor cells (24,25). Understanding and inhibiting this niche, alongside current surgical resection, could improve patient outcome.

1.1.3 - Epidermal growth factor receptor

Epidermal growth factor receptor (EGFR) signaling plays an essential role in gliomagenesis and neural stem-cell regulation. EGFR amplification is associated with the formation of GBM, being coupled with direct links to growth of astrocyte precursors and neural stem cells (26)(27). It was estimated that 50 percent of GBM demonstrate EGFR amplification, potentially driving the transformation process toward GBM over normal astrocytes. EGFR amplification phenotypic link to GBM unveils a promising therapeutic target for researchers (28).

1.2 - Risk factors

Considering GBM arises *de novo* there is limited knowledge on the risk factors leading up to its development. With the use of genome-wide association in retrospective studies, a few risks are correlated with GBM. Prior radiation increases risk for GBM, while increased susceptibility to allergies is protective against GBM (29,30). A lower risk of GBM has been associated with reaction to allergen exposure and atopic disease (e.g. psoriasis, eczema, asthma)

(31–33). While unclear as to why such susceptibilities may alter risk for GBM, it can be inferred that the immune involvement in glioma formation, and in ultimately all cancers, requires researchers undivided attention.

A few nucleotide polymorphisms were detected by a genome-wide search to increase GBM risk, however, no distinct genes appear to be the route cause for its formation. Suspect to a protective effect against GBM, the use of cyclooxygenase-2 (COX-2) inhibitors as routine anti-inflammatory medication was shown to reduce risk to GBM, albeit evidence is controversial (34).

1.3 - Prognosis

Being an aggressive and invasive cancer, GBM has a median survival of only 3 months if left untreated (4,35). Surgery remains the standard treatment when managing GBM. Factors identified in MRI images before or during surgery, such as ability to resect tumour, geo-biological location, size and multifocality can help determine patient's prognosis (36). Furthermore, histological and genetic confirmation, in addition to providing data for research, is enabled by surgical intervention.

Tumour fluorescence via 5 aminolevulinic acid has aided in accuracy of surgical resection, significantly increasing patient survival. Moreover, a combinatorial approach of both radiotherapy and temozolomide (TMZ) chemotherapy as post-operative therapeutics also significantly increases patient survival, then when administered alone (37). While appealing, treating a complex disease with a simple singular therapy will often be insufficient to significantly improve outcome. Understanding and treating with complex but rational combinational therapies are becoming more permitted when striving for optimal patient survival

and quality of life. Resent advancements in genetic and molecular diagnostics techniques in research will spearhead a new line of therapeutics to combat the consistent poor prognosis of the most malignant primary brain tumour, GBM.

1.4 - Management

The national comprehensive cancer network (NCCN) recommends ongoing participation in clinical trials to patients with cancer to improve standard of care. Patients with GBM should have multidisciplinary consultation to optimize treatment plans. Standard of care for GBM is maximal surgical resection following with radiotherapy adjuvanted with concomitant temozolomide (TMZ) with almost all patients reaching mortality with a median survival of 14 months, with a 2-year survival rate of 26-33% (4). No standard treatment has been established in recurrent or progressive GBM. Notwithstanding numerous clinical trials and advancements in diagnostic and surgical equipment, GBM continues to challenge patients, caregivers and doctors. Treatment of GBM should go beyond just improving survival but also preserving the patients and caregiver's quality of life.

1.4.1 - Surgical resection

Standard protocol follows maximal safe resection regardless of patient age, performance status or tumour histology (EMSO Level II, Grade C, NCCN Category 2A). Utilizing MRI with and without Gadolinium contrast 24-72 hours prior to resection aids in determining the extent of safe tumour debulking. Images should be taken every 2-4 months following surgery to monitor tumour prognosis and estimate possible treatment options with a potential second resection.

Surgical intent is for complete resection, debulking/cytoreduction of tumour, decompression to reduce symptoms of increased intracranial pressure, preserve neurological function, obtain tissue specimen for pathological diagnosis, improve disease conditions for complementary treatment and delay clinical progression to improve quality of life (38–42). It should be noted that steroids can be utilized to control cerebral edema and hypertension (43). Continuously shown, the strongest predictor of outcome is the extent of resection (EOR) of tumour in surgery, more extensive tumour resection is correlative with longer survival (44). Greater than 98% EOR was thought to be required for increased survival but was later estimated to only 78% EOR for significant survival increase (45). More recently shown, the amount of residual volume after surgical resection is a more accurate at determining post-operative prognosis (46,47).

To enhance peri-operative EOR, fluorescent agents have been pursued, specifically the 5-aminolevulinic acid (5-ALA). 5-ALA is a naturally occurring amino acid biosynthesized by animal and plant mitochondria. ALA being a precursor of porphyrin, heme and bile pigments, is metabolized into protoporphyrin IX (PpIX) during heme synthesis, of which PpIX preferentially accumulates in tumour cells. This accumulation of 5-ALA produced PpIX in cancer cells can be identified as red fluorescence following irradiation with violet light (48). This fluorescence guided resection improved EOR and progression-free survival in a randomized controlled studies (49).

Implanting biodegradable carmustine wafers (BCNU) peri-surgical resection has been approved by the FDA for a first line-treatment, however, some adverse events (e.g. brain necrosis) has made their use questionable (50). Further evidence and investigation is required to determine their relevancy.

Bevacizumab additive to TMZ treatments showed no increase in direct overall survival (OS), however, this combinatory therapy appears to increase progression-free survival (PFS) (51,52). Ongoing clinical trials are corroborating this conclusion, increasing PFS but not OS (53–56).

1.4.2 - Recurrent GBM

While no treatment standard is currently stated for recurrent GBM, possible alternatives have been globally attempted. Supportive care, reoperation, re-irradiation, and further combinational therapies have been provided. A review of 28 studies (n=2279) of patients who underwent a second surgical resection, showed a significant increase in median OS(57). However, pursuing a second resection is on a per patient basis, with consideration of quality of life in conjunction with the increase in OS. Re-irradiation of patients GBM has been trialed in a variety of doses and techniques, however, no standard approach has been distinguished (58). A review by Mayer and Sminia, combed through 21 studies on re-irradiation of gliomas, concluding in younger patients' focal re-irradiation may improve outcomes compared to supportive care. Albeit, inter-study comparison was limited by heterogeneity of samples, dose and endpoint settings. It was further described that radiation at 100 Gy, incidence of brain necrosis increases alongside patient quality of life drastically diminishing. With limited increase in OS or PFS, continued irradiation is not a preferred line of treatment for recurrent GBM.

1.4.3 - Complementary treatment

The discovery of multiple chemotherapeutic agents has improved patient outcome in many situations involving varying types of cancer. Temozolomide (TMZ) is an oral alkylating pharmaceutical that is readily bioavailable and can actively bypass the blood brain barrier (BBB) into the cerebrospinal fluid, making it an excellent candidate for GBM (39). Concurrent TMZ (75 mg/m^2/day for 6 weeks) and radiotherapy (60 Gy in 30 fractions), followed by a maintenance regime of 6 cycles of TMZ (150-200 mg/m^2/day for the first 5 days of a 28-day cycle) significantly improved OS shown in the findings of a phase III trial (EORTC 26981)(59) and supplemented by several other trials (60–63). TMZs anti-cancer function depends directly on its ability to alkylate/methylate DNA, particularly O-6 positions of guanine residues. This DNA methylation triggers a cascade leading to cellular apoptosis. In some cases, cancer cells express a protein O^6-alkylguanine DNA alkytransferase, encoded by the O-6-methylguanine-DNA methyltransferase (MGMT), that repairs such methylation and diminishes its treatment efficacy. In newly diagnosed GBM, methylation rate of MGMT promoter has demonstrated to predict response to such alkylating agents, possibly helping choose single modality therapies in the elderly and comorbid populations (64,65). TMZ effects are seen by the accumulation of O6-methylguanine DNA adducts, which are naturally repaired by MGMT, unless otherwise methylated. However, the clinical benefit for identifying MGMT methylation is questionable as patients with unmethylated MGMT promoter lack an effective alternative option (66).

The number of cancer therapies approved by the FDA has substantially increased over the past decade, however, on the contrary only a handful of new treatments have been approved for GBM since 2005 (37,67,68). Tumour-treating fields (TT-fields) with TMZ therapy has been

the first to show potential with limited or no contradictions, and should be considered in patients (69).

1.5 - Holistic thinking (or just the immune system)

Immune surveillance hypothesis first formed in 1959, stated that malignant cells arise consistently, but are rapidly recognized and cleared via the immune system. This hypothesis was later proven in mice in 2001 by Schreiber et al and later corroborated by an abundance of literature in both animal models and human conditions.

The immune system consistently guards the body against cancer, mounting responses against tumour specific characteristics (e.g. tumour associated antigens) clearing any identified malignant cells (70). The level of this immune response is generally a good predictor of cancer patient survival (71,72). Typically, the immune system clears malignant cells before they become threatening and symptomatic. It is when the tumour can evade or outgrow the immune response that malignant cells proliferate and become dangerous to their host. Immunotherapy harnesses the patient's natural ability to clear cancer through the modulation of one or more immune related systems. Check point inhibitors (e.g. anti-PDL-1 antibodies), adoptive T-cells therapy coupled with chimeric antigen receptors, and CD8 T-cell cancer vaccines are all promising cancer immunotherapies (73,74). Viruses have also been recognized to stimulate the immune system, with a bias to replicate in and kill cancer cells (75).

Dynamic, vigorous and safe therapeutics for cancer is an ongoing objective that the scientific community unremittingly strives for. Increased access to molecular and genetic tools and the increase scope of access to our ever-increasing list of knowledge provides a new frontier for science to understand our complex human bodies. The immune system, once thought to be

exclusive to defending from pathogens exogenous to our body, is now confidently looked to as a key cancer regulator. With recent developments in the use of immune checkpoint inhibitors, attention has been brought to the potency of immunotherapeutics in an array of cancers. Antibodies targeting PD-1/PDL-1 and CTLA-4 have laid a path of opportunity for an unlimited amount of combinational therapies that can continue into a clinical setting. Whilst not every treatment will work in complete synergy with such check-point inhibitors, it has brought a much-needed spotlight to the field of immunotherapy.

1.5.1 - Passive versus active immunotherapy

Immunotherapy is treatment that modulates the patient's own immune system to combat disease, such as cancer. Passive and active methods of immunotherapy act through either the direct exploitation of a pre-existing cancer-specific immune response (e.g. adoptive transfer of *ex vivo* stimulated patient immune cells or immune checkpoint inhibitor) or to stimulate a novel immune response to generate *de novo* anti-cancer immune responses (e.g. cancer vaccine)(76), respectively.

1.5.2 - The complicated immune system of the brain

A once thought immune-privileged organ, the brain is now understood to have developed heightened immune regulatory mechanisms to resolve and protect from peripheral stimuli. Immune trafficking into the brain has to be kept under strict control, preventing any auto-immune bystander death in the event of an infection or lesion. In the 1800's Paul Erlich, injected vital dyes into the circulatory system of mice, observing all tissues become stained, except the brain. The brain was then thought to be a distinct immune privileged site, later coining the phrase

blood-brain barrier (BBB) as the boarder protecting it. The BBB has been developed to not only prevent large neurotoxic chemicals from reaching the brain, but also to help regulate cellular signalling and trafficking. Its components consist of endothelial cells, choroid epithelium and the arachnoid layer. Naturally, the BBB was believed to be consistent among all access sites, however, it was later described to have circumventricular organs (CVO) or "leaky" sites (e.g. area postrema; subcommissural organ; pineal gland; neurohypophysis; median eminence; subfornical organ). CVO's carry out a multitude of homeostatic functions, particularly ensuring bidirectional movement of select molecules between the blood and regions of the brain. In addition, septic or chronic inflammatory situations can disrupt the BBB allowing for free inflow into the brain. While the BBB provides a strong line of defence toward unwanted molecules from entering into the brain parenchyma, it does pose challenging when delivering therapeutics for a brain associated disease. Cancer therapies that are effective in peripheral tumours are limited if they are unable to cross the BBB, making immunotherapy a more promising candidate. The BBB is preserved during the initial development of the glioma, up to ~ $2mm^3$. Growth above that and the angiogenetic pressure caused by the GBM, releases the tight and adherent junctions between the endothelial cells; molecules up to 12nm are then able to pass through. The continued growth of GBM furthers this separation, increasing the maximum particle for entry into the brain (77,78). However, the invasiveness of GBM allows certain sections of tumour to remain protected by the BBB, even after surgical resection.

Resident microglia and dendritic cells expressing major histocompatibility complex (MHC) class II are potent immune stimulators, presenting antigen and exiting to cervical and nasal draining lymph nodes. These antigen presenting cells can come into contact with naïve T cells at the lymph node, inducing an adaptive immune response (79). Furthermore, it is well

understood that T cells gain access to the brain (e.g. via VLA-4 CD49d interaction) and are critical for keeping neurotropic viral infections at bay (80).

"If the human brain were so simple that we could understand it, we would be so simple that we couldn't" – Quoted by Emerson W. Pugh in the *The Biological Origin of Human Values*. This quote may now not only explain the complexity the human brain in psychology research fields, but in the neuroimmunology as well. As previously stated, the brain, while not particularly immune-privileged, has a detailed system of regulatory mechanisms to safely protect and provide optimal function. It is well established that macrophage resident or microglial cells represent a substantial part of the mammalian brain immune system (81–85) When not directly faced with a threat, microglia are consistently surveilling the surrounding microenvironment with motile processes and protrusions. In the event of a BBB disruption, these microglia cells can promptly end surveillance and begin foci production, safeguarding the site of injury (86). Comprising of up to 20% of the glial cell population and as numerous as neurons, microglia have significant control within the brain (87,88). In addition, upon activation microglia upregulate MHC class I and II, and co-stimulatory molecules assisting CD4- and CD8-specifc immune responses (89,90). In terms of chronic neoplastic events that continue on to form a tumour, microglia appear to promote tumour growth by facilitating immunosuppression. Microglia appear deficient in proper antigen presentation for cytotoxic and helper T-cell activation (91), and the downregulate proinflammatory signals (82), in addition to secreting tumour proliferation factors (epidermal growth factor (EGF) and vascular endothelial growth factor (VEGF))(92,93). Also expressing PD-1 (94,95) microglia can induce apoptotic cell death in effector T cells. While not the only cell failing to clear GBM, microglia are directly involved in its preservation.

Recently, Pinton *et al.* discovered the immune suppressive microenvironment in GBM is dependent on the presence of bone marrow-derived macrophages within the central locus of the lesion. Myeloid and lymphoid infiltrate of gliomas were examined and contrasted to circulating and resident immune cells. Interestingly, resident microglia showed no immune suppressive phenotypes, with the majority stemming from bone marrow-derived macrophages. The highest percentage of bone marrow derived macrophages appeared in grade IV gliomas (GBM), accumulating from tumour periphery to core (96). A seemingly complicated organ with a coupled complicated immune network, makes treating disease like GBM require an in-depth understanding.

1.6 - T cells: A potential therapeutic target

Thymus lymphocytes, or more cordially known as T cells, play crucial roles in pathogen and tumour surveillance and clearance. Augmenting their safe and specific killing with their ability to help produce conducive microenvironments has been a sought after therapeutic for cancer treatment. T cells are immune cells distinguished by their T cell receptor (TCR), which can recognize short unique amino acid sequences presented on major histocompatibility complexes (MHC), for mice, and human leukocyte antigen (HLA), for human. MHC class I presents a general range of 8-11 amino acid long peptides to varying degrees on all nucleated cells (97). Incidents of up to 15 amino acid long peptides have been reported (98–100), however, MHC class I preferentially binds to 9 amino acid long peptides (97). Conversely, MHC class II bound peptides are not constrained to size and can be 11 to 30 amino acids long, but are generally between 13 to 17 amino acids long (101). These longer peptides bound to MHC class II are solely presented on antigen presenting cells (APC): macrophages, dendritic cells and B-

lymphocytes (102). Traditionally speaking, CD8+ T cells recognize the internally processed peptides (e.g. self or viral antigen) on MHC class I, and CD4+ T cells recognize the exogenously processed peptides (e.g. phagocytosed antigen) on MHC class II. However, cross presentation from exogenous peptides onto MHC class I (103) and endogenous peptides onto MHC class II have been recorded (104–106). Particularly, dendritic cells can present antigen on MHC class I during efferocytosis, targeting for CD8+ T cell activation (107).

All peptide presentation analyzed within this thesis will be in the context of mouse MHC, specifically C57Blk6 H-2Db and H-2Kb class I alleles.

Transformed from the lymphoid lineage of multipotent progenitors in the bone marrow, T cells complete maturation in the thymus. Maturation involves positive and negative selection (central tolerance) by MHC and self-antigen recognition. This process ensures T cells can recognize self MHC but not become activated when faced with self-antigen. Being presented on all nucleated cells, MHC class I serves as a mechanism of immune communication to surveilling immune cells. In the event a cell infected with a foreign pathogen (i.e. not present during initial immune maturation), or has incurred mutations leading to the presence of a novel antigen (neoantigen), their protein is processed into peptides that bind to MHC and are presented to surveilling T cells (108). As aforementioned, recognition of these peptides by CD8+ cytotoxic T-cells, which in the context of MHC is known as an epitope, occurs frequently to keep cancer at bay. The cancer mutanome is responsible for producing mutated peptides that can binding MHC class I, creating a target known as neoepitopes. Neoepitopes are a preferred target when compared to over expressed self-protein or foreign based antigens. Targeting the mutanome for cancer treatment is a promising up and coming field of research that will have a large impact on the way we approach treating on a per patient basis (109).

1.7 - Immunotherapies for GBM

Dynamic, potent and safe therapeutics for cancer is an ongoing objective scientists assiduously strive for. Recent developments in the use of immune checkpoint inhibitors, have brought attention to the potency of immunotherapeutics for cancer.

1.7.1 - Checkpoint inhibitors

After establishing an entirely new principle for cancer therapy, Dr. Allison and Dr. Honjo, received the 2018 Nobel Prize of Physiology or Medicine for their research in immune checkpoint blockade. Immune checkpoint inhibitors augment the inherent immune response against cancer by blocking the inhibitory signals T cells often receive in tumour microenvironments, dramatically improving survival of many aggressive tumours (110,111).

The immunosuppressive GBM microenvironment prevents entry and maintenance of endogenous immune responses. Manipulating this immunosuppressive environment logically warrants trial and investigation. Immune checkpoint inhibitors anti-CTLA-4 (Ipilimumab), -PD-1 (Nivolumab) and -PDL-1 (Avelumab) in combination with a variety of other innovative therapies are currently being tested in Canada and worldwide, in ongoing GBM clinical trials.

Ipilimumab, a humanized antibody targeting CTLA-4, which was the first immunoregulatory molecule to be targeted for a therapy, was approved by the FDA and EMA in 2011 for melanoma (112). CTLA-4 is expressed on both effector and regulatory T cells to interact with CD80 and CD86 on APCs to inhibit costimulation (113). The expression of CTLA-4 on CD4+ and CD8+ T-cells in GBM is inversely correlated with outcome, making its inhibition a promising treatment candidate (114).

PD-1 on T-cells, and its ligand PD-L1 on APCs and tumours cells, are major immunosuppressive molecules targeted today. Their direct interaction simultaneously obliterates T cell cytotoxic activity and interferes with the production of inflammatory cytokines, substantially reducing the inherent anti-tumour response (115,116). Licenced in 2014 and 2016, Nivolumab and Pembrolizumab are two antibodies that target and block PD-1. Later being licenced in 2016 and 2017, Atexolizumab and Avelumab were manufactured to block PD-L1. Expression of PD-L1 on gliomas and PD-1 on infiltrating T cells is well documented, however, their functional and clinical significance remains unclear. Particularly in two cohort studies of GBM, there was no correlation between PD-L1 expression and OS (23,117). In contrast, another study found a correlative decrease in survival with PD-1/PD-L1 expression in the TME (118). A level of heterogeneity within these cohorts, along with undefined cut offs and no standardized experimental parameters may explain the conflicting findings. Nonetheless, PD-L1 expression in linked to negative immune prognostic factors in GBM, with multiple clinical trials testing efficacy of its blockade.

Additional immune checkpoint molecules to target for inhibition may include IDO and Tim-3. IDO, while not a classical immune checkpoint molecule having no receptorial capacity, suppresses properties of T-cell activation (119). On the other hand, Tim-3 is expressed by CD4+ and CD8+ T cells, and is involved with inducing T-cell exhaustion and promoting tumour escape (120). Tumour infiltrating lymphocytes in GBM are not capable of cytokine secretion, along with inability to exert their regular physiological function. Tim-3 overexpression is thought to contribute to this cellular phenotype and is associated with higher cancer malignancy (121,122).

A double-edged antibody

Immune checkpoint inhibitors may not be the complete silver bullet science wished it were. PD-L1/PD-1 and CTLA-4 expression is a normal physiologic feedback function that prevents autoimmune scenarios and maintains immunologic homeostasis. Capable of affecting all organs, the adverse side effects of checkpoint inhibitors tend to involve the gastrointestinal tract, endocrine glands, skin, and liver (123). The general normal function of these immune checkpoint molecules is described with mouse knock-out models; CTLA-4 gene KO mice die from lymphoproliferation; PD-1 gene KO mice have more variable responses, with model-dependent autoimmunity (e.g. arthritis and cardiomyopathy). Similarly, patients treated with checkpoint blockade therapy can exhibit immune adverse events. Currently, adverse events to anti-CTLA-4 treatment are generally more severe than anti-PD-1. Colitis and hypophysitis tend to be reported more with anti-CTLA-4 therapy, while pneumonitis and thyroiditis appear more common with anti-PD-1 therapy. The potent therapeutic effect observed with checkpoint inhibitor therapy can come at a cost, however, they often still have a better safety profile when compared to chemotherapy (124,125).

1.7.2 - Chimeric antigen receptor T cell immunotherapy

Chimeric antigen receptor (CAR) T cell therapy has produced unparalleled clinical results in hematologic malignancies, however, progress in solid tumours remains elusive. CAR T-cells harness the potency and accurateness of a cytotoxic T-cell, while utilizing the selectivity of immunoglobulins. The CAR can recognize a specific protein on a cell surface activate the bound T cell to secrete cytokines, undergo cytolytic degranulation and proliferation, rapidly clearing its target (126). Multiple clinical trials targeting EGFRvIII are currently, and have been,

pursued for GBM. EGFRvII is the most common variant of EGFR in human tumours and arises from an in-frame deletion of exons. The amino acid alteration resulting from the in-frame shift, generates a tumour-specific epitope within the extracellular domain of EGFR, making it a target for both vaccine and CAR T cell therapy. Patients who received EGFRvIII-CAR T cells experienced no improvement in outcome (127). Interestingly, their tumour explants showed decreased or completed loss of EGFR expression, when expression is normally stable with GBM progression (128). Additional studies have targeted human epidermal growth factor receptor (HER2), a tyrosine kinase over expressed in GBM, with virus-specific CAR T-cells to enhance the expansion and subsequent tumour recognition (129,130). Having the natural TCR recognize a particular tumour associated antigen (TAA), in addition to the CAR against HER2, could help fight the heterogeneity of GBM. A recent study of 17 patients tested HER2 CAR T cells, specific to adenovirus, Epstein-Barr virus, or cytomegalovirus, being peripherally administered. HER2 CAR T cells were detected in serum for all patients, with 1 showing partial response lasting for 9 weeks, and 7 patients having stable disease for 8 weeks to 29 months (131). The feasibility and safety this study demonstrated will assist in future experiments optimizing CAR T cell therapy and discovering novel therapeutics.

1.7.3 - Vaccines technologies against cancer – GBM

Vaccines are publicly known for their prophylactic ability to protect against specific pathogens. When targeting cancer, vaccines must be considered to act as a treatment rather than preventative measure. In doing so, cancer vaccines must modulate the immune system in a different way. Most often, producing new or targeting pre-existing T cell repertoires that can recognize TAA. Traditionally, research was dedicated to finding a conserved set of TAA across

all patients, however, the shear mass of HLA heterogeneity makes it difficult to vaccine against a conserved set of peptides, as epitopes change drastically between people.

Vaccines targeting over expressed self-antigens have to face inherent tolerance, which abolishes self-reactive T cells, or they can induce autoimmunity. Other promising targets, aim to vaccinate against foreign peptides, including pathogen-based peptides (e.g. from a viral infection) or peptides derived from the cancer mutanome. In some cases, viral infections can be the cause of neoplastic activity or chronic viral infections preferentially replicate in neoplastic cells. In these cases, vaccinating against the virus is also vaccinating against the neoplastic cells. Not every situation will promise the replication of a foreign pathogen, thus, targeting the mutanome unveils the most promising, but difficult avenue, for future cancer vaccines.

Epidermal growth factor receptor variant III (EGFRvIII) targeted vaccine

EGFR is a key regulator for cellular differentiation, migration and apoptosis (132). As previously mentioned, EGFRvIII arises from an in-frame deletion mutation that permits further receptor activation contributing to cellular malignancy, but also produces a targetable immunogenic epitope.

A synthetic EGFRvIII peptide vaccine was tested in phase I and phase II trials for newly diagnosed GBM. There were modestly improved outcomes observed with PFS between 12.3 and 15.3 months, and OS at 24 months. Current standards of care produced median PFS at ~8 months and median OS of 16-19 months. Therapies targeting EGFRvIII have demonstrated its safety and validity to date. Targeting this single antigen has shown again to selectively delete the EGFRvIII population and produce recurrent resistant tumours (133). It is promising that therapies have the

potential to eliminate complete populations from GBM, however, heterogeneity of cancer remains a colossal challenge for researchers.

Tumour lysate-pulsed DC vaccine

To begin targeting tumour heterogeneity at per patient level, a tumour lysate-pulsed DC vaccine was built to combat GBM. The specificity of this vaccine stems from pulsing DCs with patient derived tumour surface protein associated with MHC, that was isolated *ex vivo*. Tumour lysate provides a broad antigen pool that is patient-specific and is available to all GBM patients with a resectable tumour.

An inaugural study published by Liau *et al.*, investigated the safety and feasibility of a tumour lysate-pulsed DC vaccine in a phase 3 clinical trial (n=331) (NCT00045968)(134). After surgery and chemoradiotherapy, patients would receive temozolomide with DCVax-L or placebo, following recurrence all patients could receive DCVax-L. Of the intent-to-treat patients 90% received the DCVax-L, optaining a median OS 23.1 months. Methylated MGMT patients (n=131) median OS was 34.7 months. Interestingly, a sub-population of patients (n=100) had a median OS of 40.5 months, requiring further investigation.

Current tumour-lysate pulsed DC vaccines face challenges before their full potential can be reached. Surgery, in combination with the lengthy vaccine production process, increases duration to begin treatment, likely reduces median OS (135). Additionally, when attempting to achieve a therapeutic level of immune response against tumour antigens, autoimmunity to self-protein becomes a possibility (136,137). Tumour-lysate pulsed DC vaccines are also not protected from tumour-induced immune suppression and microenvironment niches. Further

investigation into such personalized vaccines will provide a avenue for promising cancer therapies.

1.8 - Oncolytic viruses therapy

Anecdotal evidence of farmers cancer being reduced or cured after a cowpox viral infection and other case reports from 1950's to 1980's of varicella-induced remission of acute lymphoblastic leukemia (138) and measles-induced remissions of leukemia's (139), Burkitt's lymphomas (140) and Hodgkins Lymphoma (141), initiated the research field of oncolytic viruses (OV). An OV is a replication competent virus that preferentially infects and replicates in cancer cells leading to the further replication, tumour lysis, and dispersion within the tumour. In addition to cell death, oncolytic virus therapy (OVT) clinical trials discovered an *in situ* vaccination effect after treating patients. Viral replication and tumour lysis promote release and presentation of TAA to infiltrating and draining immune systems. Consequently, research delved into the immune modulatory effects of OV's (142–146).

OVT has pushed through boundaries that many cancers therapies had previously faced and has become a major interest for all fields of cancer research. OVT particularly attracted interest in treating GBM, as the poor prognosis has been long unchanged. GBM is generally located within the brain, with limited cases of metastases, and is surrounded by non-replicating cells making it a promising candidate for OVT. As with all GBM treatment OVT still faces the requirement of strict inflammatory control within a such delicate organ, the brain.

The era of producing clinical viable OV's began in the 1990's and has since published over 400 articles on glioma oncolytic virotherapy, producing at least 8 clinical trial candidates tested in over 20 clinical trials.

Herpes simplex virus (HSV) is the most extensively studied GBM OV, with its research beginning in 1991 when Martuza *et al.* created the very first genetically engineered OV, HSV-dIsptk (147). This thymidine kinase deficient HSV showed potent tumour-killing efficacy in murine models of GBM, prompting the further creation of a multitude of HSV mutants: HSV-1716, R3616, hR3, M032, G207, and G47Δ. Such mutant strains provide better safety profiles with higher potency and are being tested in varying stages of clinical trials: NCT00028158, NCT02062827, NCT02031965, NCT00157703; making HSV the most studies OV for GBM (148).

Following HSV, adenovirus is another extensively studied virus for its oncolytic potential against GBM. Initial investagtions of a tumour-selective replication mutant of adenovirus (ONYX-015) were tested in phase 1 clinical trials, but achieved low patient median survival (149). Other more promising adenovirus subtypes, such as Delta42-RGF virus, are being pursued for pre-clinical and clinical trials (NCT01582516, NCT00805376) (150).

Attenuated strains of virus, such as poliovirus, measles virus and vaccinia virus have demonstrated potent oncolytic activity against tumours of varying origins (151). A poliovirus mutant (PVS-RIPO), replacing its IRES with human rhinovirus type 2, lacking neurotoxicity progressed to phase 1 trials for GBM (NCT01491893). The Edmonston vaccine strain of measles virus is being tested in an ongoing phase 1 clinical trial against GBM for its strong oncolytic potential (NCT00390299). Research into vaccinia virus has developed recombinant strains that show promising oncolytic potential. For example, a strain of vaccinia virus that is genetically engineered to express GM-CSF (JX-594) has prolonged survival in animal glioma models, currently being tested on hepatocellular carcinoma and other solid tumours NCT00554372, NCT00429312, NCT00625456, NCT02630368 (151).

Other viruses from non-human pathogenic backgrounds have also been recognized for their oncolytic abilities in human tumour cells. Newcastle disease virus, vesicular stomatitis virus, myxoma virus, parovirus, reovirus and Sindbis virus are a few important to note. Variations of these viruses have and are being tested in preclinical and clinical trials for GBM and various other cancers (150,151).

OVs are inherently a multi-functional based therapy. With their high tolerable doses and absence of associated death or severe side effects makes, make OVs a remarkable candidate for cancer therapeutics. However, their therapeutic efficacy depends on a delicate balance of virus-mediated tumour lysis, virus-induced host anti-tumour immune response and anti-viral host immune responses. As historically shown, cancer is immensely good at forming resistance to treatment, therefore, utilizing OVT alongside other potent immunotherapeutics, warrants further investigation.

1.8.2 - Oncolytic rhabdovirus – Farmington

The Stojdl Lab has developed of a novel OV platform for brain cancer therapy that is non-neurotoxic and exhibits potent anti-tumour efficacy. This novel platform is based on native Farmington virus (FMT), a rhabdovirus identified from dozens of isolates worldwide for its potent oncolytic properties. FMT was especially efficacious in tumours originating in the central nervous system when tested on a panel of 60 human cancer cell lines (152). FMT cannot replicate productively in healthy mammalian cells with intact interferon signalling pathways, as FMT cannot block type I IFN production. Furthermore, FMT narrows its tropism through an IFN-independent tumour selectivity mechanism targeting only replicating cells, which may explain its unique lack of neurotoxicity when injected into the brains of susceptible mice. FMT is

efficacious in multiple *in vivo* models of glioblastoma multiforme, generating robust cures in U87 and BTIC human xenograft models. Notably, syngeneic cancer models cured with FMT reject subsequent tumour implantation, elucidating a critical role of anti-tumour CD8+ T cell populations in tumour treatment. In comparison to other viruses, FMT is inherently safe and can be easily rescued with desired transgenes encoded into its genome. Encoding FMT with immunogenic transgenes has also been successful when vaccinating for tumour specific CD8+ T cells. Data shows FMT can infiltrate into mouse gliomas following IV injection, and to achieve optimal vaccination, FMT can to be administered, in part or whole, by IV injection after an initial prime vaccination. Allowing the possibility for both engineering, tumour-selectivity and safety of both IC and IV routes of administration, FMT merits further investigation into GBM applications.

1.9 - A prime-boost rhabdovirus vaccination

Oncolytic viral immunotherapy can involve the introduction of tumour associated antigens (TAA) into the viral vectors genome to induce a specific adaptive immune response. The selection of a safe and effective tumour antigen to vaccinate against is challenging. As Pol et al demonstrated, vaccination using Maraba virus encoded with human dopachrome tautomerase (hDCT), which is overexpressed in melanoma models, in mice showed efficacy when the mice were primed beforehand with an adenovirus also encoded with hDCT. The side effect of breaking natural immune tolerance was autoimmune toxicity. The cured mice from this experiment developed vitiligo, induced by autoimmune T cells (153). The safer antigen choice would be derived from the expressed mutanome, mutations found in the cancer genome. The proteins expressed from the mutanome appear as entirely foreign to the immune system,

avoiding any related autoimmune toxicity. These foreign proteins would be processed into neoantigens and placed on MHC to be recognized by T cell receptors as a neoepitope. Establishing the ability to vaccinate against multiple neoepitopes will combat the antigen loss variants seen with many single targeted vaccinations. With advances in Next Generation Sequencing, targeting the mutanome in a clinical setting is now possible.

1.9.1 - Finding a target

CD8+ T cells are key drivers of naturally occurring and therapeutic anti-cancer immune responses. As discussed before, the abundance of tumour-infiltrating CD8+ T cells positively correlates with a favorable prognosis (154). Augmenting a tumour specific antigen response shows incredible promise and safety at both pre-clinical and clinical stages, however, discovering a on-target tumour specific antigen currently bottlenecks the available therapeutics (155–157). Survivn, a self-antigen, or human cytomegalovirus proteins have been conserved targets for vaccination against GBM. However, relying on a few antigens to be present across a whole cohort of patients remains a concern today. Elucidating CD8+ epitopes specific to cancer on a per patient basis could provide the ammunition required for current cancer vaccine strategies.

Extensive work has been dedicated to discovering targetable tumour specific antigens for cancer vaccine therapies. The traditional method relies on a reverse immunology method, which performs exome sequencing on tumour cells to identify mutations, and then MHC-binding prediction software (e.g. ANN, SMM, NetMHCpan) is used to identify the potential actionable neoepitopes, with possible mRNA sequencing to identify expression (155,158). Albeit this method provides an abundance of potential neoepitopes, greater than 90% are considered false-

positives (159,160). The common *in silico* algorithms are typically used to predict MHC binding, but often lack peptide processing events that leads up to MHC binding, assuming part contribution to the high false positive rates. Updates in some *in silico* prediction methods have improved their predictions in proteasomal cleavage sites, but there is still much work to be done (159). To combat this, some researchers use mass spectrometry to provide a more rigorous definition of the tumour specific peptides, however, only a handful of neoepitopes are ever identified (159,161,162). Laumont *et el* produced a publication in December 2018, discussing a strategy to elucidate detection of more neoantigens by leveraging the non-coding regions of the genome for antigen prediction (157). Enhancing *in silico* neoepitope prediction algorithms and the increasing availability of Next Generation Sequencing will enable a new form of personalized medicine.

Concluding remarks

In light of advancements in the ability to rapidly characterize tumour phenotypes via Next Generation Sequencing, the opportunity has come to provide patients with personalized vaccines to ameliorate and offer durability to cancer therapeutics. One such treatment is to insert a targeted neoantigen cassette into the Farmington genome and administer in a heterologous prime-boost approach to treat glioblastoma multiforme. Farmington's unique neuro-safe ability to replicate in brain tumours and its ability to create robust anti-tumour immune responses can work in co-operation to combat the aggressive and invasive phenotypes glioblastoma multiforme presents.

We hypothesize that using publicly available MHC prediction algorithms we will be able to predict actionable neoepitopes that will produce efficacious CD8+ T cell responses when used

with an FMT-encoded heterologous prime-boost vaccination procedure in tumour-bearing mice. For reasons of proof-of-concept and accuracy of algorithms, MHC class I, H-2Kb and H-2Db ,of the C57Blk6 mouse strain were a chosen focus for our studies. This thesis will primarily discuss experiments surrounding the mouse glioblastoma model GL261. Our first objective was to validate and evaluate the potential of encoding a neoantigen transgene into FMT. A previously well-described neopeptide from mutant Imp3 (previously cited as mutant GARC-1) would be used in a heterologous synthetic peptide-prime FMT-encoded boost approach (163,164). Alongside these experiments, our next objective was to obtain a list of potential neoepitopes from exome and mRNA Next Generation Sequencing of GL261 cells, utilizing a Stojdl Lab neoepitope prediction pipeline and validating with *in vivo* vaccination experiments. After identifying novel GL261 neoepitopes, our final objective would test the therapeutic efficacy and observe the involved immune responses of a multi-neoepitope based vaccine strategy.

2 - MATERIALS AND METHODS

Cell culture

Cell concentrations were calculated using a hemocytometer (Corning™) under a 10X magnification.

Vero, HEK293T and GL261 cell lines were maintained in 1 X Dublecco's Modified Eagle's Medium (DMEM), HyClone™ Thermo Scientific supplemented with 10% fetal bovine serum (FBS), Sigma-Aldrich® at 37°C and 5% CO_2.

Vero cells were maintained in 15 cm tissue culture plates (Corning™) with 25 mL of 10% FBS 1 X DMEM (Corning™) and passaged at 85% confluency, unless otherwise stated. When passing Vero cells media was aspirated with vacuum and washed with pre-heated (37°C) 10 mL of phosphate buffered saline (PBS). PBS was aspirated with vacuum and 3 mL of pre-heated (37°C) 0.25% trypsin was added to the plates for a 5-minute incubation at 37°C for complete dissociation. Dissociated cells were quenched with pre-heated (37°C) 22 mL of 10% FBS 1 X DMEM, and pipetted up and down until single cell suspension was obtained, checking with a 4x microscope. Appropriate volumes were aliquoted and diluted with pre-heated 10% FBS 1 X DMEM.

GL261 cell lines were maintained in T75cm^2 flasks (Corning™) with 25 mL of 10% 1 X DMEM and passaged at ~80% confluency. When passing GL261 cells media was aspirated with vacuum and cells were washed with 10 mL of pre-heated (37°C) Dulbecco's Phosphate Buffered Saline (dPBS) solution (HyClone™). dPBS was aspirated off with vacuum and 3mL of room temperature (RT) 1 X Versene (Gibco™) was added for a 10-minute incubation at 37°C. Cells were then quenched with pre-heated (37°C) 22 mL of 10% FBS 1 X DMEM and pipetted up and down until single cell suspension was obtained. Appropriate aliquoting and dilution of cells were

done using pre-heated (37ºC) 10% FBS 1 X DMEM, and live/dead cell count staining done via 1:1 dilution with 0.4% Trypan Blue (Gibco™).

RMA-S cells were maintained in 1 X RPMI 1640 media (HyClone™) supplemented with 10% FBS (Sigma-Aldrich). RMA-S cells were cultured in T75cm^2 (Corning™) flasks. When suitable for passage, cells were centrifuged at 1500RPM at room temperature for 5 minutes in a 50 mL Falcon tube. Supernatant was aspirated and cells were resuspended to a single cell suspension by pipetting and cells were diluted to appropriate concentrations with a pre-heated (37ºC) 10 % FBS 1 X RPMI 1640 media.

Murine peripheral blood mononuclear cells were maintained in DC media: Hyclone™ RPMI 1640 media supplemented with 10% FBS (Sigma-Aldrich), 1% non-essential amino acids, 1% penicillin-streptomycin (Hyclone™), 1% HEPES (Gibco™) and 55nM beta-mercaptoethanol (Sigma-Aldrich).

Mice and cell lines

C57BL/6 mice (8-10 weeks old) were purchased from Charles River Laboratories (ON, CA). All animal procedures and housing were completed following strict rules and regulations of the University of Ottawa Animal Care and Veterinary Services (ACVS).

Vero cells (P15+) (ATCC®, CCL-81TM) were used to amplify and titre viruses. GL261 (P29-31) mouse astrocytoma cells were obtained from ATCC and used for intracranial mouse models of GBM. RMA-S cells (P2) (ATCC®, CVCL-2180) were generously donated from the Auer Lab and used for a peptide-MHC binding assay. HEK293T cells were donated from the Children's Hospital of Eastern Ontario's Research Institute, in addition to the Cowan Lab and were used for transduction of viral genomes.

Farmington Virus

Chimeric virus production

Chimeric virus transgenes were ordered from GenScript®. Transgenes were codon optimized via OptimumGene™ (GenScript®) for mus musculus (mouse). Each novel transgene was DNA synthesized and purified in pUC57 plasmid, flanked by NotI (GCGGCCGC) and BsiWI (CGTACG) restrictions sites. Digestion of 1.5µg of pUC57 transgene and Farmington genome plasmid with 20 units of NotI and BsiWi restriction enzymes (New England BioLabs®) in NEBuffer™3.1 for 1 hour was completed to obtain two sticky ends. Transgene plasmid digest was run on a 0.8% agarose TAE gel with GelRed™ (Biotium®), and extracted following QIAquick gel extraction kit (Qiagen®). Ligation, using a T4 DNA ligase (New England BioLabs®), of the transgene extraction and digested Farmington genome plasmid was completed in a 10µL reaction following T7 ligation kit (New England BioLabs®).

The ligation solution was transformed into TOP10 *E. coli* cells by pipetting 10µL's of ligation into 100µL's of competent TOP10 *E. coli* cells. Cells were gently mixed with the pipette tip and incubated on ice for 30 minutes. Following incubation, cells were heat shocked in a 42°C water bath for 42 seconds and then on ice for 2 minutes. 900µL of preheated (37°C) SOC was then added and cells were incubated at 37°C for 1 hour. Cell were centrifuged at 13000rpm for 2 minutes at RT in 1.5mL Eppendorf tubes. 900µL of supernatant was aspirated with vacuum and the remaining 100µL was used to resuspend the cells with a pipette. Cell solution was then spread on to 1% Bacto™ agar LB plates supplemented with Kanamycin (Sigma-Aldrich®), inverted and incubated at 37°C overnight. 4 to 12 colonies were picked the following day and placed into 15 mL white capped Falcon tubes with 3mL of LB supplemented with Kanamycin

(Sigma-Aldrich®) in a shaking incubator at 37°C overnight. QIAprep spin miniprep kit (Qiagen®) was used to isolate plasmids. Positive transformation clones were identified with a NotI and BsiWi (New England BioLabs®) digest run on a 0.8% agarose TAE gel with GelRed™ (Biotium®). 10µL of the positive clone solution was transferred into 300mL of LB supplemented with Kanamycin and placed in a shaking incubator at 37°C overnight. GenElute ™ HP plasmid maxiprep kit was then used to extract newly ligated plasmid DNA.

Chimeric Farmington genome plasmid was combined with helper Farmington N,P and L helper plasmids in an opti-mem solution, and incubated with PEI for 15 minutes at room temperature. Following incubation, 200uL of solution was added to confluent HEK293T cells pre-seeded in 6-well (Corning®) plates and incubated at 37°C with 5% CO_2 overnight. The following day media was changed, and cells were incubated for another 72 hours. Following incubation 100µL of cellular supernatant was transferred onto pre-seeded 6-well confluent Vero cells. Cytopathic effect was used to indicate a positive rescue after a 48-hour incubation. Media stocks of positive rescues were frozen at -80°C.

Virus amplification and purification

Farmington virus rescues were grown in either 15 cm tissue culture plates or 10-stack CellSTACK® cell culture chambers on Vero cells with 1X DMEM + 10% FBS. Multiplicity of infection (MOI) of 0.01 was used at an infection duration of 40 hours for all chimeric Farmington viruses. Briefly, virus was incubated with Vero cells at 37°C for 40 hours before media was collected and centrifuged in 500mL Beckman® bottles at 1500 rpm to remove whole cell lysate. Supernatant was removed and 0.2µm filtered with bottle top filter apparatus (Millipore, ON, CA;SCGPU05RE). Filtered virus media was pelleted in sterile 500mL

Beckman® bottles by centrifugation at 10,000 rpm for 2 hours at 4°C. Virus pellet was resuspended in 2 mL of Solution C and incubated overnight at 4°C. The following day the 2 mL virus pellet was centrifuged at 900 rpm for 5 minutes to remove any large aggerates. The remaining supernatant was purified by OptiPrep™ (Sigma-Aldrich®) density gradient centrifugation. A gradient of 15% to 35% was prepared using a BioComp Gradient Master™. Virus solution was pipetted onto the SWI gradient filled tubes and centrifuged at 300,000 rpm for 1.5 hours at 4°C. Virus band was extracted and aliquoted for titration and *in vivo* experiments, stored at -80°C.

Virus titre

Virus concentrations were determined by a traditional plaque assay. In brief, virus stocks were serial diluted using a 96-well Assay Block (Corning®) by pipetting 100µL of the previous wells solution into following well containing 900µL of cold 1X DMEM, pipette mixing 7 times before discarding the tip and proceeding to the following well. Once desired dilutions were achieved, 100µL of each dilution was pipetted directly onto 6-well plates (Corning®) of Vero cells containing no media. 200 µL of pre-heated (37°C) 1X DMEM + 10% FBS was additionally added to all wells. 6-well plates were rocked every 15 minutes for 1 hour before an 0.5% agarose 1X DMEM + 10% FBS was layer was drip pipetted on top. Plaques were fixed with Methanol: Acetic Acid (3:1) and stained with 0.04% CV after 72 hours, allowing for visual counting of plaques.

Sanger Sequencing

Virus RNA was extracted from infected Vero cells media stocks using QIAmp viral RNA extraction kit (Qiagen®). RNA sequences were amplified by RT-PCR into 4 sections of virus genome. Each PCR was agarose gel purified and extracted with QIAquick gel extraction kit (Qiagen®). Purified cDNA was sent with appropriate primers to Genome Quebec (Montreal, QC) for sanger sequencing. Chromatograms were analyzed using Geneious© software. All virus and transgene specific primers were designed from the Stojdl Lab Farmington reference genome and purchased from IDT® (Cambridge, ON).

Next Generation Sequencing

Cellular DNA was extracted from GL261 cells with a Blood and Cell Culture DNA Mini Kit (Qiagen®). RNA was also extracted using RNeasy RNA isolation kit (Qiagen®). DNA and RNA were sent to Genomic Quebec for Exome and mRNA Next Generation Sequencing on an Illumina HiSeq4000. The bioanalysis of quality, mRNA isolation, and library preparation were all completed at Genome Quebec following their standardized operating procedures.

***In silico* neoepitope prediction pipeline**

Exome and mRNA sequencing data were analyzed by the Stojdl Lab bioinformatician, Philippe Charron. In brief, exomes files were converted to fastq from bam, and quality filtered with Trimmomatic. Filtered reads were mapped to GRCm38 mouse genome with BWA-MEM and filtered for quality of reads with Picard Tools. Following, mapped reads were analyzed for variants with three, predetermined for sensitivity and specificity, publicly available variant callers (Platypus, Haplotype Caller, and Freebayes). Variants called from at least two of the

variant callers were then filtered for missense and frameshift mutations, where a list of novel amino acids are produced.

mRNA files were also converted to fasq from bam files and quality filtered using Trimmomatic. Reads were then mapped to GRCm38 mouse genome with STAR aligner. Fragments per kilobase million were updated with Cufflinks, and matching mutations were applied to the variants called from exome data.

Potential neoepitopes were then tested against MHC binding and processing algorithms (NetMHCpan, NetCTL, IEDB-ANN, IEDB-SMM). All candidates predicted were inputted into an interactive table using R Shiny®. From this list of MHC ranked neoepitopes could be identified and validated.

RMA-S peptide binding assay

RMA-S cells were grown in suspension until desired concentrations were obtained. Cells were then incubated at 26°C and 5% CO_2 overnight to increase MHC class I surface expression. Cells were aliquoted and pulsed with a serial dilution of peptide for 1 hour at 37°C. Following incubation, cells were then stained for MHC class I markers with fluorescent antibodies and cells were fixed and permeabilized with Cytofix/Cytoperm (BD Biosciences). Mean fluorescence was measure and analyzed with flow cytometry.

Liposome production

Materials

Lipids 1,2-dioleoyl-sn-glycero-3-ethylphosphocholine (EDOPC), 1,2-dioleoyl-sn-glycero-3-phosphoethanolamine (DOPE), N1-[2-((1S)-1-[(3-aminopropyl) amino]-4-[di(3-

amino-propyl)amino]butylcarboxamido)ethyl]-3,4-di[oleyloxy]-benzamide (MVL5), 1,2-distearoyl-sn-glycero-3-phosphoethanolamine-N-[methoxy(polyethylene glycol)-2000] (DSPE-PEG), and α-Galactosyl Ceramide (α-GalCer or KRN700) were purchased from Avanti® Polar Lipids Inc.

Preparation and characterization of liposomes

All lipids were dissolved in chloroform and used to prepare thin lipid films by rotary evaporation in a Rotavapor (Buchi) under 200mbar vacuum. Peptides dissolved in chloroform:methanol solution (4:1) were added pre-lipid film production, those dissolved in ddH_2O were added when resuspending the lipid film. The lipid film produced was either composed of either Gen1: EDOPC:DOPE:DSPE-PEG (49:49:2)or Gen2 MVL5:DOPE:DSPE-PEG (16:82:2), as stated. Each formulation included 0.5μg of α-GalCer.

Hydrodynamic size and zeta potential of the peptide-loaded liposomes were measured with a Zetasizer Nano ZS dynamic light scattering instrument (Malvern).

Manufacturing mRNA

DNA plasmids, ordered from GenScript®, containing a chain of neoepitopes connected by AAY sites, were digested and ligated into a starting vector contain SP- and MITD-domains (SP, MRVTAPRTLILLLSGALALTETWAGS; MITD, IVGIVAGLAVLAVVVIGAVVATVMCR RKSSGGKGGSYSQAASSDSAQGSDVSLTA), to enhance MHC-peptide presentation (155). The starting vector also contained a 5' and 3' sequence from beta 2 microglobulin (B2M-ENSG00000166710) with a 120bp polyA tail, to enhance expression and stability of mRNA (165). Plasmid DNA was linearized at the end of the

polyA tail using a class II restriction enzyme, BbsI (New England BioLabs®). *In vitro* transcription of DNA plasmid was completed following mMESSAGE mMACHINE kit T7 transcription kit (Invitrogen™). mRNA was analyzed on a 1% agarose/formaldehyde gel contain GelRed™ (Biotium).

In vivo mouse vaccinations

Unless otherwise stated, Farmington virus was injected intravenously (via tail vein) with a dose of $3x10^8$ pfu (plaque forming units) in 100μLs. Virus was given 9 days post-prime vaccination, either on Day 9 for non-tumour bearing mice, or on Day 12 for tumour bearing mice, unless otherwise stated.

Liposome encapsulated peptide based prime vaccines were administered intravenously (via tail vein) with a lipid dose of 0.05 mM plus either 10 μg or 60 μg of peptide. Liposome prime vaccinations were given on Day 0, for non-tumour bearing mice, or Day 3 for tumour bearing mice.

Synthetic peptides with adjuvant were administered as an intraperitoneal prime vaccination. 50μg of synthetic peptides resuspended in DMSO were mixed with 50 μg of anti-CD40 antibody (Clone FGK4.5, BioXcell) and 100μg of Poly(I:C), and diluted to 200 μL with dPBS.

Checkpoint inhibitor anti-PD-1 (programmed death-1) (Clone J43 BioXCell) was administered IP in 6 injections 3 days apart, starting day 6 after tumour implantation, at 200μg/mouse (mice averaged 20 grams in weight).

Peripheral blood mononuclear cell isolation

Blood was taken from mice by puncturing the saphenous vein with a 25G needle tip. Approximately 100 uL of blood was collected into heparinized blood collection tubes (Microvette® CB 300 LH, Sarstedt) and briefly agitated. Blood was transferred into 5mL Falcon® round-bottom polystyrene tubes. 2mL of ACK Lysis buffer was added and mixed by flicking prior 5-minute incubation. Following lysis 2mL of dPBS (HyClone®) was added and tubes were centrifuged for 5-minutes at 1500 rpm. ACK Lysis was complete once more before resuspending to desired amounts for intracellular staining with DC media.

Peptides

All peptides used were synthesized from Biomer Technologies (San Francisco, CA) with no N- or C-terminal modifications and at a purity of >90%, delivered in lyophilized form. Peptides used for *in vitro* PBMC stimulation were resuspended in DMSO at a concentration of 10 mg/mL. Peptides prepared for liposomal encapsulation were resuspended in either water or a solution of chloroform:methanol (4:1) at 10 mg/mL.

Antibodies

Fluorochrome conjugated monoclonal antibodies used in PBMC flow cytometry assays include: CD8-Alexa488 Clone 53-6.7, IFN*y*-Alexa Flour 647 Clone XMG-1.2, TNF*a*-PE-Cy7 Clone MP6-XT22, and IL-3-PE Clone JES6-5H4. RMA-S peptide binding assay used antibodies: H-2Kb-PE-AF6-88.5 PE and H-2Db-FITC-KH95. All flow cytometry antibodies were purchased from BD Biosciences (Missisauga, ON) and BioLegend (Burlington, ON).

Detection of antigen-specific T cell response

Antigen-specificity of CD8+ T cells were measured by their response to stimulation of synthetic peptides. For CD8+ T cell stimulation, isolated PBMCs were incubated in DC media with 50μg of desired peptide for 5 hours at 37°C, Golgiplug™ (BD Biosciences) added after 1 hour. After 5 hours, cells were centrifuged at 5 minutes at 1500 rpm in 4°C. Subsequent T-cell surface staining was completed with fluorescent-conjugated antibodies on ice. Cells were fixed and permeabilized with Cytofix/Cytoperm (BD Biosciences) and stained for intracellular markers of activation.

Flow cytometer

All flow cytometry experiments were followed out using a BD LSRFortessa X-20 at the Children's Hospital of Eastern Ontario Research Institute II. All cells were run in FACS buffer; 0.05% Bovine Serum Albumin (Sigma-Aldrich®) in azide-free dPBS (HyClone®). While running samples, FCS data was analyzed using FACSDiva software (BD Biosciences). Later analysis and data configuration of FCS files was completed with FlowJo Mac software (Treestar, Ashland, OR).

Intracranial mouse tumour model

For mouse intracranial injection of GL261 GBM model, GL261 cells were harvested in T75 flasks at 80% confluency. Cells were dissociated with Versene, and washed 2x with dPBS. Cells were counted and a final concentration of 5000, 10000, or 20000 cells/2μL was made in serum-free, 1% HEPES buffered 1X DMEM. Cells were kept on ice for a maximum of 3 hours before discarding and preparing fresh cells. Mice were anesthetized using isofluorane gas and

prepared by subcutaneous injection of 1mL of 0.9% sodium chloride solution and 30 μL of buprenorphine (0.03mg/mL). Hair was shaved, tear gel added over eyes, and incision site was cleaned with chlorahexidine solution. Mice were then transferred and secured in a stereotaxic apparatus. An incision down the centre of the mouse's head was made with a scalpel to expose the skull. The injection site was marked with a surgical pen, 0.5mm forward and 2.5mm to the right of bregma. A 25G needed was rotated to provide a small hole in the skull. Using a Hamilton® syringe, cells were loaded, and the needle tip was lowered 4mm past the punctured hole. After 30 seconds the needle tip was raised by 0.5mm, and cells were injected at 1μL/minute using the stereotaxic pump. 30 seconds after the injection finished, the needle was slowly removed, and the mouse incision site was amended with VetBond™ tissue adhesive. Topical 2% bupivacaine hydrochloride was applied to the incision directly and 4-6 hours after surgery. Mice recovered for a minimum of 10 minutes in a 29°C incubator. 4-6 hours after surgery mice received a second dose of buprenorphine.

DNA and RNA concentration analysis

All DNA and RNA concentration were estimated with a Nanodrop1000 spectrophotometer (Thermo Fisher), using the 260/280 and 260/230 ratio for a level of purity.

Statistical analysis

Statistical analyses were completed using Graphpad Prism 7.0 software (GraphPad Software, Inc., CA, USA), including: student's t-test, one-way AVOVA with Tukey's test. Mean and standard deviation (SD) or standard error of the mean (SEM) were shown. Significance is shown with p-values as *=$p<0.05$, **=$p<0.01$, ***=$p<0.001$ and ****=$p<0.0001$.

3 - RESULTS

3.0 - Engineering a virus to express tangible neoepitopes

As previously described in Maraba and VSV (153,166), rhabdoviruses possess the ability to replicate, while expressing a desired transgene. Particularly, the Stojdl Lab has produced an efficient pipeline to produce chimeric FMT viruses. Briefly, the chimeric FMT engineering pipeline, described in Fig. 1, begins at transgene design. Transgenes are gene synthesized, digested, and ligated into a plasmid containing the entire FMT genome. All viruses produced within this thesis, have the transgene located following the viral N-protein. Transgenes can also be inserted following viral G-protein, however, results show maximal protein expression following viral N protein (data not shown), with no observed inhibition to the virus life cycle. Chimeric plasmids, along with helper plasmids containing viral N, P, and L proteins, can be transfected into susceptible cell lines using PEI. Vaccinia T7 or ribozyme promoting systems are used, obtaining a ~70-100% virus rescue. To isolate a single virus population, plaques were picked across three consecutive plaque assays. Viral RNA was taken from media stocks and sanger sequenced to confirm absence of mutations and presence of transgene. Chimeric virus media stocks at ~$5x10^8$ pfu/mL require amplification and purification for *in vivo* experiments. Viruses are amplified in cell stack chambers or plates, pelleted, and gradient purified. Aliquots are then kept in -80°C for further dilution and use. Similar to other rhabdoviruses, FMT is sensitive to freeze-thaw cycles, losing ~50% pfu each cycle. All aliquots used within this thesis underwent one cycle of freeze-thawing.

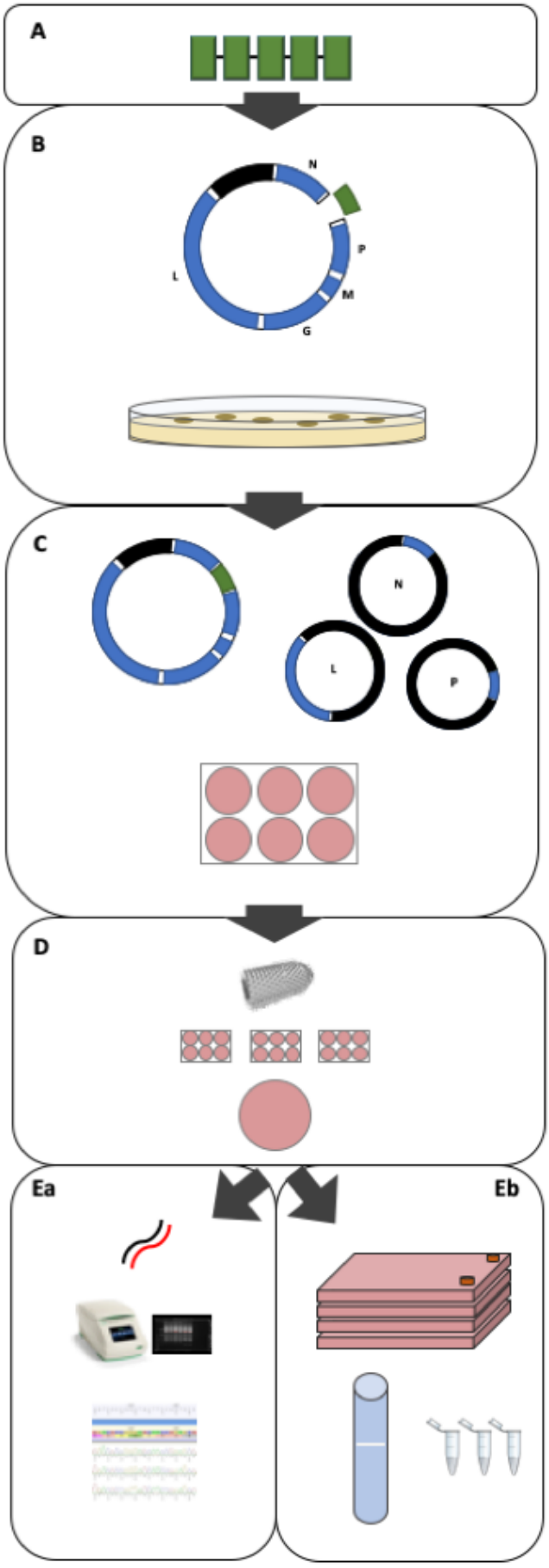

Figure 1: Chimeric Farmington engineering and production pipeline for *in vivo* virus testing. (A) Neoepitope, 'beads on a string', gene insert design and plasmid gene synthesis. (B) Digestion and ligation of designed insert into linearized Farmington plasmid following viral N protein. Transformation, cloning and chimeric plasmid amplification in TOP10 competent cells. (C) Chimeric, helper -N, -P, and -L plasmid transfection in HEK293T cells. Positive virus rescue identified on Vero cells by visual CPE. (D) Triple plaque purification to isolate for a single lineage of chimeric virus. Media stock amplification of isolated chimeric virus. (Ea) Viral mRNA isolation with carrier RNA. RTPCR of virus mRNA and Sanger sequencing to identify mutations when analyzed against original FMT genome. (Eb) Large scale amplification of chimeric virus product. Gradient purification of virus pellet, and subsequent aliquoting and storage at -80°C.

3.1 - Validating a vaccination strategy against neoepitopes by targeting verified mImp3 neoepitope

To demonstrate the applicability of the heterologous prime-boost vaccination approach using a rhabdovirus-boost, previously described by Pol et al. 2014, (153) to neoepitope-based vaccines we decided to target a previously described neoantigen, mImp3 (previously cited as GARC1). The aspartic acid to asparagine non-synonymous mutation can produce 54 potential neoepitopes as 8-,9-, or 10-amino acid long peptides between H-2Kb and H-2Db alleles. Upon analysis (supplementary table 1), we discovered the 10-amino acid version, AALLNKLYAM, produced the lowest MHC IC50 score on NetMHCpan algorithm at 35.7nM. The 9-amino acid peptide, AALLNKLYA, also produced low scores, beating the 10-amino acid form in the SMM algorithm analysis. Both forms were chosen for further investigation. To corroborate the presence of mImp3 in the GL261 GBM mouse cell line, sanger sequencing was done on PCR amplified products with primers flanking the mutation (Fig. 2).

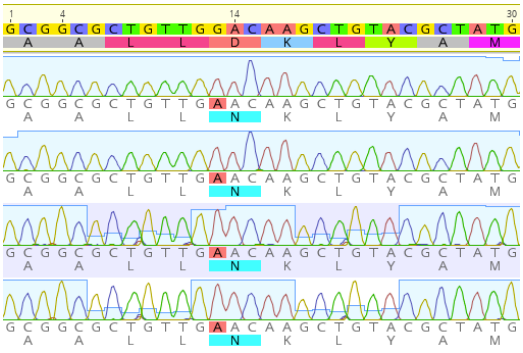

Figure 2: Non-synonymous mutation: aspartic acid (GAC) to asparagine (AAC), of the published mutant Imp3 (GARC1) exists in the GL261 cell line used. Sanger sequencing of forward and reverse primers flanking the known mutation was completed for the GL261 cell line to confirm the existence of the single nucleotide polymorphism.

3.1.2 - Vaccination method with peptide-prime FMT-boost targeting the mImp3 neoepitope

To establish vaccination capability of FMT as a boost, in a prime-boost approach, the 10-amino acid version, AALLNKLYAM, was inserted into the FMT genome. The insert consisted of the peptide sequence repeated five times, spaced by AAY proteasome sites, flanked by in-line restriction enzyme sites; labeled as FMT-mImp3 (Fig.3,4,5,6,7,12). The prime, based on peptide vaccination method by Yadav and colleagues, consisted of 50 μg of synthetic peptides mixed with an adjuvant containing 50μg of anti-CD40 antibodies and 100μg of Poly (I:C) (167) (Fig.3,4,5,6,7).

3.1.3 - *In vivo* prime-boost vaccination targeting the mImp3 neoepitope

All immune response kinetics of CD8+ T cells specific to target neoepitopes, herein, were followed by blood PBMC isolation and stimulation, using synthetic target peptides and staining for IFNg, TNFa, and IL-2 as markers of activation. Immune responses are displayed in frequency of IFNg+ CD8+ cells of total CD8+ T cell populations. In the case of mImp3 vaccination, PBMCs were split and stimulated with either the 10- or 9-amino acid version of mImp3. Initial trials using only the 10-amino acid version of mImp3, AALLNKLYAM, produced sub-optimal results (data not shown), leading to experiments comparing the 10-amino acid versus the 9-amino acid version of mImp3 (Fig. 3). No observable immune response was detected after a single peptide-prime. Five days following the boost, mice who received the 9-amino acid version of mImp3 as a prime and the FMT-mImp3 boost, produced significantly higher immune responses (5.904 ±1.255) than the 10-amino acid version prime FMT-mImp3 boost (0.951±0.375), or FMT-mImp3 alone (0.531 ±0.131) (Fig. 3). Immune responses within the blood were observed to contract over another 7-34 days, losing significant to only FMT-

mImp3 vaccinated groups. Upon stimulation *in vitro* of CD8+ T cells from PBMCs there was no difference in IFNg+ cells between using the 10- or 9- amino acid versions of mImp3.

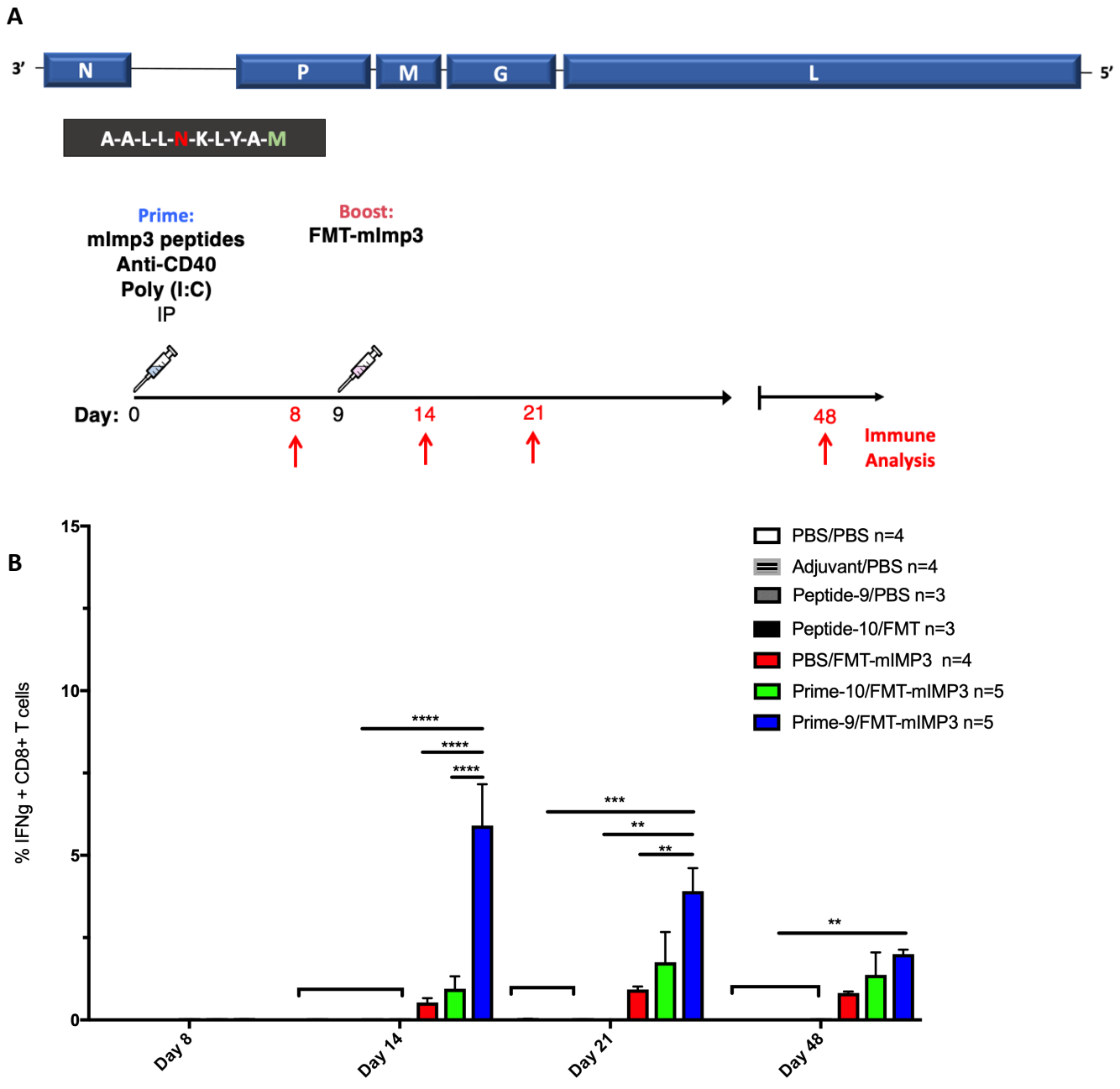

Figure 3: The 9-amino acid long version of mImp3 synthetic peptide provides a stable prime for FMT encoded with mImp3 to boost. (A) 50 µg of synthetic peptides (AALLNKLYAM or AALLNKLYA) were injected on Day 0 with 50 µg of anti-CD40 antibodies and 100 µg Poly (I:C) via IP route. On Day 9, $3x10^8$pfu of FMT-mImp3, that encoded 5 repeats of the 10-amino acid long mImp3 neoepitope linked by AAY proteasome site, was administered to mice through IV injection. (B) Blood was taken for PBMC immune analysis of mImp3 specific CD8+ T cells by stimulated IFNg stain-positive cells, on Day 8, 14, 21, and 48. Data is plotted as mean ±SEM, with asterisks representing significance: *p<0.05, **p<0.01, ***p<0.001, **** p<0.0001.

Considering the mouse survival timeline in the GL261 GBM mouse model is ~23 days, the 9 day duration between prime and boost was used within this thesis. Figure 4 leveraged the ability to wait in a naïve mouse vaccination model and waited 15 days between prime and boost. As shown in Fig. 4, the 9-amino acid version of mImp3 is again required to produce significantly higher immune responses. The increase in time between prime and boost improved vaccine responses, achieving mImp3 IFNg+ CD8+ frequencies of 10.891 (±2.154) five days following boost. Additionally, 9-amino acid prime vaccinated mice did not lose significance to 10-amino acid prime with FMT-mImp3 boost after 34 days (Fig. 4) (Fig. 5). When measuring the kinetics of polyfunctionality of immune responses between all responding vaccination groups, the IFNg+ cells contract, with the remaining populations testing positive for both IFNg and TNFa (Fig. 5).

Based upon vaccination results against mImp3 being positive, their application to the GL261 tumour model was tested (Fig. 6, Fig. 7). Survival was determined based upon ACVS designated end-point symptoms and graphed in Kaplan-Meirer curves. Mice were IC injected with $2x10^4$ (Fig.6) or $1x10^4$ GL261 cells (Fig. 7). No immune responses were observed prior to FMT-mImp3 boost vaccination. mImp3 specific immune responses were observed following FMT-mImp3 boost, achieving frequencies of 5.373±2.206 (Fig.6) and 6.212±1.544 (Fig. 7). However, vaccination did not increase mouse survival rates.

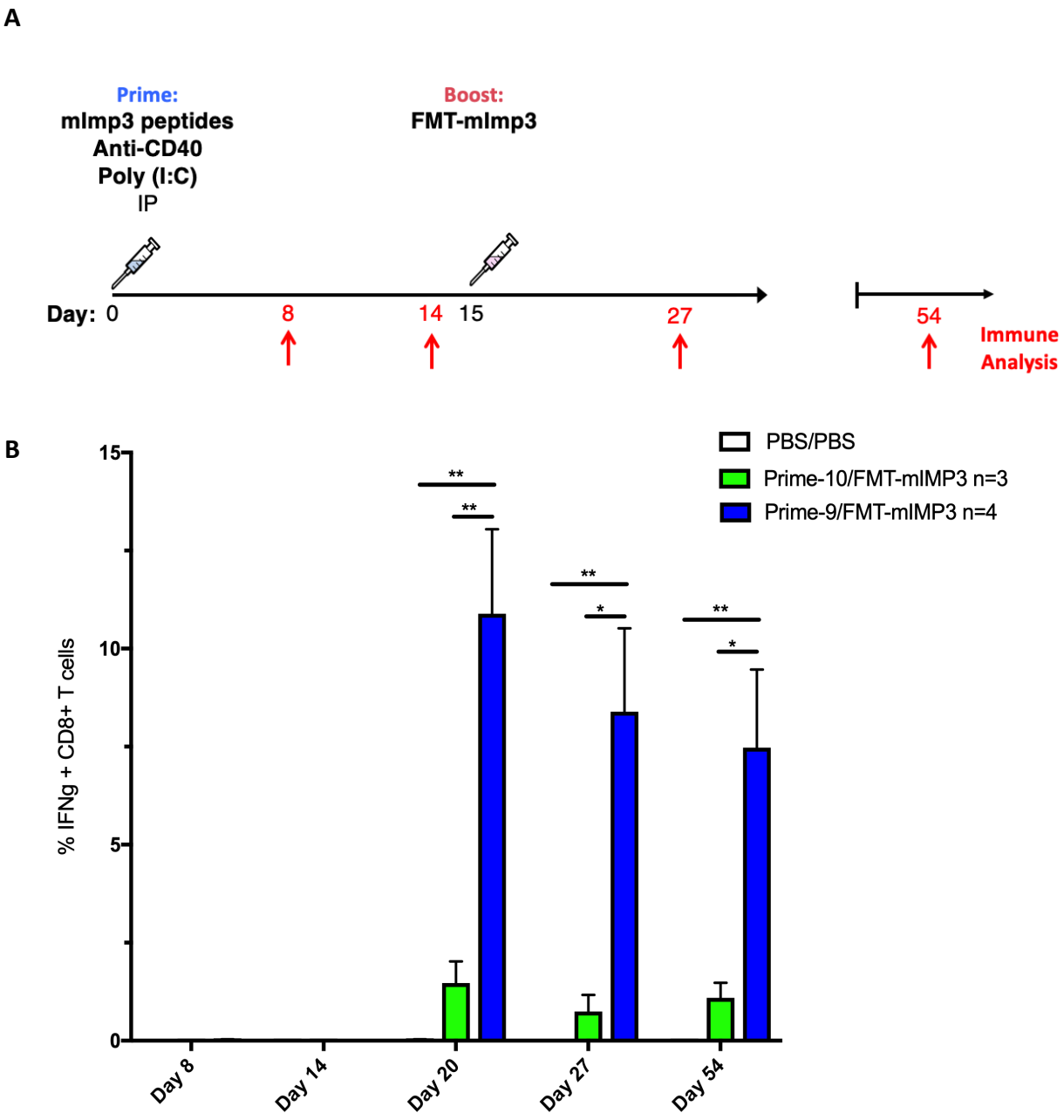

Figure 4: Increasing duration between prime and boost to 15 days increases immune response to mImp3 in only mice primed with the 9-amino acid mImp3 peptide. (A) 50 µg of synthetic peptides (AALLNKLYAM or AALLNKLYA) were injected IP on Day 0 with 50µg of anti-CD40 antibodies and 100 µg Poly (I:C). 15 days following mice were IV injected with $3x10^8$pfu of FMT-mImp3, that encoded 5 repeats of the 10-amino acid long mImp3 neoepitope linked by AAY proteasome site. (B) Blood was collected and analyzed by flow cytometry on Days 8, 14, 20, 27 and 54, for mImp3 specific CD8+ T cells staining for IFNg in peptide stimulated lymphocytes. Data is plotted as mean ±SEM, with asterisks representing significance: *p<0.05, **p<0.01, ***p<0.001, **** p<0.0001.

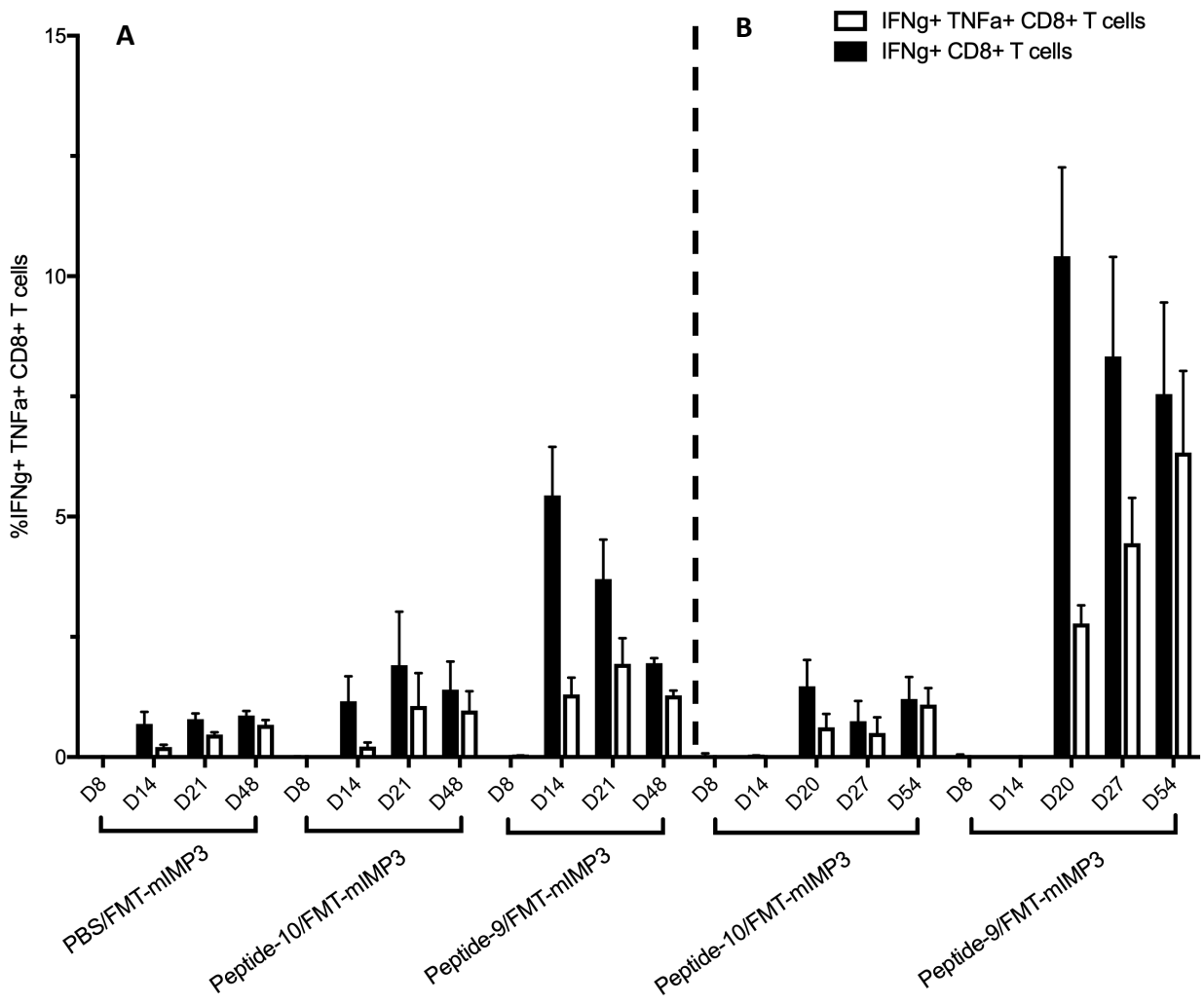

Figure 5: Independent of the amount of mImp3 specific immune response recorded by vaccination technique, overtime, the remaining specific CD8+ T cells population is polyfunctional, expressing both IFNg and TNFa. The following is a consolidation of two different experiments run in parallel. Mice were prime vaccinated with synthetic peptides (AALLNKLYAM or AALLNKLYA) mixed with 50µg of anti-CD40 antibodies and 100µg of Poly(I:C) by IP route. Mice were either followed up with an FMT-mImp3 boost vaccination (A) 9 days after, or (B) 15 days after. Blood samples were collected 1 day prior to prime vaccination, and 5,12, and 40 days after boost vaccination. Blood PBMCs were stained for IFNg and TNFa markers of activation.

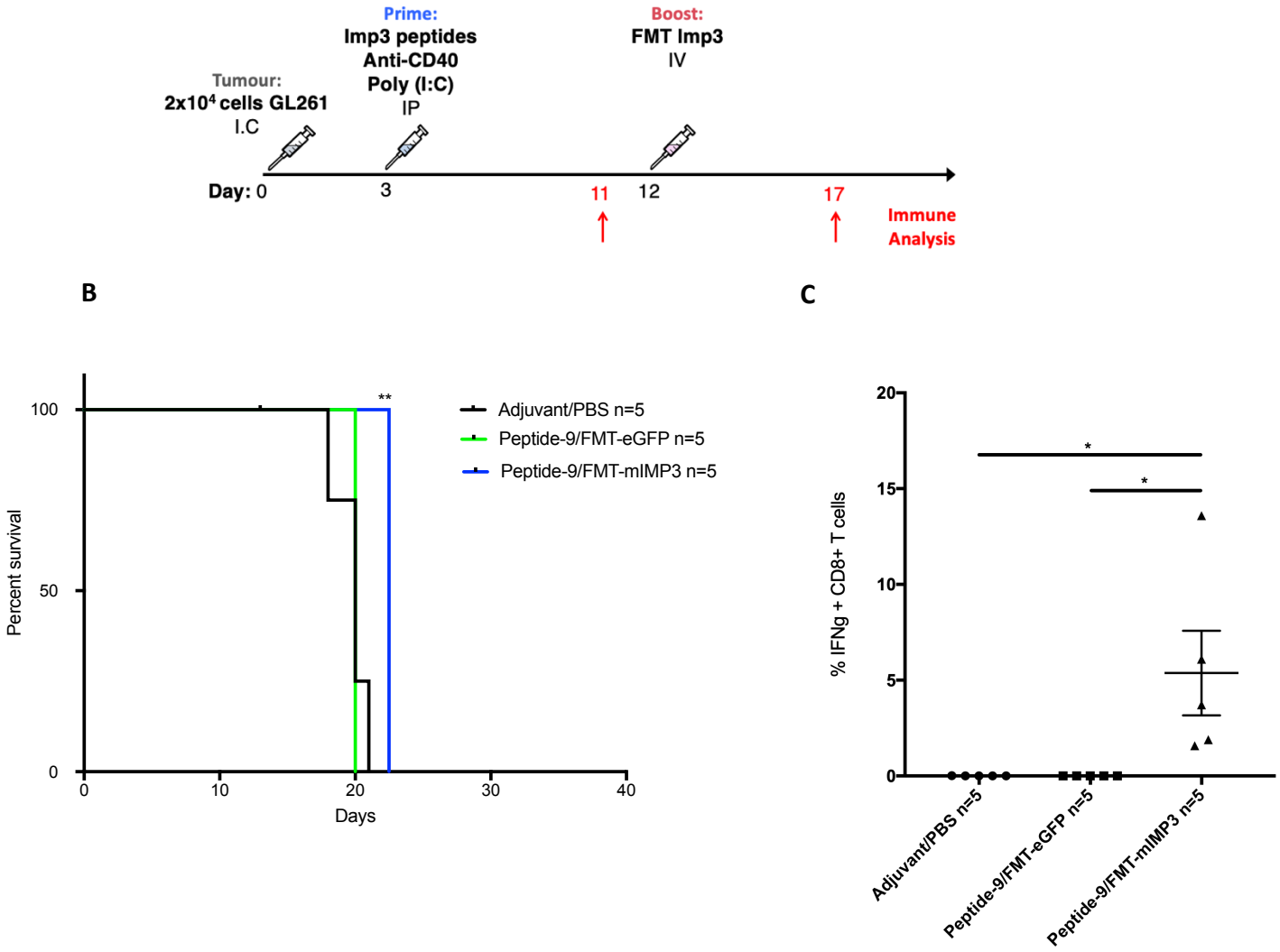

Figure 6: mImp3 immunity induced by peptide-prime FMT-mImp3 boost does not increase survival in mice implanted by IC injection of GL261 mouse GBM cells. (A) Mice underwent stereotaxic IC implantation of $2x10^4$ GL261 cells on Day 0. Day 3 mice were primed with synthetic mImp3 peptides (AALLNKLYA) mixed with 50µg of anti-CD40 antibodies and 100 µg Poly (I:C) via IP administration. On Day 12, mice were immunized with FMT-mImp3 or FMT-eGFP by IV injection. (C) Blood was collected on Day 11 and 17 (pre- and post-FMT boost) and analyzed by flow cytometry for mImp3 CD8+ specific T cells, Day 17 results are shown. Data is plotted as mean IFNg positive cell frequency of CD8+ T cell populations with ±SEM, with asterisks representing significance: *p<0.05, **p<0.01, ***p<0.001, **** p<0.0001. (B) Survival was determined by designated end-point symptoms.

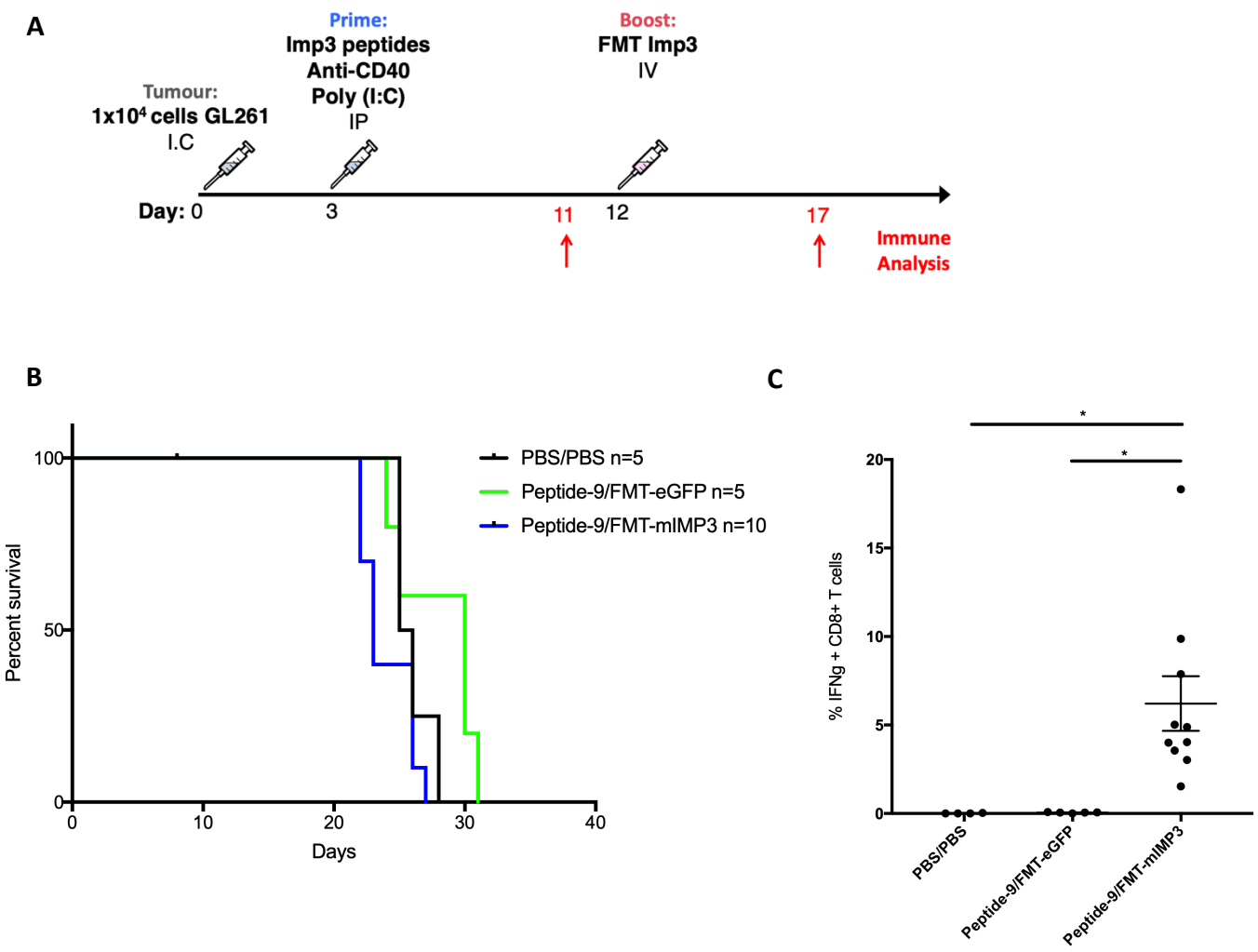

Figure 7: Decreasing tumour burden does not increase survival of mice vaccinated with a peptide-prime FMT-mImp3 boost approach. (A) On Day 0 mice underwent surgical implantation of 1x10^4 GL261 cells via IC injection. Day 3 mice were primed with synthetic mImp3 peptides (AALLNKLYA) mixed with 50µg of anti-CD40 antibodies and 100 µg Poly (I:C) via IP administration. On Day 12, mice were immunized with FMT-mImp3 or FMT-eGFP by IV injection. (C) Blood was collected on Day 11 and 17 (pre- and post-FMT boost) and analyzed by flow cytometry for mImp3 CD8+ specific T cells, Day 17 results are shown. Data is plotted as mean IFNg positive cell frequency of CD8+ T cell populations ±SEM, with asterisks representing significance: *p<0.05, **p<0.01, ***p<0.001, **** p<0.0001. Survival was pre-determined by designated end point symptoms.

3.2 - Producing an efficient neoepitope prediction pipeline

Understanding the limitations of single target vaccinations, we planned to discover a list of novel immunogenic neoepitopes to, ultimately, build a dynamic multi-epitope vaccination. Genomic DNA and RNA was extracted from a GL261 homogenous cell line (passage 28). Exome sequencing of extracted DNA obtained a raw total read count of 101,606,251, with an average coverage of 157 reads. mRNA sequencing of RNA had a depth of 53,303,150 reads. These sequence data were inputted into the Stojdl Lab neoepitope prediction pipeline created by Philippe Charron (Fig.8b). Briefly, the exome sequencing was quality filtered and mapped to the mouse genome. Mapped reads were then analyzed for variants by three predetermined variant callers. Variants called between, at minimum, two variant callers were considered for further investigation; 52,951 variants were called with 39,315 being shared. Missense and frameshift mutations were then isolated, producing 5,930 possible target mutations. Lastly, mRNA was used to determine possible expression, further filtering to 2,223 mutation targets.

Novel 8-,9-, and 10-amino acid long peptides flanking the mutation were analyzed for MHC binding potential by *in silico* binding algorithms. Following NetMHCpan, 15 of the top scored MHC binding peptides for H-2Db and H-2Kb alleles were chosen for further investigation (Fig. 8a).

A

GENE	MUTATION	PEPTIDE	NetMHC IC50
Tmem2	K.1042.N	VMLENGYTI	11.41
Rtn2	L.405.F	GAIFNGFTL	17.42
Imp3	D.81.N	AALLNKLYAM	37.19
Fut10	R.175.M	FSMHSHLPL	91.4
Tm9sf3-Db	V.231.L	FSIFNSFMML	95.45
Slc36a1	I.298.V	MAIVTVLYI	102.97
Extl1	E.540.D	TGMTNDFSM	104.09
Slc7a1	R.59.L	VALENAGPAI	104.09
Slc2a12	Q.214.K	KAIAMYFL	130.69
Qars	E.168.D	KMIKNDVDM	177
Clint1	N.446.S	FSLMSTSTV	208.24
Fbxo34	V.21.M	SALSSWSASM	222.23
Ifi47	S.16.N;G.11.S	SASENNFQQL	234.6
Ube4b	Q.817.L	MFMTNPSVL	279.01
Gal3st1	D.304.Y	ATAWNLLYV	294.54

GENE	MUTATION	PEPTIDE	NetMHC IC50
Lrrk1	T.1768.S	VMYHSASYQL	36.39
Sfxn2	R.111.M	FMLQFYMTM	38.83
Myo9a	R.440.L	ISYKKKTYL	43.28
Rad51d	R.54.M	LSYKALVALM	47.71
Myh14	G.135.V	LIYTYSVLF	52.6
Mrps18b	Q.28.L	SSYVAQVPLL	53.17
Hlcs	Q.487.P	LMFEMPPEM	54.93
Col4a3bp	R.158.L	SSFKKGHSLL	57.98
Zfp106	K.1567.M	RVYNLVSRM	69.71
Mb21d1	H.422.Y	CSYYVKTAIF	69.71
Pcyox1	L.454.F	ILHDRFYYL	71.24
Wipi1	A.35.S	SGYKLFSL	73.59
Hhat	T.181.A	LYYASFSLEL	74.39
Tm9sf3-Kb	V.231.L	SIFNSFMMLI	74.39
Snx6	S.250.F	IGFSLYAL	76.85

B

NAME	PEPTIDE
INDEL #1	VSTAWNPM
INDEL #2	VSVRSQRL
INDEL #3	FVFELEARL
INDEL #4	VWPWFIPSL
INDEL #5	AMRARWSLV
INDEL #6	VAHFSAFV

Figure 8: Stojdl neoepitope prediction pipeline, using GL261 sequencing results, produces potential vaccination neoepitope candidates efficiently. Next-generation sequencing was completed on the homogenous GL261 cell line. (B) Sequencing results were input into the Stojdl Lab mouse neoepitope prediction pipeline, created by Philippe Charron. 2,223 expressed mutations were predicted as feasible targets. (A) The top 15 strongest MHC binding neoepitopes from SNPs, predicted by MHC IC50 affinity scores (nM) generated by NetMHCpan 2.3, were chosen for further analysis. From the available INDELs the top 6 neoepitopes were also chosen based on their MHC IC50 *in silico* score generated by NetMHCpan 2.3.

3.3 - Screening for immunogenic neoepitopes

To further validate the predicted peptides for immunogenicity, a prime-boost vaccination method was implemented to confirm immunogenicity *in vivo*. To produce the boost vaccination, FMT was encoded with sets of 10 predicted neoepitopes (Fig. 9). The FMT inserts were designed based upon the top 30 neoepitopes predicted by NetMHCpan, ordered down from best IC50 score, alternating between alleles (e.g. top 5 neoepitopes of H-2Db and top 5 neoepitopes of H-2Kb for the first virus). The prime, consisted of one targeted neoepitope peptide (10μg) encapsulated in a liposome nanoparticle (Gen1 lipo-peptide).

The model to analyze the immunogenicity is consistent with previous prime-boost experiments; mice (n=3) receive one injection of prime with a virus boost 9 days after, measuring blood immune responses 1 day pre- and 5 days post-boost (Fig 10a). Figure 10b is a combination of five experiments, with grouped PBS and PMA/Ionomycin controls. (*) are immune responses from an experiment where mice (n=5) were vaccinated with a pooled 10 peptide liposome prime with all mouse blood pooled for stimulation. Immune responses 1-day pre-boost are shown in red, and 5-days following boost are represented in black. Immunogenicity of peptides were determined by frequency of immune response induced by prime-boost vaccination. Six predicted neoepitopes were identified to have clear IFNg+ CD8+ T cells populations above background following boost immunization: mutant(m)- Rtn2 (0.79), **Imp3**(23.81), Myh14 (0.95), Slc7a1 (24.06 ±5.359), Ube4b (4.222 ± 1.331), and Tm9sf3-Kb (14.563 ± 6.829). Only mice vaccinated with mutant Tm9sf3-Kb peptides were observed to have a peripheral immune response (0.867 ± 0.133) following just prime vaccination. Consolidated immunes responses of positive responders are shown in Fig. 11. Varying frequency of polyfunctional T-cells (IFNg+ and TNFa+), following virus boost, of each immunogenic peptide

was observed (Fig. 11b): Rtn2 (30.12), Imp3 (26.91), Myh14 (49.26), Slc7a1 (15.073 ± 2.468), Ube4b (61.938 ± 2.912), Tm9sf3-Kb (67.497 ± 3.584). Dot plots of flow cytometry results of the best mouse responders in each group is shown in Fig.11c,11d.

	GENE	MUTATION
1	Tmem2	K.1042.N
2	Lrrk1	T.1768.S
3	Rtn2	L.405.F
4	Sfxn2	R.111.M
5	Imp3	D.81.N
6	Myo9a	R.440.L
7	Fut10	R.175.M
8	Rad51d	R.54.M
9	Tm9sf3-Db	V.231.L
10	Myh14	G.135.V
11	Slc36a1	I.298.V
12	Mrps18b	Q.28.L
13	Extl1	E.540.D
14	Hlcs	Q.487.P
15	Slc7a1	R.59.L
16	Col4a3bp	R.158.L
17	Slc2a12	Q.214.K
18	Zfp106	K.1567.M
19	Qars	E.168.D
20	Mb21d1	H.422.Y
21	Clint1	N.446.S
22	Pcyox1	L.454.F
23	Fbxo34	V.21.M
24	Wipi1	A.35.S
25	Ifi47	S.16.N;G.11.S
26	Hhat	T.181.A
27	Ube4b	Q.817.L
28	Tm9sf3-Kb	V.231.L
29	Gal3st1	D.304.Y
30	Snx6	S.250.F

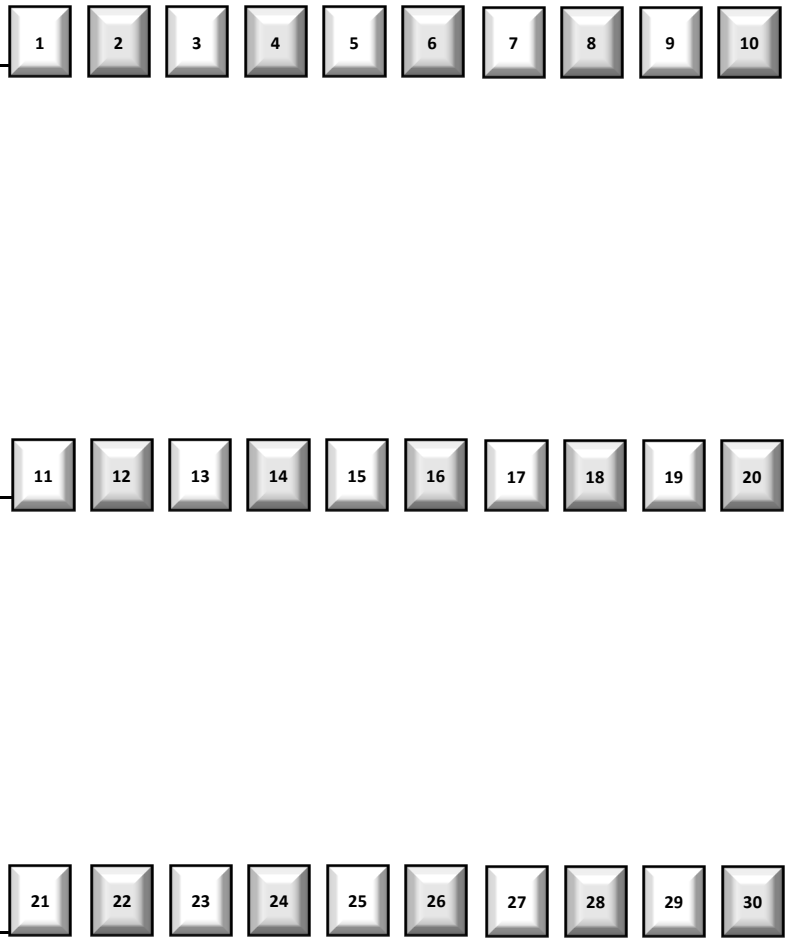

Figure 9: Chimeric Farmington engineering production pipeline produces viruses encoded with predicted neoepitopes in a designed insert following viral N protein. Transgenes were designed using the predicted neoepitopes from GL261 sequencing. Neoepitopes were ordered from lowest IC50 score to highest, with alternating MHC alleles. Three transgenes were created containing 10 neoepitopes each, spaced by AAY proteasome sites, repeated once, and inserted into the viral genome following N protein, using inherit upstream promoting sequences.

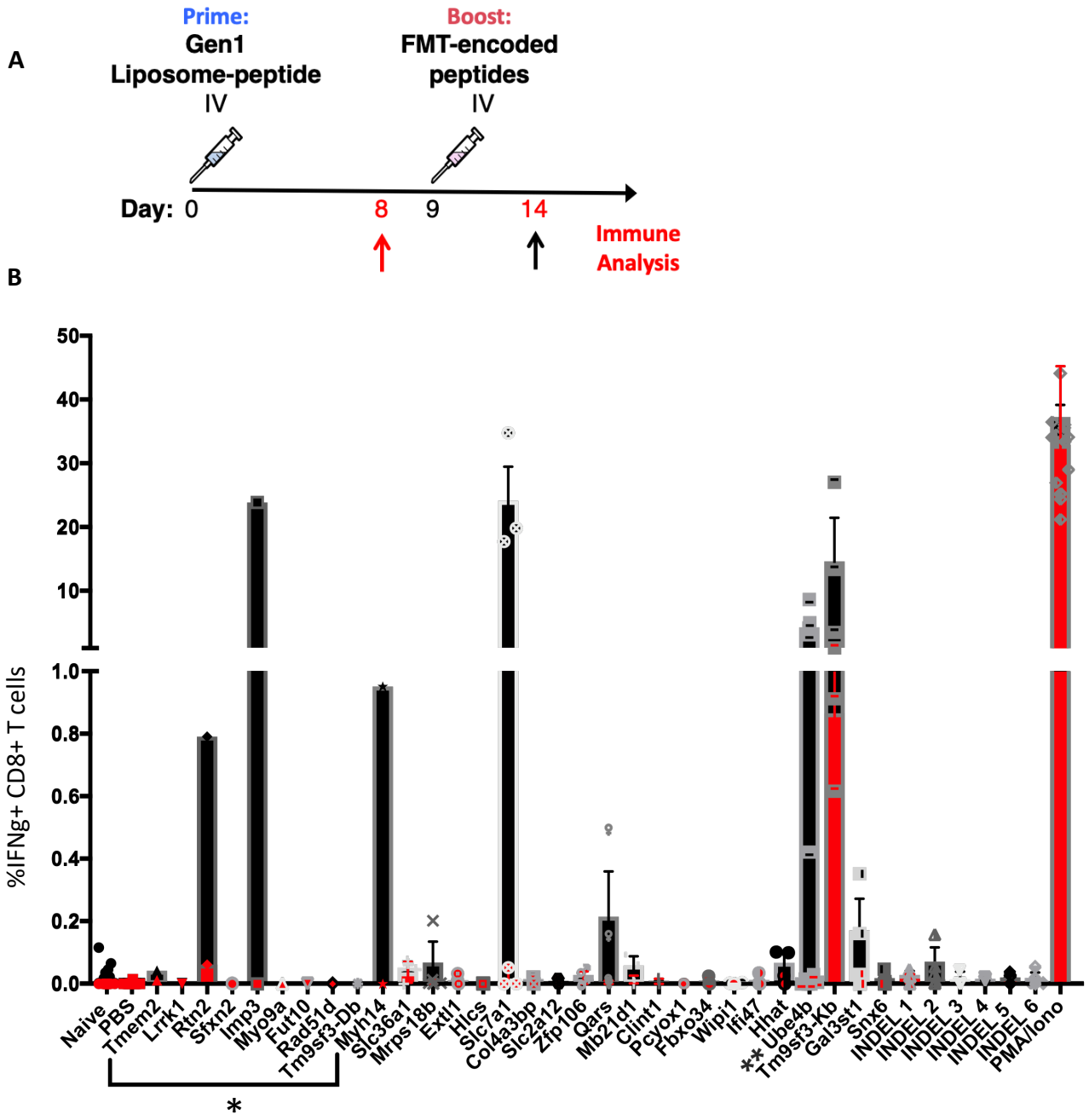

Figure 10: Vaccinating mice against a single neoepitope as a prime allows for specific amplification of CD8+ T cells following Farmington-encoded virus boost, enabling identification of immunogenic neoepitopes. The following is a consolidation of five experiments to properly display the discovered immunogenic neoepitopes from the screen. (A) 3 mice were vaccinated per group (targeting one peptide per group) with a single liposome-peptide prime by IV, marked at Day 0. On Day 9, mice were followed up with a boost vaccination with $3x10^8$ pfu of chimeric FMT virus encoded with the respective neopeptide, by IV administration. (B) Blood was collected on Day 8 (marked by red bars) and Day 14 (marked by black bars), and analyzed for neoepitope specific immune responses by flow cytometry for IFNg+ CD8+ T cells by peptide stimulation. Naïve, PBS, and PMA/Ionomycin (positive control) were grouped from all experiments. (*) marks blood collections that were pooled from n=5 mice that were vaccinated with a $1x10^8$ pfu FMT. (**) marks the grouping of 2 separate experiments vaccinating against Ube4b. Data is plotted as mean IFNg positive cell frequency of CD8+ T cell populations ±SEM.

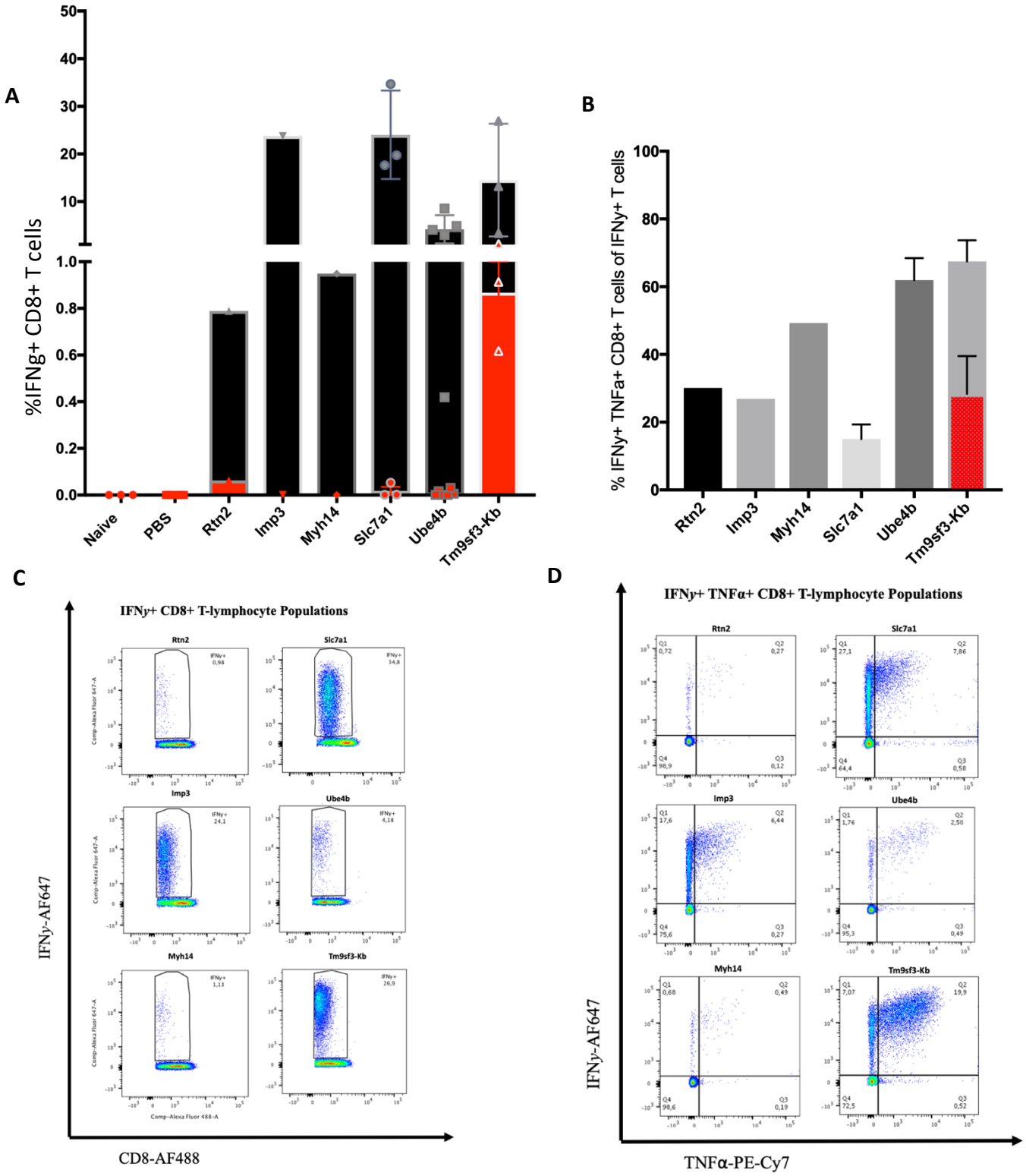

Figure 11: Screen positive immunogenic predicted neoepitopes produced varying polyfunctional immune responses. (A) Top six immune responses collected from the prime-boost screen of 36 predicted neoepitopes, plotted as mean IFNg positive cell frequency of CD8+ T cell populations ±SEM. (B) The top 6 immunogenic peptides polyfunctionality, plotted as frequencies of IFNg+ TNFa+ of the IFNg+ CD8+ population ±SEM. (C)(D) Corresponding dot plots of flow cytometry results of best responding mouse response in each group.

3.3.2 - RMA-S peptide binding assay

To continue corroborating the *in silico* and *in vivo* data of peptide immunogenicity, a peptide-binding assay was applied to synthetic peptides derived from immunogenic neoepitopes (Fig. 13). RMA-S cells were pulsed with peptides and stained for both H-2Kb and H-2Db alleles. Mean florescence intensity was measured via flow cytometry as a surrogate for MHC surface expression. H-2Db (Fig. 13a) and H-2Db (Fig. 13b) expression stabilized by DMSO (background), OVA (ovalbumin 257-264; SIINFEKL, positive control), Adpgk (MC38 – H2-Db based neoepitope; ASMTNMELMl, positive control), mImp3 (*in silico* predicted for H-2Db; AALLNKLYAM) or Tm9sf3 (*in silico* predicted for H-2Kb; SIFNSFMMLI). As predicted, Adpgk and mImp3 peptides increased H-2Db surface expression, but not H-2Kb, designating their binding selectivity to the H-2Db allele. Similar, Tm9sf3 and OVA peptides increased H-2Kb allele, while Tm9sf3 peptides did not change H-2Db expression. Of note, OVA appeared to increase expression of H-2Db and H-2Kb alleles.

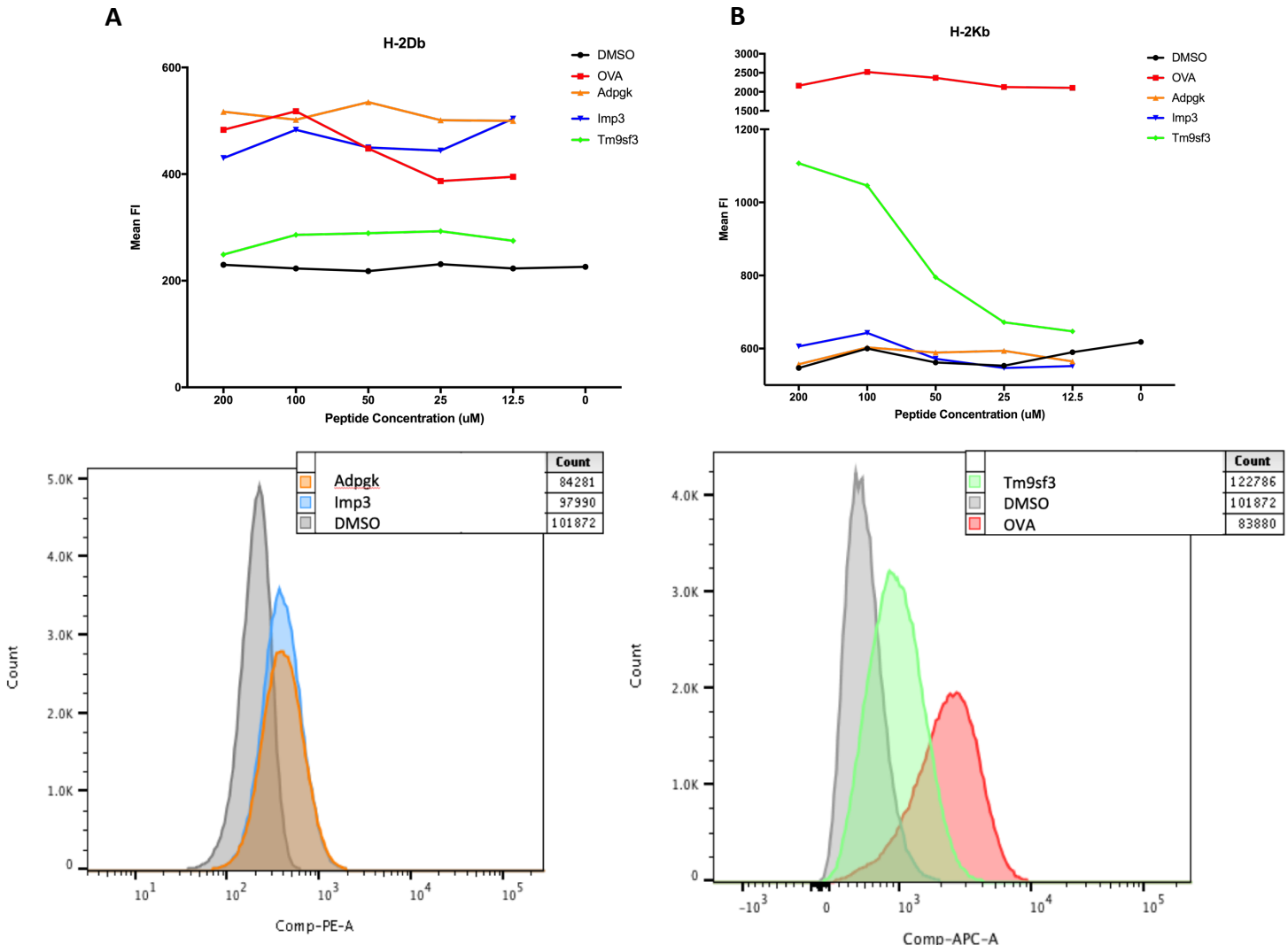

Figure 13: RMA-S peptide binding assay shows potential to identify peptide-MHC binding ability. RMA-S cells were pulsed with different peptides, stained for MHC alleles, and analyzed by flow cytometry for fluorescence intensity. (A) H-2b, stained with PE and (B) H-2Kb, stained with APC, were pulsed with DMSO (negative control), OVA (ovalbumin 257-264; SIINFEKL), Adpgk (MC38 – H2-Db based neoepitope; ASMTNMELMl), mImp3 (*in silico* predicted for H-2Db; AALLNKLYAM), and Tm9sf3 (*in silico* predicted for H-2Kb; SIFNSFMMLI). Peptide-MHC binding was measured by fluorescence intensity of MHC alleles following peptide-pulsing and incubation.

3.4 - Multi-epitope vaccinations and their tumour efficacy

The chimeric FMT virus containing the top 10 predicted peptides from the neoepitope screen was tested in a survival efficacy experiment (Fig. 12). The prime consisted of a pool of 10 peptides wrapped, 1μg each peptide, together in liposomes (Gen1 Lipo-peptide), administered IV 3 days following tumour implantation of $2x10^4$ GL261 cells by stereotaxic IC injection, and FMT encoded boost 9 days later (Fig. 12b) (n=5). This multi-epitope vaccine was compared to the previous mImp3 prime-boost single epitope vaccination methods, with a mImp3 peptide (1μg) liposome prime. Of note, the 10-amino acid form of mImp3 was used, and by wrapping with lipids the peptide was observably protected, shown by the substantial increase in the mImp3 specific immune response present (Fig. 12d). Blood between mice was pooled for further separation and peptide stimulation, giving an average value per 5 mice. No target immune response was detected prior to boost. Following boost, the multi-epitope vaccination achieved higher mImp3 frequency (23.81) than the single epitope vaccination (8.02), in addition to responses against mRtn2 (0.79) and Myh14 (0.95), versus no response with the single epitope vaccination (Fig.12d). No significant extension in survival between groups was detected.

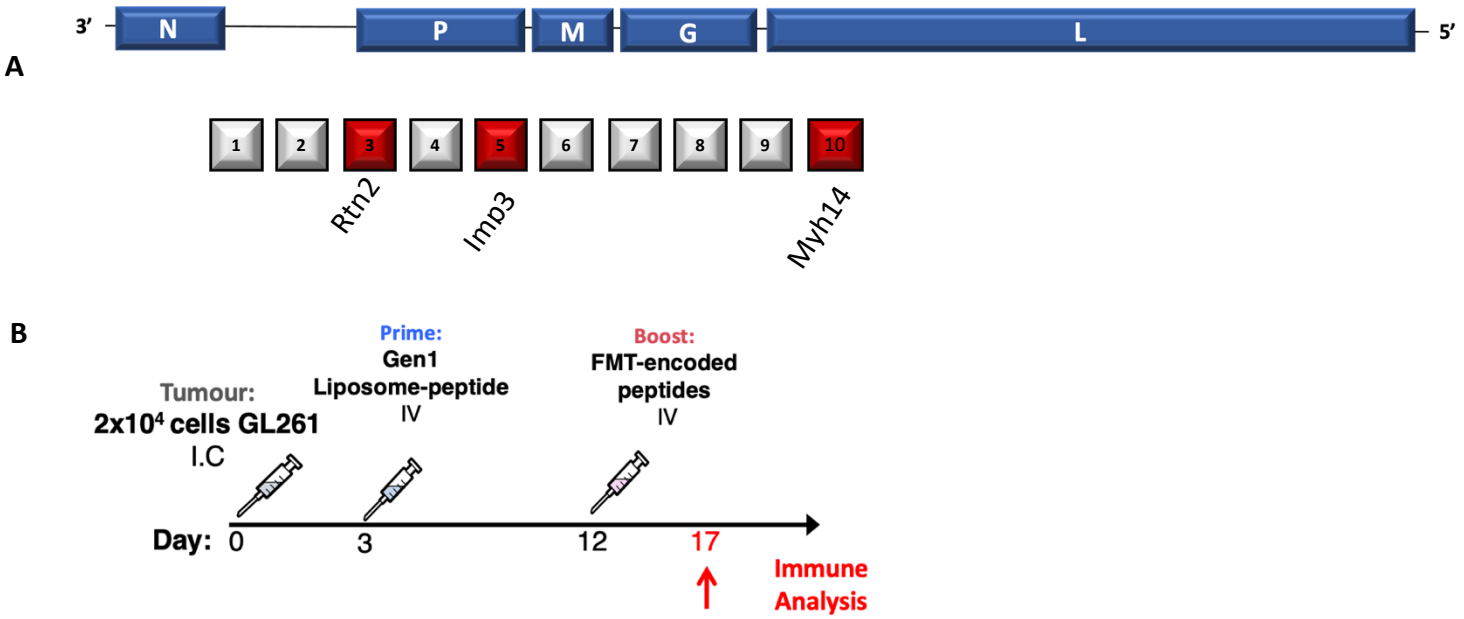

Figure 12: Vaccination against three immunogenic neoepitopes does not increase survival in GL261 mouse GBM model. (A) Chimeric Farmington rescued containing the top five predicted neoepitopes from each allele was tested in a survival experiment. (B) Mice underwent stereotaxic IC implantation of $2x10^4$ GL261 cells on Day 0. Day 3 mice were primed with liposome-peptide (Gen1) by IV administration. On Day 12, mice were immunized with FMT-mImp3 or FMT encoded with the top 10 neoepitopes. Blood collection from Day 17 was analyzed and shown as pooled (n=5) PBMC responses to peptide stimulation. (C) Survival plotted in a Kaplan-Meirer curve, with survival being determined by designated end-point symptoms. (D) Day 17 immune responses plotted as frequency of IFNg+ cells of the CD8+ T cell population of pooled blood per group.

To examine the efficacy ability of therapeutically targeting all six immunogenic neoepitopes, a multi-epitope vaccine was created to test against the GL261 mouse GBM model. A novel chimeric FMT virus was rescued containing all six epitopes separated by AAY proteasome sites, in two repeats (Fig. 14a). Mice underwent IC injection of $2x10^4$ GL261 cells on Day 0, followed by a Gen2 liposome-peptide prime, where peptides were wrapped individually before being pooled at injection, on Day 3 (Fig. 14b). On Day 12, mice were injected with FMT-encoded with the respective peptides. Checkpoint inhibitor, anti-PD-1, was administered 6 times by IP injection every three days beginning on Day 6. Blood was collected for analysis on Day 11 and 17. Day 11 (Fig.14c) immune responses were dominated by Slc7a1 and Myh14 specificity, in groups receiving both targeted prime and boost: Gen2 Lipo-peptides/IgG/FMT-peptides (Slc7a1: 2.612 ± 0.457, Myh14: 1.032 ±.0167) and Gen2 Lipo-peptides/**anti-PD-1**/FMT peptides (Slc7a1: 1.948 ± 0.434, Myh14 ± 0.791 ± 0.157). Prior to boost, no difference was observed in absolute total CD8+ T cell blood counts. Post boost Day 17 immune responses revealed immune responses, again, dominated with specificity toward Slc7a1 and Myh14, with modest response to mImp3, mRtn2, and mUbe4b. CD8+ T cell absolute counts were also substantially increased in targeted prime-boost vaccination groups, presenting with a ~log more peripherally circulating CD8+ T cells. Targeted vaccination did not improve survival outcome in targeted vaccination groups, also reducing the ability of anti-PD-1 to incur survival as seen in non-targeted vaccination control (Fig.14e). Efficacy was repeated with a reduced tumour burden of 4000 GL261 cells implanted IC into mice on Day 9 (Fig. 15). Prime immune responses appeared less, but still dominated with specificity toward Slc7a1 and Myh14. Following boost, total immune frequency appeared reduced, with the majority of specificity on mSlc7a1 and mMyh14, followed by modest response to mRtn2 (Fig. 15c). Responses toward mUbe4b and mImp3 were

completely reduced. Absolute total of peripheral blood CD8+ T cell counts also increased in targeted vaccination groups (Fig. 15c). Reducing tumour burden (Fig.15d) allotted to indistinguishable survival between control and treated groups. Again, anti-PD-1 survival rates were depleted with the addition of a targeted vaccine therapy.

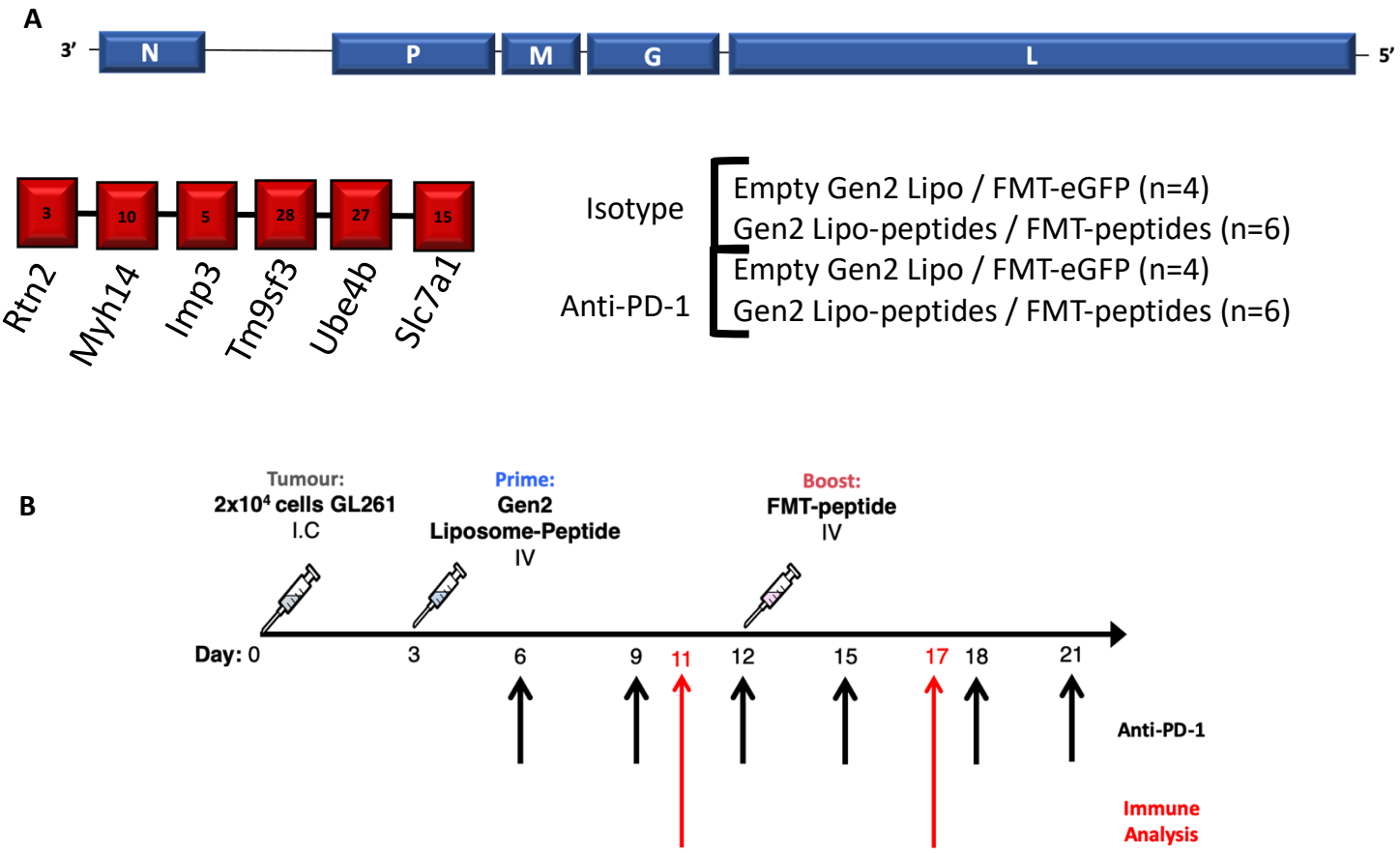
A
3'
N
P
M
G
L
5'
3
10
5
28
27
15
Rtn2
Myh14
Imp3
Tm9sf3
Ube4b
Slc7a1
Isotype
Empty Gen2 Lipo / FMT-eGFP (n=4)
Gen2 Lipo-peptides / FMT-peptides (n=6)
Anti-PD-1
Empty Gen2 Lipo / FMT-eGFP (n=4)
Gen2 Lipo-peptides / FMT-peptides (n=6)
B
Tumour:
2x10⁴ cells GL261
I.C
Prime:
Gen2
Liposome-Peptide
IV
Boost:
FMT-peptide
IV
Day: 0
3
6
9
11
12
15
17
18
21
Anti-PD-1
Immune
Analysis
C
GBM Specific % IFNγ+ CD8+ T-cells
100
80
60
40
20
10
8
6
4
2
0
Slc7a1
Myh14
Imp3
Rtn2
Ube4b
Tm9sf3
CD8+ T-cells/mL
10⁸
10⁷
10⁶
10⁵
Empty Gen 2 Lipo / IgG / FMT-eGFP
Gen2 Lipo-peptides / IgG / FMT-peptides
Empty Gen 2 Lipo / anti-PD-1 / FMT-eGFP
Gen2 Lipo-peptides / anti-PD-1 / FMT-peptides

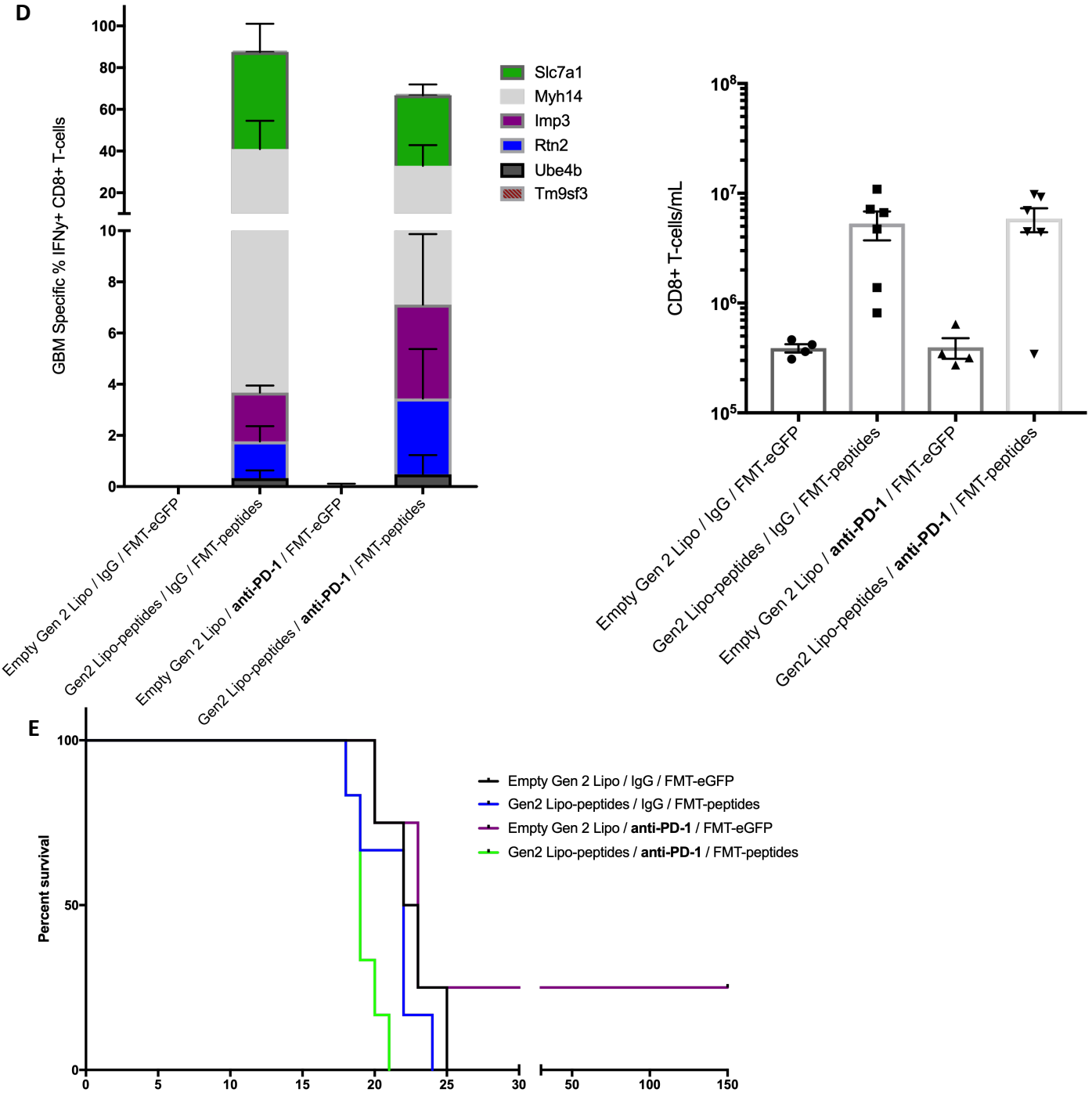

Figure 14: Multi-neoepitope vaccine provides robust immunity against dominate epitopes but does not increase survival. (A) The six identified immunogenic peptides were designed into a gene insert, to produce a chimeric FMT virus. (B) Mice underwent stereotaxic surgery to implant $2x10^4$ GL261 cells IC, marked as Day 0. On Day 3, mice were primed with individually wrapped six immunogenic peptides (Gen2 liposome-peptide) vaccination by IV injection. Mice were boosted with FMT- encoded with the respective peptides on Day 12. Mice were also either administered anti-PD-1 checkpoint inhibitors or isotype control IgG antibodies six times, 3 days apart, starting on Day 6. Blood was collected on Day 11 and 17, for PBMC analysis by flow cytometry. (C)(D) Immune blood analysis of Day 11 and 17 were plotted as cumulative frequencies of separate blood-peptide stimulations of IFNg stained cells of CD8+ T cell mouse populations. Total CD8+ T cell counts were plotted in absolute numbers of CD8+ T cells per mL of mouse blood. Data was plotted in mean values ±SEM. (E) Survival was determined by pre-designated end-points and graphed on a Kaplan-Meirer curve.

A

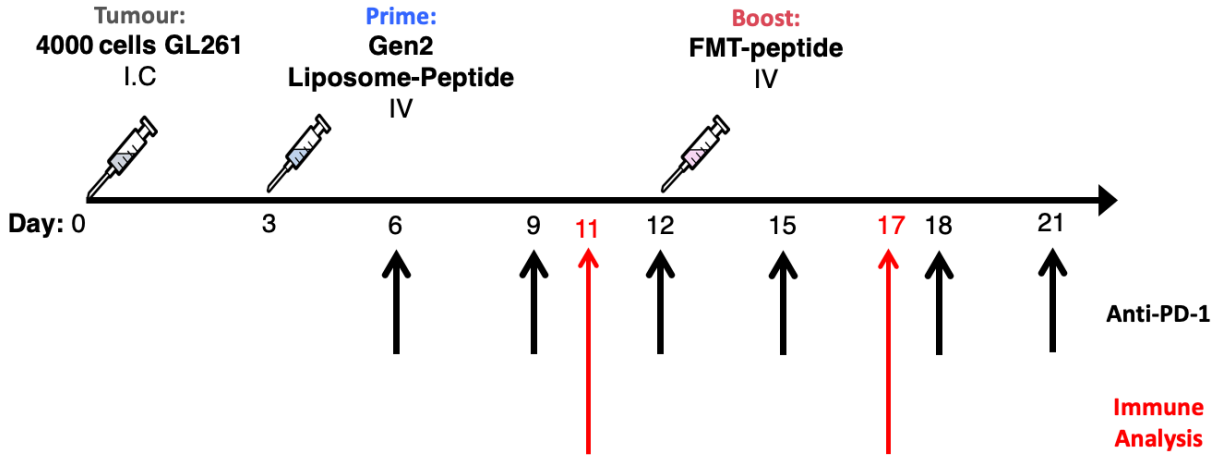

Isotype
- Empty Gen2 Lipo / FMT-eGFP (n=4)
- Gen2 Lipo-peptides / FMT-peptides (n=6)

Anti-PD-1
- Empty Gen2 Lipo / FMT-eGFP (n=4)
- Gen2 Lipo-peptides / FMT-peptides (n=6)

PBS - PBS / PBS (n=4)

B

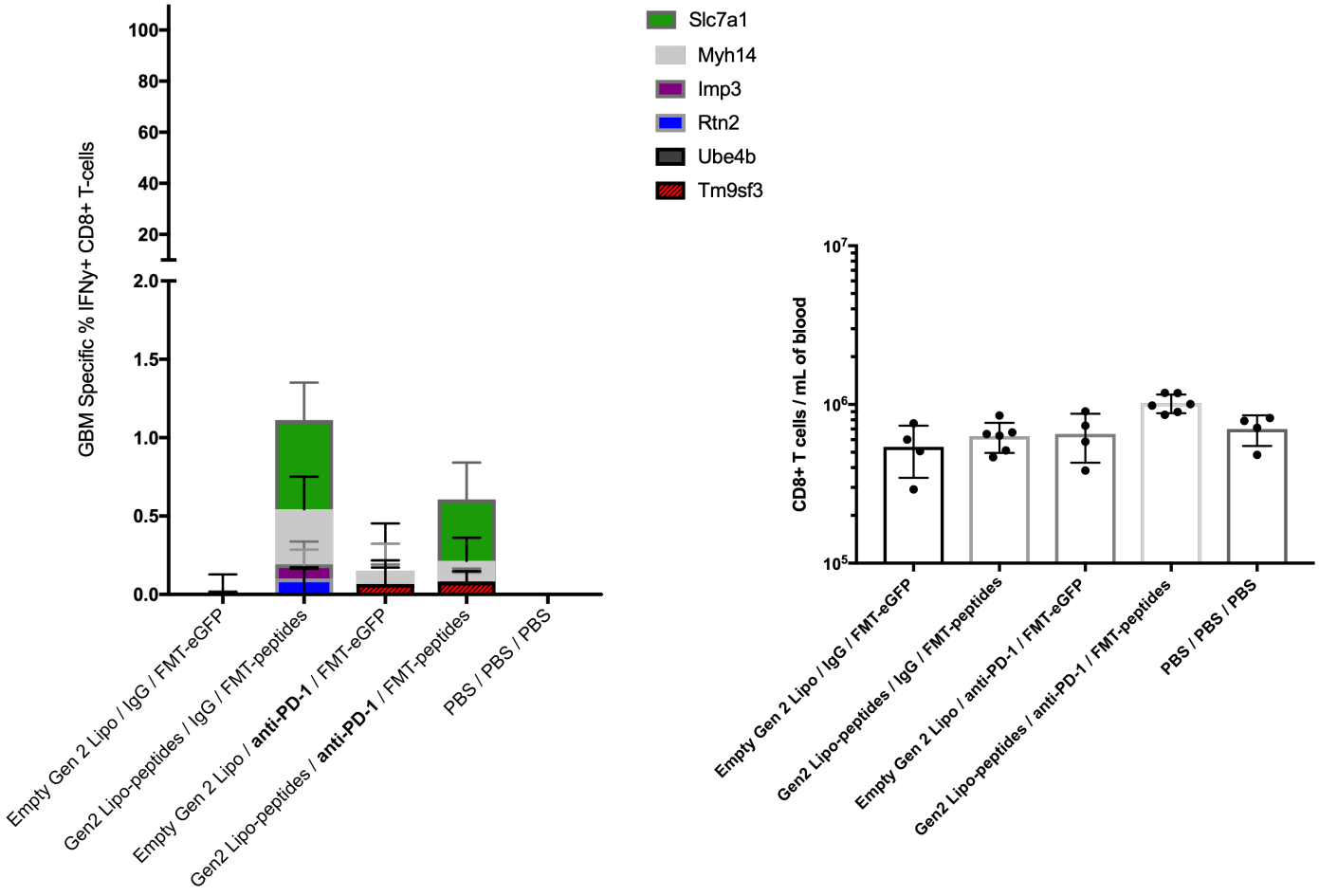

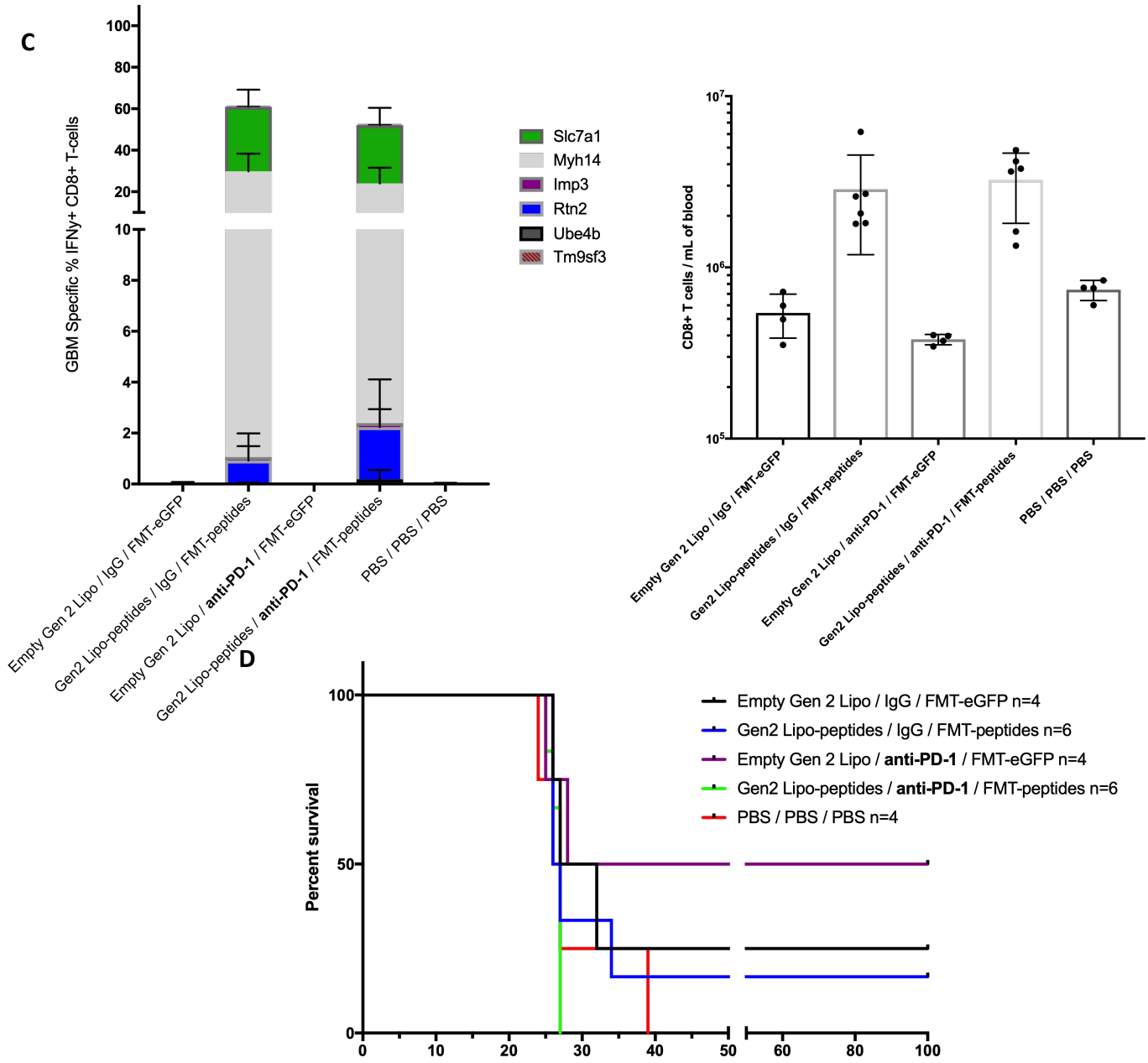

Figure 15: Reducing tumour burden in GL261 GBM mouse model with prime-boost vaccination produces indistinguishable cures between treated and control groups. (A) Mice underwent stereotaxic surgery to have 4000 GL261 cells implanted IC, marked as Day 0. On Day 3, mice were primed with individually wrapped six immunogenic peptides (Gen2 liposome-peptide) vaccination by IV injection. Mice were boosted with FMT-encoded with the respective peptides on Day 12. Mice were also either administered anti-PD-1 checkpoint inhibitors or isotype control IgG antibodies six times, 3 days apart, starting on Day 6. Blood was collected on Day 11 and 17, for PBMC analysis by flow cytometry. (C)(D) Immune blood analysis of Day 11 and 17 were plotted as cumulative frequencies of separate blood-peptide stimulations of IFNg+ stained cells of CD8+ T cell mouse populations. Total CD8+ T cell counts were plotted in absolute numbers of CD8+ T cells per mL of mouse blood. Data was plotted in mean values ±SEM. (E) Survival was determined by pre-designated end-points and graphed on a Kaplan-Meirer curve.

3.5 - Preventative vaccine strategy and mRNA for a new prime

To test the impact of targeting six neoepitopes on the GL261 tumour model, a prophylactic vaccine experiment was completed (Fig. 16). Mice were vaccinated with the Gen2 liposome-peptide prime FMT-peptides boost, with immune responses observed pre- and post-boost to confirm GBM specific immunity (Fig. 16a). Gen2 liposomes containing a mRNA polyplex was also implemented in attempt to diverge from peptide-based vaccine therapies. mRNA construct, previously designed by Dr. Sahin's group (155), was used to insert a targeted cassette of the six neoepitopes separated by AAY proteasome sites with or without PADRE (AKFVAAWTLKAAA) and tetanus toxoid (QYIKANSKFIGITE; 830-843) sequences to enhance CD4+ T cell help. Only mice vaccinated with the Gen2 liposome-peptide prime had immune responses observed prior to FMT boost, consisting of only specificity to mSlc7a1. No substantial effect on CD8+ T cell absolute blood counts were observed after prime (Fig. 16b). Following the viral boost vaccination, immune responses with specificity to mSlc7a1 and mMy14 dominated vaccinated mice. Mice vaccinated with the targeted Gen2 Liposome-peptide prime produced the highest total immune frequency against neoepitopes and was the only one to substantially increase absolute total CD8+ T cell blood counts. Gen2 liposome-mRNA without CD4 help sequence had an observable larger total immune response compared to mice vaccinated with Gen2 liposome-mRNA with CD4 help. No vaccination protection was observed across all treated groups (Fig 16d).

A

Gen2 Lipo-peptides / FMT-peptides n=5
Gen2 Lipo-mRNA / FMT-peptides n=5
Gen2 Lipo-mRNA (CD4 help) / FMT n=4
PBS / PBS = 4

B

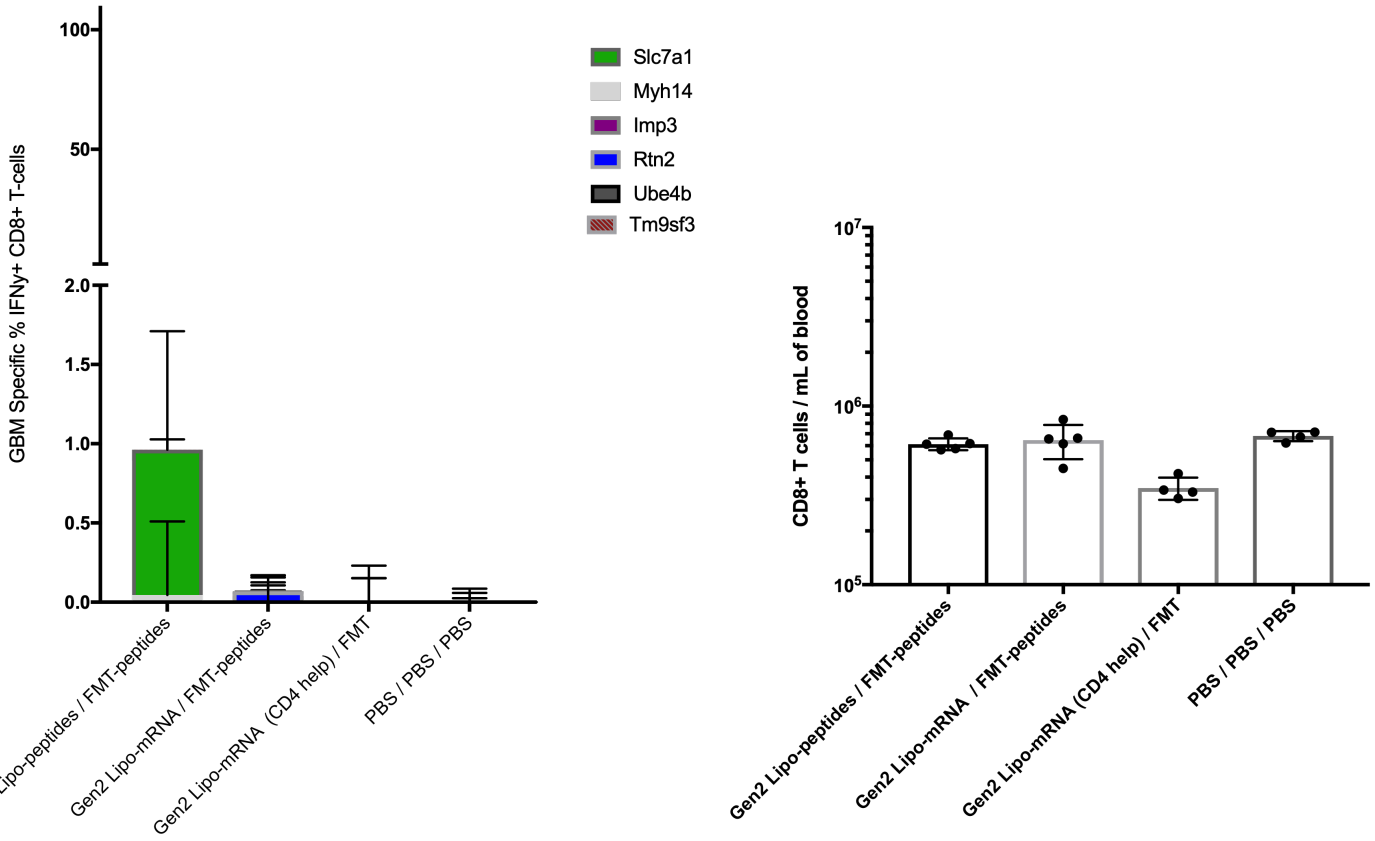

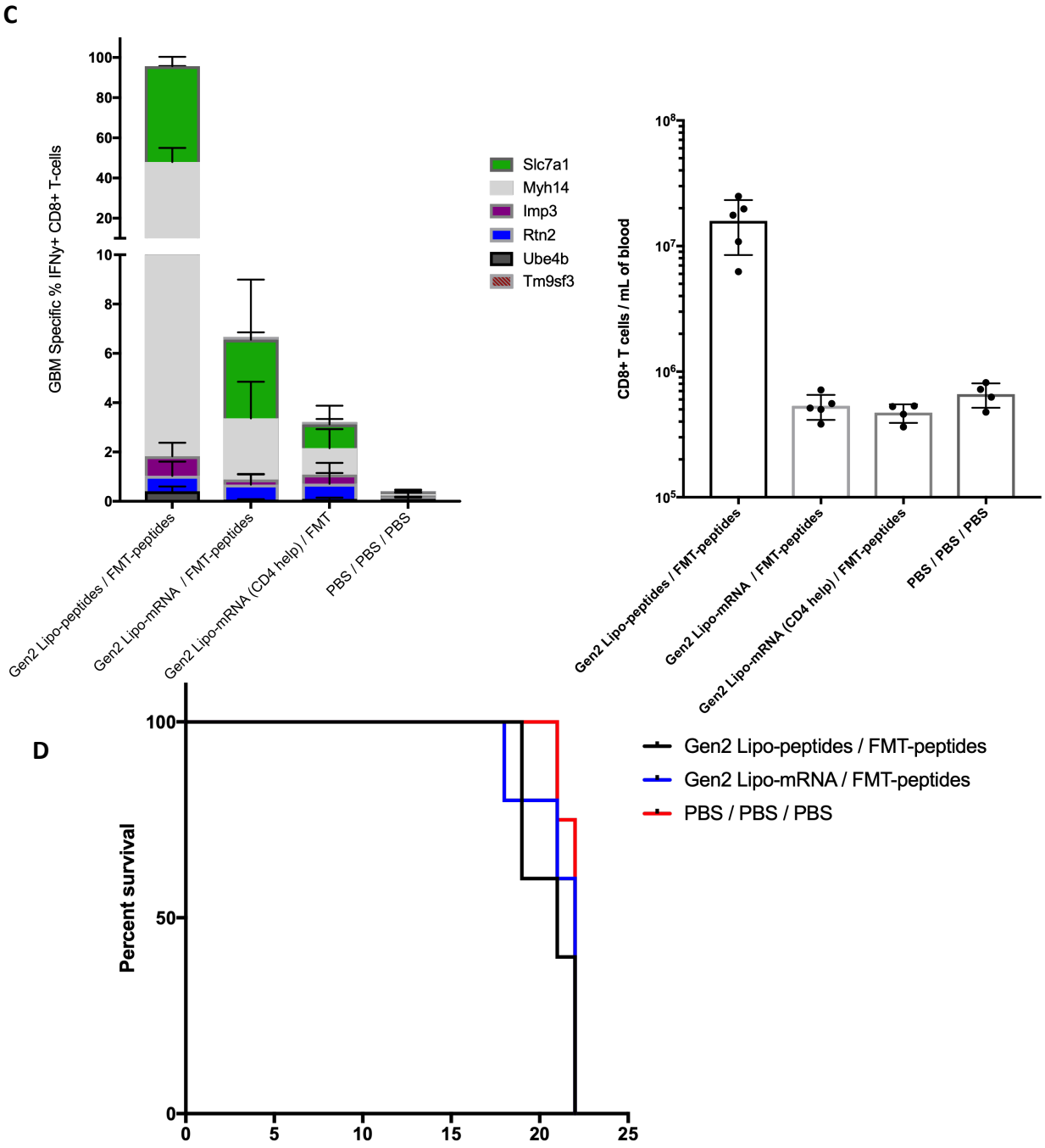

Figure 16: Targeting immunogenic neoepitopes as a prophylactic therapy does not provide protection in the GL261 GBM mouse model. (A) Mice were primed with the six immunogenic individually wrapped peptides (liposome-peptides) at Day 0 and boosted with FMT-encoded with the respective peptides on Day 9. On Day 30, vaccinated mice were challenged by IC injection of $2x10^4$ GL261 cells. Blood was collected on Day **8**, **14**, and 28, for immune analysis by flow cytometry. (B) (C) Immune analysis of blood collections are plotted in cumulative frequencies of separate blood-peptide stimulations of IFNg+ stained cells of the CD8+ T cell mouse populations. Total CD8+ T cell counts were plotted as absolute numbers of CD8+ T cells per mL of mouse blood. All data is plotted in mean values ±SEM. (D) Survival was determined by pre-designated end-points and graphed on a Kaplan-Meirer curve.

4 - DISSCUSSION

A multimodal approach is required for success when treating cancer directly. Considering natural responses present across the body inherently prevents cancer, cancer must become dynamic to overcome these defenses and present clinically. Treatment designed to fight such a dynamic and precarious disease should also be dynamic and a multi-mechanistic based approach to overcome and eliminate cancer. Treatment for glioblastoma multiforme (GBM), the most common primary malignant brain tumour, continually faces these challenges, struggling to provide any significant improvement (37). Targeted potent combinational therapies are needed for patients facing the poor prognosis of GBM.

4.1 - Engineering Farmington to express tangible neoepitopes for clinical application

Direct tumour oncolysis, immune cell recruitment and tumour microenvironment alterations are just a few of the mechanisms that successful oncolytic viruses possess. Knowing the potency and selectivity oncolytic viruses have, the Stojdl Lab focused efforts on finding a virus with a particular selectivity to brain tumour cells. Upon results of bioprospecting for viruses, Farmington (FMT) was discovered (152). FMT is unique by safe intracranial (IC) injection into mice, with the ability of both priming for tumour associated antigens (TAA) and boosting pre-existing TAA-specific immune memory (unpublished data), collectively making FMT a prime candidate for GBM immunotherapy.

Engineering FMT to express neoantigens was a major tool for the production of the results completed within this thesis. Efforts, notable by Charles Lefebvre, were completed previously by the Stojdl Lab to understand and manipulate FMTs genome in order to rescue chimeric virion. Shown previously with the Maraba rhabdovirus, the Stojdl lab was able to

effectively express hDCT, achieving tumour vaccination and increased survival with durable cures. However, targeting single TAA in cancer patients leads to antigen loss variants (168,169), thus we focused on designing inserts for FMT that target multiple antigens to be incorporated into the virus production pipeline, by using short peptides (Fig.1). From cancer target discover to ready-to-administer chimeric virus takes approximately 3 weeks, which we believe can be clinically relevant.

The design and location of the transgene must ensure both expression of the targeted antigens, while not effecting the virus replication. For all experiments shown herein, the transgene was located following viral N-protein. Due to 'linear attenuation', that occurs in negative sense RNA viruses where the polymerase transcribes 3' proteins most with decreasing expression the further away each protein is positioned, transgenes are expressed at a higher rate inserted after viral N-protein then compared to after viral G-protein (unpublished data). On the contrary, inserting cumbersome transgenes following viral N-protein may change the natural replication course by preventing downstream proteins from optimally being presented; though no data of this phenomena has been observed. Currently, the maximum transgene size inserting follow viral N-protein in FMT was ~4000bp long (unpublished data), however, the size threshold may become stricter if short repeating sequences are use. Further investigation into the size and format limitations is required to understand the limitations of FMT engineering.

The optimal vaccine transgene allows for maximum expression of protein, which then becomes accurately digested by cellular processes preceding strong interaction with MHC proteins. To ensure target vaccination peptides remain uncut, implementing proteasome cleavage sites as spacers between peptides has been tested, producing a string-of-beads transgene. Velders and colleagues discovered increased protection from tumour challenge in a epitope-based DNA

vaccination that applied AAY spacer between target antigens (170). In contrast, Wang et al. found a decrease in humoral and cellular immune responses when testing HIV vaccines with AAY spacers versus GGGS flexible linkers (171). Furthermore, Schubert and Kohlbacher proposed a mathematical model for epitope specific spacer design, showing highest immune epitope recovery when compared to AAY or no spacers. Interestingly AAY spacers provided the highest immunogenicity in each vaccine design (172). A likely possibility for this increase in immunogenicity seen with AAY can be described by the protein rigidity/instability when containing multiple AAY repeats. If unstable, these proteins are swiftly processed by the proteasome, increasing the likelihood of binding MHC.

A general consensus is currently held that AAY spacers are most effective when flanking MHC class I epitopes and flexible linkers, GGGS or GPGPGP can provide stability when surrounding larger MHC class II epitopes (170–177). AAY spacers were used to separate target epitopes in all data within this thesis, likely contributing to a level of immunogenicity and preventing unwanted protein folding through its rigidity. However, it potentially altered viral replication by having repeats, though further investigation is required. Other vaccine design tactics, such as introducing universal MHC class II restricted epitopes (e.g. PADRE, tetanus toxoid) or signaling proteins to increase shuttling to the endoplasmic reticulum and MHC, could be implemented to enhance either prime or boost within these vaccination experiments (155,178).

4.2 - Validating the ability to target single epitopes with a prime-boost approach

To test our ability to efficiently produce a chimeric virus to express a beads-on-a-string transgene and generate tangible immune responses, we decided to target a validated GL261

mouse model antigen, mutant (m)Imp3. The aspartic acid (GAC) to asparagine (AAC) mutation in the GL261 Imp3 (GARC-1) (1190002L16Rik) protein was originally found by Iizuka et al. (2006) to produce anti-tumour immunity in HSV vaccinated mice bearing GL261 tumours (163). Following, in 2016, Gavin Dunn's group rediscovered this mutation while *in silico* searching for neoepitopes, finding CD8+ T cells specific to mImp3 epitopes within the tumours and draining lymph nodes of C57Blk6 mice IC implanted with GL261 mouse GBM cells. While it is clear that mImp3 peptide is immunogenic and produces anti-tumour immune responses, there remains no effective treatment vaccine against this mouse model.

Firstly, to confirm our cell line also had the $Imp3_{D81N}$ mutation, sanger sequencing was done with PCR products produced by flanking primers (Fig.2). Confirming the presence of this mutation allotted for future vaccination efficacy-based studies. To test the possibility of inserting repeated sequences in a string-of-beads format, we designed an insert with five repeats of mImp3 peptide (AALLNKLYAM) linked with AAY spacers. To remain consistent and replicate future clinical trials, insert designs were codon optimized by a third party, for maximal protein expression, and were gene synthesized into a purified plasmid. From here, the chimeric FMT genome was made and transfected into cells, rescuing a novel FMT virus: FMT-mImp3. After confirming the correct genome was present by sanger sequencing, the new virus was successfully amplified and purified for *in vivo* trials. With cloning and virus rescue reaching ~100% success rate, the virus production pipeline proved its ability to handle creating neoepitope targeted FMT viruses.

To test mImp3 vaccination *in vivo*, we implemented a prime-boost vaccination, where the chimeric virus provided the boost. Previous successful data of the prime-boost model using a rhabdovirus, leveraged an encoded non-replicating adenovirus for the prime. While effective,

chimeric adenovirus engineering is not as successful as FMT or Maraba, also taking a much longer duration before being able to produce a ready-to-administer virus. In addition, pre-existing cellular and humoral immunity in patients that have been previously infected with adenovirus mediates acute toxicity and reduced therapeutic outcomes (179). Currently, adenovirus candidacy for a personalized vaccine vector approves unfruitful. A more simplistic adjuvant-peptide vaccine method, described by Yadav et al., was pursued as a stand-in prime vaccination for our prime-boost method (167). The vaccination method mixes synthetic peptides with anti-CD40 and Poly(I:C) for an IP injection. Preliminary evidence indicates that anti-CD40 may be unsafe as an adjuvant for vaccine therapy in humans. Furthermore, free peptides face several challenges which result in sub-optimal immunogenicity of target antigens (180), requiring nanoparticle carriers. Utilizing the capability of liposomes to encapsulate peptides was investigated to overcome such obstacles.

The mImp3$_{D81N}$ mutation produces a potential 54 neopeptides between H-2Db and H-2Kb alleles in 8-, 9-, and 10-amino acid long forms. When tested against peptide-MHC binding algorithms IC50 (nM) scores can be applied to each peptide. In the case of mImp3 (supplementary table 1), two peptides: AALLNKLYAM (10-amino acid) and AALLNKLYA (9-amino acid), had optimal scores, particular the 10-amino acid form. Staying consistent with future peptide prediction, being the best IC50 score peptide would be chosen, we chose to test the 10-amino acid peptide of mImp3. Longer 27-amino acid peptides are more clinically relevant, as they overlap the mutation by 13 amino acids, delivering the possibility of all 54 MHC class I neoepitopes as well as MHC class II neoepitopes produced by the single nucleotide polymorphism. In terms of observing the immune response of a 27-amino acid long peptide vaccination, pools of overlapping peptides would be required to begin to distinguish which

peptide is immunogenic. For purposes of this experiment we decided to vaccinate and follow a single neoepitope.

Initial results (data not shown) had low vaccination frequencies against mImp3, when using a synthetic peptide-prime and FMT-mImp3-boost approach. The extra methionine added to the 10-amino acid peptide makes it susceptible to oxidation, possibly reducing stability upon injection. Considering the peptides encoded into FMT were in 10-amino acid versions, FMT-mImp3 could potentially vaccinate against either 9- or 10-amino acid form (**AALLNKLYA**M). A peptide-prime containing either form was tested with FMT-mImp3 as a boost (Fig.3, Fig.4, Fig.5). Interestingly, the 9-amino acid mImp3 vaccinated sufficiently for the secondary immune boost of FMT-mImp3 for amplification. Peripheral blood mononuclear cells (PBMCs) were stimulated with either version of the peptide to identify the specificity of our intracellular staining assay (data not shown). All mImp3 specific immune responses recorded showed no difference between stimulation with either size peptide, likely indicating that either peptide can bind and be recognized by the same T cell population.

Targeted vaccination of mImp3 (Fig.4 & Fig.5), when using the 9-amino acid peptide-prime, bears a mImp3 specific CD8+ T cell population, further validating our ability to produce a vaccination targeting specific neoepitopes. As expected, when the time between prime and boost was increased, a larger immune amplification was detected (Fig.5 & Fig.6). This can be explained by the natural progression of immunity following a primary response, as a longer wait would produce more memory T cells eligible to become reactivated. However, due to the shortness of the GL261 IC tumour model, a 9-day wait was pursued for efficacy experiments. Lower frequencies were detected with the shorter wait between prime and boost, and possibly a different T cell phenotype was also be produced. A full functionality examination of these

shorter timed boosted CD8+ T cells would be required to understand their activation state. It could be these T cells are in exhaustion, often seen in chronic virus or other chronic disease states (181,182). Furthermore, when tested in IC tumour mouse models, this vaccination did not improve survival (Fig.6 & Fig. 7). To understand why mImp3 vaccination does not improve mouse survival an analysis of the tumour environment would be required. Tumour cell RNA can be measured for expression of mImp3, with the hypothesis that antigen loss variants continued tumour progression. Immune responses were measured from peripheral blood samples, which may not indicate the amount of tumour infiltrating lymphocytes (TIL) specific to mImp3. Extracting TIL and staining brain samples for TIL, immune exhaustion or checkpoints, would expedite our understanding of why these treatments failed.

Polyfunctional T cells, expressing IFNg, TNFa, and IL-2 perform better when in contact with target antigens. While IL-2 was stained, the time points T cells were analyzed showed no expression. IL-2 is generally at peak expression 12 hours following T cell activation, possibly indicating why no expression was seen (79). TNFa was also stained for polyfunctionality analysis, which showed increasing frequencies of IFNg+ TNFa+ CD8+ populations with time following boost vaccination. To determine whether the number of polyfunctional T cells increase in time or the increase in frequency was from a contraction of IFNg+ T cells, an analysis of absolute numbers in a similar experiment must be had. Nonetheless, our vaccination against mImp3 produced lasting polyfunctional immunity.

Producing a chimeric FMT virus that expresses a targeted neoepitope, in string-of-beads format, is possible with our virus production pipeline. Chimeric FMT-mImp3 has the capability to produce large specific immune responses when injected following an initial peptide-adjuvant prime. These immune responses do not correlate with increased survival in the respective mouse

model and require further investigation for a complete understanding. Peptides as a prime vaccination can produce a false-negative peptide immunogenicity when given freely and should be delivered with a carrier to preserve their integrity.

4.3 - Producing an *in silico* prediction pipeline to predict immunogenic mouse neoepitopes

The Stojdl Lab neoepitope prediction pipeline introduced here is a product of the bioinformatician, Philippe Charron. The pre-determined choice of variant callers was based upon sensitivity and specificity testing using mutations from a known data base (unpublished data). This prediction pipeline was applied to GL261 sequencing data. The traditional method of discovering the mutanome from cancer takes exome sequencing and screens it against the wild-type genome, calling variants from a coding region comparison (164,167). mRNA sequencing is often used to rule out epitopes that are not expressed, but unfortunately cannot determine the level of protein expressed due the highly regulated post-transcriptional processes naturally present (183). We decided to initially form our prediction pipeline using exome and mRNA sequencing focusing on coding regions, presented in Figure 8. Alternatively, a recent publication by Laumont et al. (2018) reinforced the notion that cancer often produces proteins from non-coding regions. Laumont and colleagues discovered 40 tumour specific antigens, 90% being derived from apparent non-coding regions. With further investigation, a comparison between pipelines could be done, further corroborating the need to produce a personal cancer exome from mRNA sequencing.

Not every peptide predicted can bind MHC effectively or is even recognized by T cell receptors, making a high false-positive rate for neoepitope prediction methods (157,164), forcing further screening validation, such as mass spectrometry (184)(167). In the current method, we

implemented *in silico* public available algorithms scoring peptides based on their affinity to an MHC allele. Following the isolation of mImp3 by Johanns et al. we ordered peptides based by MHC binding affinity generated by NetMHCpan2.3. However, NetMHCpan4.0 has since emerged, implementing more proteasome mass spectrometry data. In a retrospect comparison (Supplementary Figure 1), NetMHCpan4.0, ANN and SMM appear to remove a large portion of non-immunogenic peptides tested in our original screen, while keeping the positive responding peptides. Particularly in the H-2Kb prediction, only a few non-immunogenic peptides are within the top 15, the remaining being novel untested peptides. Further immunogenicity testing of all peptides predicted between groups would aid in defining optimal prediction methods and help improve *in silico* algorithms.

4.4 - Methods to screen and validate immunogenic neoepitopes

Once variants are called, the remaining possible epitopes remain too cumbersome for complete testing, often with the majority not being immunogenic. MHC binding algorithms can help narrow down peptides to test, however, they predict at a low specificity and can miss multiple immunogenic peptides, and require further validation. Forming a proteome data base by mass spectrometry is now often used to discover MHC class I bound peptides. While not perfect, mass spectrometry has led to the discovery of multiple neoepitopes today (167,185,186). As mentioned previously, only a few antigens are found by mass spectrometry (MS) when screening predicted peptides from basic exome sequencing. This can be improved by building a personal cancer exome, looking at non-coding regions of cancer genomes through mRNA sequencing (157). In a screen, looking for neoepitopes in a sarcoma mouse cell line, by Gubin et al. used a discovery mass spectrometry approach only discovering 1 of 2 validated peptides. A more

sensitive approach, selected reaction monitoring mass spectrometry, was implemented to be able to identify both peptides. Selected reaction monitoring is the most accurate mass spectrometry method; however, it requires a synthetic peptide standard for each peptide, limiting it to known peptide standards available and making it unavailable for large peptidomic studies. Peak intensity and spectral counting are the other candidates available for neoepitope identification, however as shown, they both face limitations to predicting short peptides. Particularly, the restricted number of fragmentations each MS run, can either miss peptides or produce a fragmentation number too low for further identification (187). Experiments designed to utilize MS data could be had to compare and possibly discover more neoantigens from our current neoepitope list. Furthermore, specific peptide standards could be implemented for selected reaction monitoring MS from the 36 synthetic peptides produced during our neoepitope screen.

To discover and validate potential novel immunogenic peptides for the GL261 GBM model, an *in vivo* prime-boost vaccination was implemented (Fig.10a). A novel liposome encapsulated peptide (Gen 1 Liposome-peptide) based on work done by Persano et al. (188), was used to overcome premature denaturing of peptides seen with the previous 10-amino acid mImp3 peptide. Liposome-peptide was successful for protection, shown by immune responses generated from a 10-amino acid mImp3 liposome-peptide (Fig.10b). If immune responses were detected following a heterologous prime-boost targeted vaccination, peptide immunogenicity and vaccination capabilities could be established promptly. Considering the purpose of this screen was to discover novel GL261 neoepitopes and not provide a solution for the human neoepitope screening method, the vaccination-style screen was acceptable. Six mutant peptides were identified to produce substantially higher than background immune responses. A few mutant peptides may have shown a low level of immunogenicity (e.g. mQars, mMrps18b), but were not

chosen due to inability to produce high immune responses with our current vaccination method (Fig.10b). Initial polyfunctionality, determined by double positive staining for TNFa and IFNg, varied between peptides, possible indicating a ranging immunogenicity level amongst predicted peptides. Further functionality testing (e.g. modified CTL assays) of each peptide specific T cell may help indicate how effective these CD8+ T cell populations are. In conclusion, this method was successful in discovering 6, out of 36, immunogenic peptides that can produce robust T cell populations upon prime-boost vaccination.

To continue corroborating *in silico* and vaccination data a RMA-S cell peptide binding assay was pursued. Two immunogenic peptides were trialed to induce stable MHC expression on RMA-S cells, which lack a functional antigen transporter and therefore fail to express high levels of cell surface MHC class I proteins at 37°C (189). If temperature is decreased to 26°C, low affinity peptides are able to bind and stabilize surface expression of MHC class I proteins. If RMA-S cells are incubated at 26°C previous to being pulsed with synthetic target peptides at 37°C, low affinity peptides will detach from MHC class I and target peptides can then bind and stabilize surface MHC class I. mImp3 induced stabilization of H-2Db and not H-2Kb, while mTm9sf3 induced H-2Kb stabilization and not H-2Db, indicating their allele binding selectivity (Fig. 13). This binding assay is useful to further validate and determine allele binding but is clearly limited to requiring synthetically produced peptides. All 36 synthetic peptides produced for these experiments could be sent through this binding assay to help identify their allele binding and determine the specificity and sensitivity of this assay.

4.5 - Multi-neoepitope vaccinations and their applicability in survival studies

Passive and active cancer immunotherapies both effectively exploit that tumour cells express unique antigens on their cell surface. Overcoming autoimmune targeting by using tumour specific antigens from the cancer mutanome has aided in shifting vaccine technology away from self-antigens. Targeting these tumour specific antigens has been an ongoing goal for potent immunotherapies. However, cancer immunoediting, by both inherently and therapeutically stimulated immune responses, provide selective pressure for cancer to from variants with reduced immunogenicity (190). Tumours are found to reduce surface expression of MHC and T cell/NK cell co-stimulatory molecules, evading natural immunity. Checkpoint receptors such as anti-PD-1 and anti-CTLA-4 are also commonly increased on the surface of tumours to suppress effector function of surveilling immune cells. Moreover, tumours can form antigen loss variants that lack expression of these immunogenic proteins, escaping immunity and leading to recurrence. Chimeric antigen receptor (CAR) T cell therapy and CD8+ T cell vaccines are both notable for effectively eliminating target populations and selecting for cancer cells lacking expression of target antigen (168,169).

To help spearhead a world-wide multimodal approach for treating cancer, we decided to create a multi-epitope-based vaccine. Using the six immunogenic peptides discovered from our screen, we produced a chimeric FMT virus as our boost vaccine (Fig. 14a). A novel formulation of liposome (Gen2 liposome-peptide), discovered by Persano et al., provides a heighten CD8+ immune response and tumour selectivity, with reduced toxicity (unpublished data). This new formula was leveraged as our prime vaccination. To attempt to prevent peptide dominance, peptides were encapsulated separately, and mixed prior to vaccination. A comparison between wrapping peptides individually or as a pool would be required to understand its relevancy and

requirement. However, when peptides mRtn2, mImp3, and Myh14 were pooled before being encapsulated in the Gen1 liposome, mRtn2 and mMyh14 specific immunity was significantly less than mImp3 (Fig.12). In observable contrast in a separate experiment when all six peptides were encapsulated in liposomes individually, mRtn2 and mMyh14 specific immune responses matched or were substantially higher, respectively (Fig.14). Gen1 vs Gen2 liposomes, or 1μg vs 10μg of each peptide could explain this difference between said experiments, requiring further investigation.

Liposome-peptide prime and the encoded FMT boost induced tumour specific immunity to multiple neoantigens. Immune responses following a peptide prime, or even Gen1 liposome-peptide, vaccination generally did not elicit observable peripheral immunity alone, until Gen2 liposome-peptide was implemented (Fig.14, Fig. 15). Briefly, the Gen2 liposome utilizes a multivalent lipid rather than a monovalent lipid, so when injected IV it can obtain entry into more target cells throughout the spleen (unpublished data). Furthermore, no absolute increases in CD8+ T cell counts in the blood were seen prior to using the Gen2 liposome-peptide vaccination as a prime for FMT-boost (Fig. 14, Fig. 15). With the Gen2 liposome a change in total CD8+ T cell blood counts, 1 log higher, occurred when compared to non-targeted or PBS vaccination controls. The frequency of tumour specific immunity applies now to a substantial larger T cell population, producing 10-fold more specific T cells compared to previous vaccination trials with free or Gen1 liposome-peptide primes. The effect or safety profile of this considerable increase in circulating T cell still remains enigmatic. If on target and properly activated these effector cells could induce better survival (191). On the contrary, this large immune increase could be producing effector T cells incapable of their effector functions. Staining for markers for stages of T cell development (e.g. CD25, CD127, CD44, KLRG1, CD62L) or exhaustion state (e.g. PD-1,

TIM3, LAG3, CTLA-4, BTLA, TIGIT) would helping in determining the state this T cell population.

The inaugural survival experiment testing vaccination targeting all six neoepitopes produced observable immune specificity to mSlc7a1, mMyh14, mImp3, mRtn2, and mUbe4b, but not mTm9sf3 (Fig.14). Considering mTm9sf3 was the only peptide to produce an immune response following one prime dose (Fig.10), it can be inferred to be very immunogenic. However, due to complications in peptide stability and manufacturing it is likely that the peptide precipitated before being encapsulated into a liposome for vaccination. Synthetic mTm9sf3 peptides resuspended, for the screen vaccinations (Fig.10), in a chloroform:methanol solution precipitated out of solution over time within the -80°C freezer. The extremely hydrophobic characteristic of mTm9sf3 made manufacturing and keeping it in solution difficult. Unfortunately, new mTm9sf3 synthetic peptides were not successfully encapsulated into our further vaccination experiments (Fig.14, Fig.15). In the absence of a prime, mTm9sf3 specific immunity was solely produced by FMT. While not nonexistent, there was a small population of mTm9sf3 specific CD8+ T cells produced. The remaining CD8 T cell population was spread across the other five neoepitopes. Targeted vaccine groups of mice produced immunity to mSlc7a1 and mMyh14 following a singular prime vaccination. These neoepitopes continued on to dominate the immune response following FMT boost. While the vectors of our prime-boost method are heterologous, the neoepitopes within them are homologous and if a few peptides are immunodominant, secondary responses could be skewed to those peptides, like seen in homologous prime-boost vaccines. Bearing in mind the vaccines used contain the short (8-,9-10-amino acid long) neoepitope version, so if a 27-amino acid long version was used in

replacement, immune response may become more diverse, eliminating an immune majority to two single mutant peptides.

Mice that received a Gen2 liposome-peptide prime with FMT boost, had induced a T cell phenotype that promoted proliferation when peptide stimulated *ex vivo*. Immune responses following boost vaccination within these groups (Fig.14, Fig.15, Fig.16) had T cells from PBMC isolation divide within the 5-hour peptide incubation. Figures shown control for this duplication, by eliminating the divided population from the frequency calculation post analysis, using the DMSO stimulated samples as a CD8 T cell count baseline. T cell activation that leads to proliferation normally does not lead to cell division within 5-hours, however, cases have shown division within 2 hours *in vivo* (192). Moving forward, using tetramer staining in replace of peptide stimulation to identify CD8 T cell specificity would solve this inaccuracy of T cell induced division. Conversely, tetramer-based staining does not induce T cell activation, staining for any TCR that can recognize the neoepitope. In repeat experiments, a peptide stimulation can be monitored for proliferation to determine optimal stimulation times. In addition, stains for T cell proliferation assays could be implemented to gate out duplicated populations (e.g. CFSE).

Checkpoint inhibitors

Checkpoint blockade by PD-1 antibodies has previously been shown to induce a moderate level of survival in GL261 GBM models (193–197). We hypothesized, that in combination with our vaccine strategy mouse survival could be improved. No increase in survival was recorded with the combination of a targeted prime-boost vaccination and PD-1 checkpoint blockade (Fig14e, Fig 15d). As expected, the control mice receiving anti-PD-1 and vaccination without target peptides, had 25% survival (n=1) (Fig.14), and 50% survival (n=2) (Fig. 15) with a decreased initial tumour burden. Additionally, when the initial tumour burden

was reduced (Fig.15) vaccination with and without target peptides and IgG isotype as a control, also had survival (n=1), possibly indicating a low-level treatment affect from the adjuvanted liposome and/or FMT. Interestingly, the combination of both anti-PD-1 and a targeted prime-boost vaccination did not induce survival, like anti-PD-1 with control vaccination (Fig.14, Fig.15).

When $2x10^4$ GL261 cells were injected (Fig.14), mice who received the on target prime and boost vaccination became dehydrated and lost weight by day 17 (5 days following boost), while other controls were healthy. Rehydrating by weight food and saline helped mice return to normal activity, however, those mice reached endpoint sooner than non-targeted vaccine controls. When necropsied, mice had large blood clots within their right hemisphere, where the tumour was implanted. It is not entirely uncommon to have mice reach endpoint from a blood clot in the GL261 model, likely due to weak vasculature when the tumour becomes large. Though it is noteworthy that all treated mice were both dehydrated and succumbed to endpoint with brain blood clots before control mice. The substantial increase of CD8 T cell blood counts, along with a assuming inflammatory environment, could have put pressure on the tumour microenvironment causing the observed intracerebral hemorrhaging. Alternatively, the targeted vaccination could have induced a larger TIL count, also pressuring the tumour vasculature. This T cell infiltrate, if on target, could have induced a tumour lysis syndrome phenotype, possibly explaining the sick phenotype and early death observed with vaccinated mice (198,199). Immunohistochemistry of brain samples (e.g. TIL), along with sequencing analysis (e.g. qPCR), would help illuminate the underlying pathology and tumour state post treatment.

To combat this tumour lysis syndrome hypothesis, we decided to reduce the initial tumour burden to 4000 GL261 cells and the FMT boost to $7.5x10^7$ pfu, to provided room for

intervention (Fig.15). Mice treated with targeted vaccine and anti-PD-1 still showed no survival improvement, however, no mice lost weight or were dehydrated following boost vaccination. As aforementioned, with the decreased initial tumour burden, mice were now surviving with vaccination lacking target neoepitopes. Again, the targeted vaccination with checkpoint inhibitor anti-PD-1 showed no survival compared to 50% survival in mice with empty vaccination and anti-PD-1 treatment. The targeted vaccine appears to negatively impact the treatment efficacy induced by anti-PD-1, whether indirectly or directly. Considering nearly the entire CD8 T cell population recognizes a few neoepitopes, it is possible that resources are being taken from more effective naturally occurring immune responses that would be amplified by anti-PD-1 therapy. Additionally, when the initial tumour burden was decreased, responses specific to mImp3 and mUbe4b became absent. Perhaps indicating that the implanted GL261 cells have a priming effect on the immune system like observed previously by Johanns et al (164).

In hopes to identify the on-target ability of the neoepitopes vaccinated, a prophylaxis vaccination model was tested (Fig.16). While robust immunity against mSlc7a1 and mMyh14 neoepitopes was again recorded, a lower frequency to mImp3, mRtn2 and mUbe4b was observed than before. Unfortunately, no survival of either vaccine treated mice were recorded. The tumour microenvironment established by GL261 cells within the mouse brain could be significantly truncating the vaccinated immune response. A subcutaneous GL261 model in mice would help identify the relevancy of immunosuppression induced within the brain. More importantly, identifying if these chosen six neoepitopes are on-target via T cell cytotoxicity assay using lymphocytes from vaccinated mice against GL261 cells can be trialed to aid our understanding.

A mRNA polyplex encapsulated in the Gen2 liposome, containing the targeted neoepitopes was also trialed in attempt to remove the issue of stability that peptides face in both

manufacturing and *in vivo* vaccination (Fig.16). Control mice with just FMT vaccination were missing, however, total immune responses following boost vaccination of Gen2-Liposome mRNA primed mice appeared higher than mice vaccinated with mRNA containing PADRE and tetanus toxoid sequences (CD4 help). This could indicate that the mRNA prime helped but was suboptimal due a level of instability induced by additional repeats. The mRNA construct was based on Dr. Sahin's backbone, but varied with how the epitopes were inserted (155). Dr. Sahin inserted 27-amino acid long peptides within their backbone, spaced by GGSGGGGSG flexible linkers, where we used short 8-, 9-,or 10-amino acid long peptides flanked by AAY rigid proteasome sites as linkers. *In vitro* testing of our mRNA construct can be done to determine its ability to translate effectively. Using longer peptides overlapping the mutate target with flexible linkers could also be pursed to enhance the mRNA capability as a prime.

Concluding remarks

There is still much to understand before a personalized vaccination can produce optimal efficacy in the clinic. Albeit, data such as shown here, begins to discover the potent ability vaccine technologies can provide against cancer. Identifying novel immunogenic peptides in mice permits further exploration into prediction algorithms and cancer vaccine technologies. Discovering how tumours evolve, the impact vaccine technologies have on tumour evolution, what level of immune response is considered safe, and how can we manipulate the deleterious tumour microenvironment are important questions raised here requiring further investigation. Global efforts are being made to improve GBM patient prognosis with immunotherapy, and FMT virus has much to contribute.

REFERENCES

1. Kasten FH. Paul Ehrlich: pathfinder in cell biology. 1. Chronicle of his life and accomplishments in immunology, cancer research, and chemotherapy. Biotech Histochem. 1996 Jan;71(1):2–37.
2. Love RR, Leventhal H, Easterling D V, Nerenz DR. Side effects and emotional distress during cancer chemotherapy. Cancer. 1989 Feb 1;63(3):604–12.
3. Woods R, Louchini R, Guiot M-C, Melin B, Spinelli J, Bryant H, et al. Malignant primary brain and other central nervous system tumors diagnosed in Canada from 2009 to 2013. Neuro Oncol. 2018;(January):1–10.
4. Ostrom QT, Gittleman H, Truitt G, Boscia A, Kruchko C, Barnholtz-Sloan JS. CBTRUS statistical report: Primary brain and other central nervous system tumors diagnosed in the United States in 2011-2015. Neuro Oncol. 2018;20:iv1–86.
5. Kleihues P, Louis DN, Scheithauer BW, Rorke LB, Reifenberger G, Burger PC, et al. The WHO classification of tumors of the nervous system. J Neuropathol Exp Neurol. 2002 Mar;61(3):215–25; discussion 226-9.
6. Brandes AA, Tosoni A, Franceschi E, Reni M, Gatta G, Vecht C. Glioblastoma in adults. Crit Rev Oncol Hematol. 2008 Aug 1;67(2):139–52.
7. Song W, Ruder AM, Hu L, Li Y, Ni R, Shao W, et al. Genetic Epidemiology of Glioblastoma Multiforme: Confirmatory and New Findings from Analyses of Human Leukocyte Antigen Alleles and Motifs. Lowenstein PR, editor. PLoS One. 2009 Sep 23;4(9):e7157.
8. Chakrabarti I, Cockburn M, Cozen W, Wang Y-P, Preston-Martin S. A population-based description of glioblastoma multiforme in Los Angeles County, 1974-1999. Cancer. 2005 Dec 15;104(12):2798–806.
9. Thakkar JP, Dolecek TA, Horbinski C, Ostrom QT, Lightner DD, Barnholtz-Sloan JS, et al. Epidemiologic and molecular prognostic review of glioblastoma. Cancer Epidemiol Biomarkers Prev. 2014 Oct;23(10):1985–96.
10. Hamilton SR, Liu B, Parsons RE, Papadopoulos N, Jen J, Powell SM, et al. The Molecular Basis of Turcot's Syndrome. N Engl J Med. 1995 Mar 30;332(13):839–47.
11. Kleihues P, Ohgaki H. Primary and secondary glioblastomas: from concept to clinical diagnosis. Neuro Oncol. 1999;1(1):44–51.
12. Louis DN, Perry A, Reifenberger G, von Deimling A, Figarella-Branger D, Cavenee WK, et al. The 2016 World Health Organization Classification of Tumors of the Central Nervous System: a summary. Acta Neuropathol. 2016 Jun 9;131(6):803–20.
13. Wang R, Chadalavada K, Wilshire J, Kowalik U, Hovinga KE, Geber A, et al. Glioblastoma stem-like cells give rise to tumour endothelium. Nature. 2010 Dec 21;468(7325):829–33.
14. Dirks PB. Brain Tumor Stem Cells: Bringing Order to the Chaos of Brain Cancer. J Clin Oncol. 2008 Jun 10;26(17):2916–24.

15. Chen J, McKay RM, Parada LF. Malignant Glioma: Lessons from Genomics, Mouse Models, and Stem Cells. Cell. 2012 Mar 30;149(1):36–47.
16. Furnari FB, Fenton T, Bachoo RM, Mukasa A, Stommel JM, Stegh A, et al. Malignant astrocytic glioma: genetics, biology, and paths to treatment. Genes Dev. 2007 Nov 1;21(21):2683–710.
17. Ohgaki H, Dessen P, Jourde B, Horstmann S, Nishikawa T, Di Patre P-L, et al. Genetic Pathways to Glioblastoma. Cancer Res. 2004 Oct 1;64(19):6892–9.
18. Verhaak RGW, Hoadley KA, Purdom E, Wang V, Qi Y, Wilkerson MD, et al. Integrated genomic analysis identifies clinically relevant subtypes of glioblastoma characterized by abnormalities in PDGFRA, IDH1, EGFR, and NF1. Cancer Cell. 2010 Jan 19;17(1):98–110.
19. Arjona D, Rey JA, Taylor SM. Early genetic changes involved in low-grade astrocytic tumor development. Curr Mol Med. 2006 Sep;6(6):645–50.
20. Nakamura M, Yang F, Fujisawa H, Yonekawa Y, Kleihues P, Ohgaki H. Loss of heterozygosity on chromosome 19 in secondary glioblastomas. J Neuropathol Exp Neurol. 2000 Jun;59(6):539–43.
21. Watanabe K, Tachibana O, Sata K, Yonekawa Y, Kleihues P, Ohgaki H. Overexpression of the EGF receptor and p53 mutations are mutually exclusive in the evolution of primary and secondary glioblastomas. Brain Pathol. 1996 Jul;6(3):217–23; discussion 23-4.
22. Ohgaki H, Kleihues P. The Definition of Primary and Secondary Glioblastoma. Clin Cancer Res. 2013 Feb 15;19(4):764–72.
23. Heiland DH, Haaker G, Delev D, Mercas B, Masalha W, Heynckes S, et al. Comprehensive analysis of PD-L1 expression in glioblastoma multiforme. Oncotarget. 2017 Jun 27;8(26):42214–25.
24. Alvarez-Buylla A, Lim DA. For the long run: maintaining germinal niches in the adult brain. Neuron. 2004 Mar 4;41(5):683–6.
25. Maher EA, Furnari FB, Bachoo RM, Rowitch DH, Louis DN, Cavenee WK, et al. Malignant glioma: genetics and biology of a grave matter. Genes Dev. 2001 Jun 1;15(11):1311–33.
26. Kornblum HI, Hussain R, Wiesen J, Miettinen P, Zurcher SD, Chow K, et al. Abnormal astrocyte development and neuronal death in mice lacking the epidermal growth factor receptor. J Neurosci Res. 1998 Sep 15;53(6):697–717.
27. Seidman KJ., Teng AL, Rosenkopf R, Spilotro P, Weyhenmeyer JA. Isolation, cloning and characterization of a putative type-1 astrocyte cell line. Brain Res. 1997 Apr 4;753(1):18–26.
28. Xu H, Zong H, Ma C, Ming X, Shang M, Li K, et al. Epidermal growth factor receptor in glioblastoma. Oncol Lett. 2017 Jul;14(1):512–6.
29. Wrensch M, Fisher JL, Schwartzbaum JA, Bondy M, Berger M, Aldape KD. The molecular epidemiology of gliomas in adults. Neurosurg Focus. 2005 Nov 15;19(5):E5.
30. Schwartzbaum JA, Fisher JL, Aldape KD, Wrensch M. Epidemiology and molecular

pathology of glioma. Nat Clin Pract Neurol. 2006 Sep;2(9):494–503.
31. Brenner AV, Butler MA, Wang SS, Ruder AM, Rothman N, Schulte PA, et al. Single-nucleotide polymorphisms in selected cytokine genes and risk of adult glioma. Carcinogenesis. 2007 Dec;28(12):2543–7.
32. Lachance DH, Yang P, Johnson DR, Decker PA, Kollmeyer TM, McCoy LS, et al. Associations of High-Grade Glioma With Glioma Risk Alleles and Histories of Allergy and Smoking. Am J Epidemiol. 2011 Sep 1;174(5):574–81.
33. Scheurer ME, Amirian ES, Davlin SL, Rice T, Wrensch M, Bondy ML. Effects of antihistamine and anti-inflammatory medication use on risk of specific glioma histologies. Int J Cancer. 2011 Nov 1;129(9):2290–6.
34. Seliger C, Meier CR, Becker C, Jick SS, Bogdahn U, Hau P, et al. Use of Selective Cyclooxygenase-2 Inhibitors, Other Analgesics, and Risk of Glioma. Wallace J, editor. PLoS One. 2016 Feb 12;11(2):e0149293.
35. Malmström A, Grønberg BH, Marosi C, Stupp R, Frappaz D, Schultz H, et al. Temozolomide versus standard 6-week radiotherapy versus hypofractionated radiotherapy in patients older than 60 years with glioblastoma: the Nordic randomised, phase 3 trial. Lancet Oncol. 2012 Sep;13(9):916–26.
36. Nieder C, Grosu AL, Astner S, Molls M. Treatment of unresectable glioblastoma multiforme. Anticancer Res. 25(6C):4605–10.
37. Stupp R, Mason WP, van den Bent MJ, Weller M, Fisher B, Taphoorn MJB, et al. Radiotherapy plus Concomitant and Adjuvant Temozolomide for Glioblastoma. N Engl J Med. 2005 Mar 10;352(10):987–96.
38. Tsitlakidis A, Venetis CA, Selviaridis P, Foroglou N, Hatzisotiriou A, Patsalas I. Biopsy versus resection in the management of malignant gliomas: a systematic review and meta-analysis. J Neurosurg. 2009;112(May):1020–32.
39. Long DM, Gordon TD, Bowman H, Etzel A, Burleyson G, Betchen S, et al. OUTCOME AND COST OF CRANIOTOMY PERFORMED TO TREAT TUMORS IN REGIONAL ACADEMIC REFERRAL CENTERS. file:///Users/zacharyjilesen/Desktop/Genes Dev-2001-Maher-1311-33.pdf.
40. Hart MG, Metcalfe SE, Grant R. Biopsy versus resection for high grade glioma. Cochrane Database Syst Rev. 2000 Apr 24;(2).
41. Vuorinen V, Hinkka S, Färkkilä M, Jääskeläinen J. Debulking or biopsy of malignant glioma in elderly people - a randomised study. Acta Neurochir (Wien). 2003 Jan 1;145(1):5–10.
42. Oszvald Á, Güresir E, Setzer M, Vatter H, Senft C, Seifert V, et al. Glioblastoma therapy in the elderly and the importance of the extent of resection regardless of age. J Neurosurg. 2012 Feb 1;116(2):357–64.
43. Glantz MJ, Cole BF, Forsyth PA, Recht LD, Wen PY, Chamberlain MC, et al. Practice parameter: anticonvulsant prophylaxis in patients with newly diagnosed brain tumors. Report of the Quality Standards Subcommittee of the American Academy of Neurology.

Neurology. 2000 May 23;54(10):1886–93.
44. Wolbers JG. Novel strategies in glioblastoma surgery aim at safe, supra-maximum resection in conjunction with local therapies. Chin J Cancer. 2014 Jan 5;33(1):8–15.
45. Sanai N, Berger MS. Intraoperative stimulation techniques for functional pathway preservation and glioma resection. Neurosurg Focus. 2010 Feb;28(2):E1.
46. Chaichana KL, Jusue-Torres I, Navarro-Ramirez R, Raza SM, Pascual-Gallego M, Ibrahim A, et al. Establishing percent resection and residual volume thresholds affecting survival and recurrence for patients with newly diagnosed intracranial glioblastoma. Neuro Oncol. 2014 Jan;16(1):113–22.
47. Grabowski MM, Recinos PF, Nowacki AS, Schroeder JL, Angelov L, Barnett GH, et al. Residual tumor volume versus extent of resection: predictors of survival after surgery for glioblastoma. J Neurosurg. 2014 Nov;121(5):1115–23.
48. Ishizuka M, Abe F, Sano Y, Takahashi K, Inoue K, Nakajima M, et al. Novel development of 5-aminolevurinic acid (ALA) in cancer diagnoses and therapy. Int Immunopharmacol. 2011;11:358–65.
49. Senders JT, Muskens IS, Schnoor R, Karhade A V., Cote DJ, Smith TR, et al. Agents for fluorescence-guided glioma surgery: a systematic review of preclinical and clinical results. Acta Neurochir (Wien). 2017 Jan 22;159(1):151–67.
50. Bregy A, Shah AH, Diaz M V, Pierce HE, Ames PL, Diaz D, et al. The role of Gliadel wafers in the treatment of high-grade gliomas. Expert Rev Anticancer Ther. 2013 Dec 10;13(12):1453–61.
51. Chinot OL, Wick W, Mason W, Henriksson R, Saran F, Nishikawa R, et al. Bevacizumab plus Radiotherapy–Temozolomide for Newly Diagnosed Glioblastoma. N Engl J Med. 2014 Feb 20;370(8):709–22.
52. Gilbert MR, Dignam JJ, Armstrong TS, Wefel JS, Blumenthal DT, Vogelbaum MA, et al. A Randomized Trial of Bevacizumab for Newly Diagnosed Glioblastoma. N Engl J Med. 2014 Feb 20;370(8):699–708.
53. Herrlinger U, Schaefer N, Steinbach JP, Weyerbrock A, Hau P, Goldbrunner R, et al. Survival and quality of life in the randomized, multicenter GLARIUS trial investigating bevacizumab/irinotecan versus standard temozolomide in newly diagnosed, MGMT-non-methylated glioblastoma patients. J Clin Oncol. 2014 May 20;32(15_suppl):2042–2042.
54. Herrlinger U, Schäfer N, Steinbach JP, Weyerbrock A, Hau P, Goldbrunner R, et al. Bevacizumab Plus Irinotecan Versus Temozolomide in Newly Diagnosed O ^{6} -Methylguanine–DNA Methyltransferase Nonmethylated Glioblastoma: The Randomized GLARIUS Trial. J Clin Oncol. 2016 May 10;34(14):1611–9.
55. Carlson JA, Reddy K, Gaspar LE, Ney D, Kavanagh BD, Damek D, et al. Hypofractionated-intensity modulated radiotherapy (hypo-IMRT) and temozolomide (TMZ) with or without bevacizumab (BEV) for newly diagnosed glioblastoma multiforme (GBM): a comparison of two prospective phase II trials. J Neurooncol. 2015 Jun 29;123(2):251–7.

56. Omuro A, Beal K, Gutin P, Karimi S, Correa DD, Kaley TJ, et al. Phase II Study of Bevacizumab, Temozolomide, and Hypofractionated Stereotactic Radiotherapy for Newly Diagnosed Glioblastoma. Clin Cancer Res. 2014 Oct 1;20(19):5023–31.
57. Montemurro N, Perrini P, Blanco MO, Vannozzi R. Second surgery for recurrent glioblastoma: A concise overview of the current literature. Clin Neurol Neurosurg. 2016 Mar;142:60–4.
58. Nieder C, Adam M, Molls M, Grosu AL. Therapeutic options for recurrent high-grade glioma in adult patients: Recent advances. Crit Rev Oncol Hematol. 2006 Dec;60(3):181–93.
59. Gilbert MR, Wang M, Aldape KD, Stupp R, Hegi ME, Jaeckle KA, et al. Dose-Dense Temozolomide for Newly Diagnosed Glioblastoma: A Randomized Phase III Clinical Trial. J Clin Oncol. 2013 Nov 10;31(32):4085–91.
60. Szczepanek D, Marchel A, Moskała M, Krupa M, Kunert P, Trojanowski T. Efficacy of concomitant and adjuvant temozolomide in glioblastoma treatment. A multicentre randomized study. Neurol Neurochir Pol. 2013;47(2):101–8.
61. Kocher M, Frommolt P, Borberg SK, Rühl U, Steingräber M, Niewald M, et al. Randomized Study of Postoperative Radiotherapy and Simultaneous Temozolomide without Adjuvant Chemotherapy for Glioblastoma. Strahlentherapie und Onkol. 2008 Nov 19;184(11):572–9.
62. Karacetin D, Okten B, Yalcin B, Incekara O. Concomitant temozolomide and radiotherapy versus radiotherapy alone for treatment of newly diagnosed glioblastoma multiforme. J BUON. 2011;16(1):133–7.
63. Athanassiou H, Synodinou M, Maragoudakis E, Paraskevaidis M, Verigos C, Misailidou D, et al. Randomized Phase II Study of Temozolomide and Radiotherapy Compared With Radiotherapy Alone in Newly Diagnosed Glioblastoma Multiforme. J Clin Oncol. 2005 Apr 1;23(10):2372–7.
64. Esteller M, Gaidano G, Goodman SN, Zagonel V, Capello D, Botto B, et al. Hypermethylation of the DNA repair gene O(6)-methylguanine DNA methyltransferase and survival of patients with diffuse large B-cell lymphoma. J Natl Cancer Inst. 2002 Jan 2;94(1):26–32.
65. Esteller M, Garcia-Foncillas J, Andion E, Goodman SN, Hidalgo OF, Vanaclocha V, et al. Inactivation of the DNA-Repair Gene *MGMT* and the Clinical Response of Gliomas to Alkylating Agents. N Engl J Med. 2000 Nov 9;343(19):1350–4.
66. Hart MG, Garside R, Rogers G, Stein K, Grant R. Temozolomide for high grade glioma. Cochrane Database Syst Rev. 2013 Apr 30;(4):CD007415.
67. Stupp R, Taillibert S, Kanner AA, Kesari S, Steinberg DM, Toms SA, et al. Maintenance Therapy With Tumor-Treating Fields Plus Temozolomide vs Temozolomide Alone for Glioblastoma. JAMA. 2015 Dec 15;314(23):2535.
68. Friedman HS, Prados MD, Wen PY, Mikkelsen T, Schiff D, Abrey LE, et al. Bevacizumab Alone and in Combination With Irinotecan in Recurrent Glioblastoma. J

Clin Oncol. 2009 Oct 1;27(28):4733–40.
69. Hottinger AF, Pacheco P, Stupp R. Tumor treating fields: a novel treatment modality and its use in brain tumors. Neuro Oncol. 2016 Oct 24;18(10):1338–49.
70. Baldwin RW. Tumour-specific immunity against spontneous rat tumours. Int J Cancer. 1966 May 15;1(3):257–64.
71. Galon J, Costes A, Sanchez-Cabo F, Kirilovsky A, Mlecnik B, Lagorce-Pagès C, et al. Type, Density, and Location of Immune Cells Within Human Colorectal Tumors Predict Clinical Outcome. Science (80-). 2006 Sep 29;313(5795):1960–4.
72. Goeppert B, Frauenschuh L, Zucknick M, Stenzinger A, Mehrabi A, Hafezi M, et al. Type, Density, and Location of Immune Cells within Cholangiocarcinomas Predict Clinical Outcome. Z Gastroenterol. 2012 Jan 9;50(01).
73. Restifo NP, Dudley ME, Rosenberg SA. Adoptive immunotherapy for cancer: harnessing the T cell response. Nat Rev Immunol. 2012 Apr 1;12(4):269–81.
74. Brahmer JR, Tykodi SS, Chow LQM, Hwu W-J, Topalian SL, Hwu P, et al. Safety and Activity of Anti–PD-L1 Antibody in Patients with Advanced Cancer. N Engl J Med. 2012 Jun 28;366(26):2455–65.
75. Lindenmann J, Klein PA. Viral oncolysis: increased immunogenicity of host cell antigen associated with influenza virus. J Exp Med. 1967 Jul 1;126(1):93–108.
76. Lampson LA. Brain tumor immunotherapy: seeing the brain in the body. Drug Discov Today. 2013 Apr 1;18(7–8):399–406.
77. Schlageter KE, Molnar P, Lapin GD, Groothuis DR. Microvessel Organization and Structure in Experimental Brain Tumors: Microvessel Populations with Distinctive Structural and Functional Properties. Microvasc Res. 1999 Nov;58(3):312–28.
78. Davies DC. Blood-brain barrier breakdown in septic encephalopathy and brain tumours. J Anat. 2002 Jun;200(6):639–46.
79. Abbas AK, Lichtman AH, Pillai S. Cellular and molecular immunology. Saunders/Elsevier; 2012. 545 p.
80. Schneider-Hohendorf T, Rossaint J, Mohan H, Böning D, Breuer J, Kuhlmann T, et al. VLA-4 blockade promotes differential routes into human CNS involving PSGL-1 rolling of T cells and MCAM-adhesion of TH17 cells. J Exp Med. 2014 Aug 25;211(9):1833–46.
81. Eliason DA, Cohen SA, Baratta J, Yu J, Robertson RT. Local proliferation of microglia cells in response to neocortical injury in vitro. Brain Res Dev Brain Res. 2002 Jul 30;137(1):75–9.
82. Kostianovsky AM, Maier LM, Anderson RC, Bruce JN, Anderson DE. Astrocytic regulation of human monocytic/microglial activation. J Immunol. 2008 Oct 15;181(8):5425–32.
83. Carbonell WS, Murase S-I, Horwitz AF, Mandell JW. Infiltrative microgliosis: activation and long-distance migration of subependymal microglia following periventricular insults. J Neuroinflammation. 2005 Jan 28;2(1):5.
84. Schroeter M, Jander S, Huitinga I, Witte OW, Stoll G. Phagocytic response in

photochemically induced infarction of rat cerebral cortex. The role of resident microglia. Stroke. 1997 Feb;28(2):382–6.
85. Zhang SC, Goetz BD, Carré JL, Duncan ID. Reactive microglia in dysmyelination and demyelination. Glia. 2001 Apr 15;34(2):101–9.
86. Nimmerjahn A, Kirchhoff F, Helmchen F. Resting Microglial Cells Are Highly Dynamic Surveillants of Brain Parenchyma in Vivo. Science (80-). 2005;308(May):1314–8.
87. Lawson LJ, Perry VH, Gordon S. Turnover of resident microglia in the normal adult mouse brain. Neuroscience. 1992;48(2):405–15.
88. Lawson LJ, Perry VH, Dri P, Gordon S. Heterogeneity in the distribution and morphology of microglia in the normal adult mouse brain. Neuroscience. 1990;39(1):151–70.
89. Aloisi F, Ria F, Columba-Cabezas S, Hess H, Penna G, Adorini L. Relative efficiency of microglia, astrocytes, dendritic cells and B cells in naive CD4+ T cell priming and Th1/Th2 cell restimulation. Eur J Immunol. 1999 Sep;29(9):2705–14.
90. Aloisi F, Ria F, Penna G, Adorini L. Microglia are more efficient than astrocytes in antigen processing and in Th1 but not Th2 cell activation. J Immunol. 1998 May 15;160(10):4671–80.
91. Flügel A, Labeur MS, Grasbon-Frodl E-M, Kreutzberg GW, Graeber MB. Microglia only weakly present glioma antigen to cytotoxic T cells. Int J Dev Neurosci. 1999 Aug 1;17(5–6):547–56.
92. Lafuente J V., Adán B, Alkiza K, Garibi JM, Rossi M, Cruz-Sánchez FF. Expression of Vascular Endothelial Growth Factor (VEGF) and Platelet-Derived Growth Factor Receptor-β (PDGFR-β) in Human Gliomas. J Mol Neurosci. 1999;13(1–2):177–86.
93. Tsai J-C, Goldman CK, Gillespie GY. Vascular endothelial growth factor in human glioma cell lines: induced secretion by EGF, PDGF-BB, and bFGF. J Neurosurg. 1995 May;82(5):864–73.
94. Dong H, Strome SE, Salomao DR, Tamura H, Hirano F, Flies DB, et al. Tumor-associated B7-H1 promotes T-cell apoptosis: A potential mechanism of immune evasion. Nat Med. 2002 Aug 24;8(8):793–800.
95. Magnus T, Schreiner B, Korn T, Jack C, Guo H, Antel J, et al. Microglial Expression of the B7 Family Member B7 Homolog 1 Confers Strong Immune Inhibition: Implications for Immune Responses and Autoimmunity in the CNS. J Neurosci. 2005 Mar 9;25(10):2537–46.
96. Pinton L, Masetto E, Vettore M, Solito S, Magri S, D'Andolfi M, et al. The immune suppressive microenvironment of human gliomas depends on the accumulation of bone marrow-derived macrophages in the center of the lesion. J Immunother Cancer. 2019 Dec 27;7(1):58.
97. Trolle T, McMurtrey CP, Sidney J, Bardet W, Osborn SC, Kaever T, et al. The Length Distribution of Class I-Restricted T Cell Epitopes Is Determined by Both Peptide Supply and MHC Allele-Specific Binding Preference. J Immunol. 2016 Feb 15;196(4):1480–7.
98. Rist MJ, Theodossis A, Croft NP, Neller MA, Welland A, Chen Z, et al. HLA Peptide

Length Preferences Control CD8+ T Cell Responses. J Immunol. 2013 Jul 15;191(2):561–71.
99. Tey S-K, Goodrum F, Khanna R. CD8+ T-cell recognition of human cytomegalovirus latency-associated determinant pUL138. J Gen Virol. 2010 Aug 1;91(8):2040–8.
100. Hassan C, Chabrol E, Jahn L, Kester MGD, de Ru AH, Drijfhout JW, et al. Naturally Processed Non-canonical HLA-A*02:01 Presented Peptides. J Biol Chem. 2015 Jan 30;290(5):2593–603.
101. Rudensky AY, Preston-Hurlburt P, Hong S-C, Barlow A, Janeway CA. Sequence analysis of peptides bound to MHC class II molecules. Nature. 1991 Oct;353(6345):622–7.
102. Nelson CA, Fremont DH. Structural principles of MHC class II antigen presentation. Rev Immunogenet. 1999;1(1):47–59.
103. Espinosa-Cueto P, Magallanes-Puebla A, Castellanos C, Mancilla R. Dendritic cells that phagocytose apoptotic macrophages loaded with mycobacterial antigens activate CD8 T cells via cross-presentation. Eugenin EA, editor. PLoS One. 2017 Aug 2;12(8):e0182126.
104. Nuchtern JG, Biddison WE, Klausner RD. Class II MHC molecules can use the endogenous pathway of antigen presentation. Nature. 1990 Jan 4;343(6253):74–6.
105. Jaraquemada D, Marti M, Long EO. An endogenous processing pathway in vaccinia virus-infected cells for presentation of cytoplasmic antigens to class II-restricted T cells. J Exp Med. 1990 Sep 1;172(3):947–54.
106. Leung CSK. Endogenous Antigen Presentation of MHC Class II Epitopes through Non-Autophagic Pathways. Front Immunol. 2015;6:464.
107. Albert ML, Sauter B, Bhardwaj N. Dendritic cells acquire antigen from apoptotic cells and induce class I-restricted CTLs. Nature. 1998 Mar;392(6671):86–9.
108. Janeway C. Immunobiology 5 : the immune system in health and disease. Garland Pub; 2001. 732 p.
109. Brennick CA, George MM, Corwin WL, Srivastava PK, Ebrahimi-Nik H. Neoepitopes as cancer immunotherapy targets: key challenges and opportunities. Immunotherapy. 2017 Mar 17;9(4):361–71.
110. McDermott D, Haanen J, Chen T-T, Lorigan P, O'Day S, MDX010-20 Investigators. Efficacy and safety of ipilimumab in metastatic melanoma patients surviving more than 2 years following treatment in a phase III trial (MDX010-20). Ann Oncol. 2013 Oct 1;24(10):2694–8.
111. Schachter J, Ribas A, Long G V, Arance A, Grob J-J, Mortier L, et al. Pembrolizumab versus ipilimumab for advanced melanoma: final overall survival results of a multicentre, randomised, open-label phase 3 study (KEYNOTE-006). Lancet. 2017 Oct;390(10105):1853–62.
112. Hodi FS, O'Day SJ, McDermott DF, Weber RW, Sosman JA, Haanen JB, et al. Improved Survival with Ipilimumab in Patients with Metastatic Melanoma. N Engl J Med. 2010 Aug 19;363(8):711–23.
113. Lee KM, Chuang E, Griffin M, Khattri R, Hong DK, Zhang W, et al. Molecular basis of T

cell inactivation by CTLA-4. Science. 1998 Dec 18;282(5397):2263–6.
114. Fong B, Jin R, Wang X, Safaee M, Lisiero DN, Yang I, et al. Monitoring of Regulatory T Cell Frequencies and Expression of CTLA-4 on T Cells, before and after DC Vaccination, Can Predict Survival in GBM Patients. Castro MG, editor. PLoS One. 2012 Apr 2;7(4):e32614.
115. Francisco LM, Salinas VH, Brown KE, Vanguri VK, Freeman GJ, Kuchroo VK, et al. PD-L1 regulates the development, maintenance, and function of induced regulatory T cells. J Exp Med. 2009 Dec 21;206(13):3015–29.
116. Cheng X, Veverka V, Radhakrishnan A, Waters LC, Muskett FW, Morgan SH, et al. Structure and Interactions of the Human Programmed Cell Death 1 Receptor. J Biol Chem. 2013 Apr 26;288(17):11771–85.
117. Wang Z, Zhang C, Liu X, Wang Z, Sun L, Li G, et al. Molecular and clinical characterization of PD-L1 expression at transcriptional level via 976 samples of brain glioma. Oncoimmunology. 2016 Nov 16;5(11):e1196310.
118. Nduom EK, Wei J, Yaghi NK, Huang N, Kong L-Y, Gabrusiewicz K, et al. PD-L1 expression and prognostic impact in glioblastoma. Neuro Oncol. 2016 Feb;18(2):195–205.
119. Prendergast GC, Smith C, Thomas S, Mandik-Nayak L, Laury-Kleintop L, Metz R, et al. Indoleamine 2,3-dioxygenase pathways of pathogenic inflammation and immune escape in cancer. Cancer Immunol Immunother. 2014 Jul 8;63(7):721–35.
120. Das M, Zhu C, Kuchroo VK. Tim-3 and its role in regulating anti-tumor immunity. Immunol Rev. 2017 Mar;276(1):97–111.
121. Li G, Wang Z, Zhang C, Liu X, Cai J, Wang Z, et al. Molecular and clinical characterization of TIM-3 in glioma through 1,024 samples. Oncoimmunology. 2017 Aug 3;6(8):e1328339.
122. Han S, Feng S, Xu L, Shi W, Wang X, Wang H, et al. Tim-3 on Peripheral CD4 $^{+}$ and CD8 $^{+}$ T Cells Is Involved in the Development of Glioma. DNA Cell Biol. 2014 Apr;33(4):245–50.
123. Weber JS, Hodi FS, Wolchok JD, Topalian SL, Schadendorf D, Larkin J, et al. Safety Profile of Nivolumab Monotherapy: A Pooled Analysis of Patients With Advanced Melanoma. J Clin Oncol. 2017 Mar;35(7):785–92.
124. Reck M, Rodríguez-Abreu D, Robinson AG, Hui R, Csőszi T, Fülöp A, et al. Pembrolizumab versus Chemotherapy for PD-L1–Positive Non–Small-Cell Lung Cancer. N Engl J Med. 2016 Nov 10;375(19):1823–33.
125. Robert C, Long G V., Brady B, Dutriaux C, Maio M, Mortier L, et al. Nivolumab in Previously Untreated Melanoma without *BRAF* Mutation. N Engl J Med. 2015 Jan 22;372(4):320–30.
126. Hombach A, Wieczarkowiecz A, Marquardt T, Heuser C, Usai L, Pohl C, et al. Tumor-specific T cell activation by recombinant immunoreceptors: CD3 zeta signaling and CD28 costimulation are simultaneously required for efficient IL-2 secretion and can be integrated into one combined CD28/CD3 zeta signaling receptor molecule. J Immunol.

2001 Dec 1;167(11):6123–31.
127. O'Rourke DM, Nasrallah MP, Desai A, Melenhorst JJ, Mansfield K, Morrissette JJD, et al. A single dose of peripherally infused EGFRvIII-directed CAR T cells mediates antigen loss and induces adaptive resistance in patients with recurrent glioblastoma. Sci Transl Med. 2017 Jul 19;9(399):eaaa0984.
128. Felsberg J, Hentschel B, Kaulich K, Gramatzki D, Zacher A, Malzkorn B, et al. Epidermal Growth Factor Receptor Variant III (EGFRvIII) Positivity in *EGFR* -Amplified Glioblastomas: Prognostic Role and Comparison between Primary and Recurrent Tumors. Clin Cancer Res. 2017 Nov 15;23(22):6846–55.
129. Andersson U, Guo D, Malmer B, Bergenheim AT, Br□nnstr□m T, Hedman H, et al. Epidermal growth factor receptor family (EGFR, ErbB2?4) in gliomas and meningiomas. Acta Neuropathol. 2004 Aug 18;108(2):135–42.
130. Liu G, Ying H, Zeng G, Wheeler CJ, Black KL, Yu JS. HER-2, gp100, and MAGE-1 Are Expressed in Human Glioblastoma and Recognized by Cytotoxic T Cells. Cancer Res. 2004 Jul 15;64(14):4980–6.
131. Ahmed N, Brawley V, Hegde M, Bielamowicz K, Kalra M, Landi D, et al. HER2-Specific Chimeric Antigen Receptor–Modified Virus-Specific T Cells for Progressive Glioblastoma. JAMA Oncol. 2017 Aug 1;3(8):1094.
132. Herbst RS. Review of epidermal growth factor receptor biology. Int J Radiat Oncol. 2004 Jun 1;59(2):S21–6.
133. Gedeon PC, Choi BD, Sampson JH, Bigner DD. Rindopepimut: anti-EGFRvIII peptide vaccine, oncolytic. Drugs Future. 2013 Mar;38(3):147–55.
134. Liau LM, Ashkan K, Tran DD, Campian JL, Trusheim JE, Cobbs CS, et al. First results on survival from a large Phase 3 clinical trial of an autologous dendritic cell vaccine in newly diagnosed glioblastoma. J Transl Med. 2018 Dec 29;16(1):142.
135. Reardon DA, Mitchell DA. The development of dendritic cell vaccine-based immunotherapies for glioblastoma. Semin Immunopathol. 2017 Feb;39(2):225–39.
136. McGranahan T, Li G, Nagpal S. History and current state of immunotherapy in glioma and brain metastasis. Ther Adv Med Oncol. 2017 May;9(5):347–68.
137. Mahaley MS, Bigner DD, Dudka LF, Wilds PR, Williams DH, Bouldin TW, et al. Immunobiology of primary intracranial tumors. J Neurosurg. 1983 Aug;59(2):201–7.
138. Beirman HR, CRILE DM, DOD KS, KELLY KH, PETRAKIS NL, WHITE LP, et al. Remissions in leukemia of childhood following acute infectious disease: staphylococcus and streptococcus, varicella, and feline panleukopenia. Cancer. 1953 May;6(3):591–605.
139. Pasquinucci G. Possible effect of measles on leukaemia. Lancet (London, England). 1971 Jan 16;1(7690):136.
140. Bluming AZ, Ziegler JL. Regression of Burkitt's lymphoma in association with measles infection. Lancet (London, England). 1971 Jul 10;2(7715):105–6.
141. Taqi AM, Abdurrahman MB, Yakubu AM, Fleming AF. Regression of Hodgkin's disease after measles. Lancet (London, England). 1981 May 16;1(8229):1112.

142. Atherton MJ, Lichty BD. Evolution of oncolytic viruses: novel strategies for cancer treatment. Immunotherapy. 2013 Nov;5(11):1191–206.
143. Aurelian L. Oncolytic virotherapy: the questions and the promise. Oncolytic Virotherapy. 2013 Jun;19.
144. Chiocca EA, Rabkin SD. Oncolytic Viruses and Their Application to Cancer Immunotherapy. Cancer Immunol Res. 2014 Apr 1;2(4):295–300.
145. Toda M, Rabkin SD, Kojima H, Martuza RL. Herpes Simplex Virus as an in Situ Cancer Vaccine for the Induction of Specific Anti-Tumor Immunity. Hum Gene Ther. 1999 Feb 10;10(3):385–93.
146. Bartlett DL, Liu Z, Sathaiah M, Ravindranathan R, Guo Z, He Y, et al. Oncolytic viruses as therapeutic cancer vaccines. Mol Cancer. 2013;12(1):103.
147. Martuza RL, Malick A, Markert JM, Ruffner KL, Coen DM. Experimental therapy of human glioma by means of a genetically engineered virus mutant. Science. 1991 May 10;252(5007):854–6.
148. Hulou MM, Cho C-F, Chiocca EA, Bjerkvig R. Experimental therapies: gene therapies and oncolytic viruses. Handb Clin Neurol. 2016 Jan 1;134:183–97.
149. Chiocca EA, Abbed KM, Tatter S, Louis DN, Hochberg FH, Barker F, et al. A Phase I Open-Label, Dose-Escalation, Multi-Institutional Trial of Injection with an E1B-Attenuated Adenovirus, ONYX-015, into the Peritumoral Region of Recurrent Malignant Gliomas, in the Adjuvant Setting. Mol Ther. 2004 Nov 1;10(5):958–66.
150. Wollmann G, Ozduman K, van den Pol AN. Oncolytic Virus Therapy for Glioblastoma Multiforme. Cancer J. 2012;18(1):69–81.
151. Russell SJ, Peng K-W, Bell JC. Oncolytic virotherapy. Nat Biotechnol. 2012 Jul 10;30(7):658–70.
152. Brun J, McManus D, Lefebvre C, Hu K, Falls T, Atkins H, et al. Identification of genetically modified maraba virus as an oncolytic rhabdovirus. Mol Ther. 2010;18(8):1440–9.
153. Pol JG, Zhang L, Bridle BW, Stephenson KB, Rességuier J, Hanson S, et al. Maraba Virus as a Potent Oncolytic Vaccine Vector. Mol Ther. 2014 Feb;22(2):420–9.
154. Mlecnik B, Bindea G, Kirilovsky A, Angell HK, Obenauf AC, Tosolini M, et al. The tumor microenvironment and Immunoscore are critical determinants of dissemination to distant metastasis. Sci Transl Med. 2016 Feb 24;8(327):327ra26-327ra26.
155. Sahin U, Derhovanessian E, Miller M, Kloke B-P, Simon P, Löwer M, et al. Personalized RNA mutanome vaccines mobilize poly-specific therapeutic immunity against cancer. Nature. 2017;547(7662):222–6.
156. Castle JC, Kreiter S, Diekmann J, Löwer M, Van De Roemer N, De Graaf J, et al. Exploiting the mutanome for tumor vaccination. Cancer Res. 2012;72(5):1081–91.
157. Laumont CM, Vincent K, Hesnard L, Audemard É, Bonneil É, Laverdure J-P, et al. Noncoding regions are the main source of targetable tumor-specific antigens. Sci Transl Med. 2018 Dec 5;10(470):eaau5516.

158. Ott PA, Hu Z, Keskin DB, Shukla SA, Sun J, Bozym DJ, et al. An immunogenic personal neoantigen vaccine for patients with melanoma. Nature. 2017 Jul 5;547(7662):217–21.
159. Capietto A-H, Jhunjhunwala S, Delamarre L. Characterizing neoantigens for personalized cancer immunotherapy. Curr Opin Immunol. 2017 Jun;46:58–65.
160. Marty R, Kaabinejadian S, Rossell D, Slifker MJ, van de Haar J, Engin HB, et al. MHC-I Genotype Restricts the Oncogenic Mutational Landscape. Cell. 2017 Nov 30;171(6):1272-1283.e15.
161. Yadav M, Jhunjhunwala S, Phung QT, Lupardus P, Tanguay J, Bumbaca S, et al. Predicting immunogenic tumour mutations by combining mass spectrometry and exome sequencing. Nature. 2014;515(7528):572–6.
162. Bassani-Sternberg M, Coukos G. Mass spectrometry-based antigen discovery for cancer immunotherapy. Curr Opin Immunol. 2016 Aug;41:9–17.
163. Iizuka Y, Kojima H, Kobata T, Kawase T, Kawakami Y, Toda M. Identification of a glioma antigen, GARC-1, using cytotoxic T lymphocytes induced by HSV cancer vaccine. Int J Cancer. 2006 Feb 15;118(4):942–9.
164. Johanns TM, Ward JP, Miller CA, Wilson C, Kobayashi DK, Bender D, et al. Endogenous Neoantigen-Specific CD8 T Cells Identified in Two Glioblastoma Models Using a Cancer Immunogenomics Approach. Cancer Immunol Res. 2016;4(12):1007–15.
165. Holtkamp S, Kreiter S, Selmi A, Simon P, Koslowski M, Huber C. Modification of antigen encoding RNA increases stability , translational efficacy and T-cell stimulatory capacity of dendritic cells Modification of antigen encoding RNA increases stability , translational efficacy and T-cell stimulatory capacity of dendr. Blood. 2006;108(13):4009–18.
166. Beug ST, Pichette SJ, St-Jean M, Holbrook J, Walker DE, LaCasse EC, et al. Combination of IAP Antagonists and TNF-α-Armed Oncolytic Viruses Induce Tumor Vascular Shutdown and Tumor Regression. Mol Ther - Oncolytics. 2018;10:28–39.
167. Yadav M, Jhunjhunwala S, Phung QT, Lupardus P, Tanguay J, Bumbaca S, et al. Predicting immunogenic tumour mutations by combining mass spectrometry and exome sequencing. Nature. 2014 Nov 27;515(7528):572–6.
168. Monjazeb AM, Zamora AE, Grossenbacher SK, Mirsoian A, Sckisel GD, Murphy WJ. Immunoediting and antigen loss: overcoming the achilles heel of immunotherapy with antigen non-specific therapies. Front Oncol. 2013;3:197.
169. Majzner RG, Mackall CL. Tumor Antigen Escape from CAR T-cell Therapy. Cancer Discov. 2018 Oct 1;8(10):1219–26.
170. Velders MP, Weijzen S, Eiben GL, Elmishad AG, Kloetzel P-M, Higgins T, et al. Defined Flanking Spacers and Enhanced Proteolysis Is Essential for Eradication of Established Tumors by an Epitope String DNA Vaccine. J Immunol. 2001;166(9):5366–73.
171. Yang Y, Sun W, Guo J, Zhao G, Sun S, Yu H, et al. In silico design of a DNA-based HIV-1 multi-epitope vaccine for Chinese populations. Hum Vaccines Immunother. 2015;11(3):795–805.

172. Schubert B, Kohlbacher O. Designing string-of-beads vaccines with optimal spacers. Genome Med. 2016;8(1):9.
173. Wang QM, Sun SH, Hu ZL, Zhou FJ, Yin M, Xiao CJ, et al. Epitope DNA vaccines against tuberculosis: Spacers and ubiquitin modulates cellular immune responses elicited by epitope DNA vaccine. Scand J Immunol. 2004;60(3):219–25.
174. Livingston B, Crimi C, Newman M, Higashimoto Y, Appella E, Sidney J, et al. A rational strategy to design multiepitope immunogens based on multiple Th lymphocyte epitopes. J Immunol. 2002;168(11):5499–506.
175. Saadi M, Karkhah A, Nouri HR. Development of a multi-epitope peptide vaccine inducing robust T cell responses against brucellosis using immunoinformatics based approaches. Infect Genet Evol. 2017;51:227–34.
176. Nezafat N, Ghasemi Y, Javadi G, Khoshnoud MJ, Omidinia E. A novel multi-epitope peptide vaccine against cancer: An in silico approach. J Theor Biol. 2014;349:121–34.
177. Jones LH. Recent advances in the molecular design of synthetic vaccines. Nat Chem. 2015;7(12):952–60.
178. Alexander J, Sidney J, Southwood S, Ruppert J, Oseroff C, Maewal A, et al. Development of High Potency Universal DR Restricted Helper Epitopes by Modification of High Affinity DR Blocking Peptides. Immunity. 1994;In Press:751–61.
179. Thacker EE, Timares L, Matthews QL. Strategies to overcome host immunity to adenovirus vectors in vaccine development. Expert Rev Vaccines. 2009 Jun;8(6):761–77.
180. Li W, Joshi MD, Singhania S, Ramsey KH, Murthy AK. Peptide Vaccine: Progress and Challenges. Vaccines. 2014 Jul 2;2(3):515–36.
181. Panagioti E, Klenerman P, Lee LN, van der Burg SH, Arens R. Features of Effective T Cell-Inducing Vaccines against Chronic Viral Infections. Front Immunol. 2018;9:276.
182. Wherry EJ. T cell exhaustion. Nat Immunol. 2011 Jun;12(6):492–9.
183. Schwanhäusser B, Busse D, Li N, Dittmar G, Schuchhardt J, Wolf J, et al. Global quantification of mammalian gene expression control. Nature. 2011 May 19;473(7347):337–42.
184. Gubin MM, Zhang X, Schuster H, Caron E, Ward JP, Noguchi T, et al. Checkpoint blockade cancer immunotherapy targets tumour-specific mutant antigens. Nature. 2014 Nov 27;515(7528):577–81.
185. Bassani-Sternberg M, Coukos G. Mass spectrometry-based antigen discovery for cancer immunotherapy. Curr Opin Immunol. 2016 Aug;41:9–17.
186. Bassani-Sternberg M, Bräunlein E, Klar R, Engleitner T, Sinitcyn P, Audehm S, et al. Direct identification of clinically relevant neoepitopes presented on native human melanoma tissue by mass spectrometry. Nat Commun. 2016 Dec 21;7(1):13404.
187. Fricker L. Quantitative Peptidomics: General Considerations. In: Methods in molecular biology (Clifton, NJ). 2018. p. 121–40.
188. Persano S, Guevara ML, Li Z, Mai J, Ferrari M, Pompa PP, et al. Lipopolyplex potentiates anti-tumor immunity of mRNA-based vaccination. Biomaterials. 2017;125:81–9.

189. De Silva AD, Boesteanu A, Song R, Nagy N, Harhaj E, Harding C V, et al. Thermolabile H-2Kb molecules expressed by transporter associated with antigen processing-deficient RMA-S cells are occupied by low-affinity peptides. J Immunol. 1999 Oct 15;163(8):4413–20.
190. Dunn GP, Bruce AT, Ikeda H, Old LJ, Schreiber RD. Cancer immunoediting: from immunosurveillance to tumor escape. Nat Immunol. 2002 Nov;3(11):991–8.
191. Martens A, Wistuba-Hamprecht K, Yuan J, Postow MA, Wong P, Capone M, et al. Increases in Absolute Lymphocytes and Circulating CD4+ and CD8+ T Cells Are Associated with Positive Clinical Outcome of Melanoma Patients Treated with Ipilimumab. Clin Cancer Res. 2016 Oct 1;22(19):4848–58.
192. Yoon H, Kim TS, Braciale TJ. The Cell Cycle Time of CD8+ T Cells Responding In Vivo Is Controlled by the Type of Antigenic Stimulus. Joly E, editor. PLoS One. 2010 Nov 8;5(11):e15423.
193. Beug ST, Tang VA, LaCasse EC, Cheung HH, Beauregard CE, Brun J, et al. Smac mimetics and innate immune stimuli synergize to promote tumor death. Nat Biotechnol. 2014;32(2):182–90.
194. Reardon DA, Gokhale PC, Klein SR, Ligon KL, Rodig SJ, Ramkissoon SH, et al. Glioblastoma Eradication Following Immune Checkpoint Blockade in an Orthotopic, Immunocompetent Model. Cancer Immunol Res. 2016;4(2):124–35.
195. Genoud V, Marinari E, Nikolaev SI, Castle JC, Bukur V, Dietrich P-Y, et al. Responsiveness to anti-PD-1 and anti-CTLA-4 immune checkpoint blockade in SB28 and GL261 mouse glioma models. Oncoimmunology. 2018 Dec 2;7(12):e1501137.
196. Hung AL, Maxwell R, Theodros D, Belcaid Z, Mathios D, Luksik AS, et al. TIGIT and PD-1 dual checkpoint blockade enhances antitumor immunity and survival in GBM. Oncoimmunology. 2018 May 24;e1466769.
197. Ladomersky E, Zhai L, Lenzen A, Lauing KL, Qian J, Scholtens DM, et al. IDO1 Inhibition Synergizes with Radiation and PD-1 Blockade to Durably Increase Survival Against Advanced Glioblastoma. Clin Cancer Res. 2018 Jun 1;24(11):2559–73.
198. Howard SC, Jones DP, Pui C-H. The tumor lysis syndrome. N Engl J Med. 2011 May 12;364(19):1844–54.
199. Vogel P, Pletcher JM, Liang Y. Spontaneous Acute Tumor Lysis Syndrome as a Cause of Early Deaths in Short-Term Carcinogenicity Studies Using *p53* $^{+/-}$ Mice. Vet Pathol. 2010 Jul 30;47(4):719–24.

APPENDIX

Supplementary Table 1: Possible neoepitopes formed from D-N non-synonymous mutation with predicted MHC binding IC50 scores (nM).

Imp3_Db	D.81.N	Tumour				
Length	Position	Peptide	NetCTL IC50	NetMHC IC50	ANN IC50	SMM IC50
8	8	RASAALLN	43024.1	43805.2	48348.7	123694.4
8	7	ASAALLNK	39451.8	43759.2	45414.7	88582.9
8	6	SAALLNKL	10405.9	29433.6	22742.0	53009.0
8	5	AALLNKLY	15370.3	14934.3	13462.2	80232.4
8	4	ALLNKLYA	19507.6	17053.6	11222.4	40959.1
8	3	LLNKLYAM	14559.7	31953.8	29766.6	83243.4
8	2	LNKLYAMG	46414.2	46583.2	47965.7	93185.9
8	1	NKLYAMGL	42101.8	44773.1	44277.4	97353.1
9	9	VRASAALLN	48470.0	44511.3	48602.0	524348.5
9	8	RASAALLNK	38190.0	39249.2	47618.7	108797.8
9	7	ASAALLNKL	10749.7	11060.7	7936.9	4871.0
9	6	SAALLNKLY	31765.5	32932.7	44392.0	66775.9
9	5	AALLNKLYA	264.3	101.8	42.8	49.6
9	4	ALLNKLYAM	6253.4	7804.2	7705.6	3610.9
9	3	LLNKLYAMG	41199.2	39967.4	45788.7	323310.6
9	2	LNKLYAMGL	42560.4	39375.9	46410.7	1809755.9
9	1	NKLYAMGLV	41199.2	35116.1	40313.6	95196.3
10	10	RVRASAALLN	45419.2	39811.6	45951.9	215898.7
10	9	VRASAALLNK	47431.0	43322.0	47752.3	131295.5
10	8	RASAALLNKL	12375.7	22594.8	19286.9	23027.7
10	7	ASAALLNKLY	33899.2	34473.5	29729.3	66259.8
10	6	SAALLNKLYA	5491.0	915.6	356.6	3149.6
10	5	AALLNKLYAM	37.2	35.7	19.0	2411.3
10	4	ALLNKLYAMG	39026.7	32680.0	27279.5	59190.2
10	3	LLNKLYAMGL	30090.4	35393.0	33998.6	37346.5
10	2	LNKLYAMGLV	41199.2	34010.0	40110.4	45107.6
10	1	NKLYAMGLVP	47947.7	40413.1	43588.6	56787.1

Imp3_Db	D.81.N	Wild type				
Length	Position	Peptide	NetCTL IC50	NetMHC IC50	ANN IC50	SMM IC50
8	8	RASAALLD	44929.7	44879.8	48464.4	133767.3
8	7	ASAALLDK	40316.1	42780.3	44349.8	153585.4
8	6	SAALLDKL	6119.4	22872.5	17646.0	54745.7
8	5	AALLDKLY	30090.4	34285.6	36954.8	92971.5
8	4	ALLDKLYA	30090.4	35411.8	36866.6	117044.2
8	3	LLDKLYAM	23200.3	34531.0	38841.9	81348.6
8	2	LDKLYAMG	47431.0	47314.2	48676.2	96683.0
8	1	DKLYAMGL	45914.0	46049.0	46454.3	80417.4
9	9	VRASAALLD	48998.0	45155.0	48775.3	1243426.2
9	8	RASAALLDK	40755.3	41527.9	47764.8	138873.7
9	7	ASAALLDKL	5145.4	5056.4	3794.2	1899.4
9	6	SAALLDKLY	33899.2	32775.6	44153.0	53286.8
9	5	AALLDKLYA	10519.3	3139.3	4104.0	956.4
9	4	ALLDKLYAM	9137.2	12180.0	19286.1	8802.8
9	3	LLDKLYAMG	43966.6	41048.6	47611.0	1594483.4
9	2	LDKLYAMGL	43966.6	43206.4	47946.0	4760143.0
9	1	DKLYAMGLV	45914.0	40595.9	44591.3	180975.6
10	10	RVRASAALLD	46919.8	40226.0	45971.8	234557.9
10	9	VRASAALLDK	47947.7	44328.2	47927.8	132205.6
10	8	RASAALLDKL	8469.8	16585.4	13728.5	14297.2
10	7	ASAALLDKLY	32815.0	28578.4	24854.4	52632.0
10	6	SAALLDKLYA	17315.8	11518.6	12222.7	4448.9
10	5	AALLDKLYAM	642.6	1787.2	853.1	11648.0
10	4	ALLDKLYAMG	39881.6	35699.6	36607.4	66872.9
10	3	LLDKLYAMGL	36570.2	36497.9	40942.6	62122.7
10	2	LDKLYAMGLV	43024.1	38093.2	42221.1	45315.8
10	1	DKLYAMGLVP	48470.0	42208.8	44514.7	75726.9

Supplementary Figure 1: *In silico* algorithms NetMHCpan 2.3, NetMHCpan 4.0, ANN, and SMM, ranking top 15 predicted peptide based on MHC IC50 (nM) scores. Peptides in red represent screen negative for immunogenicity, and in green are screen positive for immunogenicity.

H-2Kb

Net MHCpan 2.3		Net MHCpan 4.0		ANN		SMM	
Lrrk1	T.1768.S	Lrrn4cl	V.200.L	Lrrn4cl	V.200.L	Lrrn4cl	V.200.L
Sfxn2	R.111.M	Myh14	G.135.V	Myh14	G.135.V	Myh14	G.135.V
Myo9a	R.440.L	Pcx	V.757.F	Snx6	S.250.F	Pcf11	D.1105.Y
Rad51d	R.54.M	Slc36a1	I.298.V	Ttbk1	C.450.R	Slc36a1	I.298.V
Myh14	G.135.V	Snx6	S.250.F	Slc36a1	I.298.V	Snx6	S.250.F
Mrps18b	Q.28.L	Pcf11	D.1105.Y	Arhgef11	S.806.A	Med1	F.596.V
Hlcs	Q.487.P	Tm9sf3	V.231.L	Eef1a1	A.355.T	Itpr1	G.877.C
Col4a3bp	R.158.L	Fut10	R.175.M	Zfhx3	R.1449.P	Tm9sf3	V.231.L
Zfp106	K.1567.M	Myo9a	R.440.L	Pcf11	D.1105.Y	Helz2	W.2486.C
Mb21d1	H.422.Y	Nsl1	Q.218.L	Cdsn	A.400.V	Rad54b	L.550.F
Pcyox1	L.454.F	Wipi1	A.35.S	Tm9sf3	V.231.L	Pcm1	Q.352.L
Wipi1	A.35.S	Txnl1	A.43.S	Txnl1	A.43.S	Gal3st1	D.304.Y
Hhat	T.181.A	Fzd1	C.326.F	Fut10	R.175.M	Eef1a1	A.355.T
Tm9sf3	V.231.L	Ifi47	C.231.R	Vars2	T.975.A	Pcdh18	Q.1012.R
Snx6	S.250.F	Arhgef11	S.806.A	Wipi1	A.35.S	Ttbk1	C.450.R

Immunogenicity	
	negative
	positive

H-2Db

Net MHCpan 2.3		Net MHCpan 4.0		ANN		SMM	
Tmem2	K.1042.N	Rtn2	L.405.F	Tmem2	K.1042.N	Tmem2	K.1042.N
Rtn2	L.405.F	Tmem2	K.1042.N	Rtn2	L.405.F	Rtn2	L.405.F
Imp3	D.81.N	Ppp4r3a	Y.581.F	Imp3	D.81.N	Imp3	D.81.N
Fut10	R.175.M	Imp3	D.81.N	Slc7a1	R.59.L	Slc7a1	R.59.L
Tm9sf3	V.231.L	Extl1	E.540.D	Ppp4r3a	Y.581.F	Rhd	V.140.M
Slc36a1	I.298.V	Tgif1	M.133.L	Extl1	E.540.D	Amacr	D.73.Y
Extl1	E.540.D	Fut10	R.175.M	Clint1	N.446.S	Qars	E.168.D
Slc7a1	R.59.L	Lrrc27	G.330.A	Lrrc27	G.330.A	Dhx35	D.246.N
Slc2a12	Q.214.K	Parp12	E.209.V	Nes	S.570.L	Sepsecs	E.300.D
Qars	E.168.D	Qars	E.168.D	Qars	E.168.D	Lrrc27	G.330.A
Clint1	N.446.S	Phactr4	V.253.L	Ube4b	Q.817.L	Clcn4	R.682.H
Fbxo34	V.21.M	Slc7a1	R.59.L	Sepsecs	E.300.D	Extl1	E.540.D
Ifi47	S.16.N; G.1	Tm9sf3	V.231.L	Phactr4	V.253.L	Hspa14	R.168.L
Ube4b	Q.817.L	Clint1	N.446.S	Hjurp	D.245.N	Rhbdd3	H.91.Y
Gal3st1	D.304.Y	Dhx35	D.246.N	Rpp25l	G.41.W	Trps1	V.813.L